Hawassa University

Institute of Technology

Department of Electrical and Computer Engineering

Damping of Low Frequency Oscillation through Optimal Sizing of Unified Power Flow Controller and Power System Stabilizer Employing Antlion Optimization

(Case study: Tana Beles 400kV Transmission Line)

A Thesis Submitted to Hawassa Institute of Technology, School of Graduate Studies Hawassa University

In Partial Fulfillment of the Requirements for the Degree of Masters of Science in Power System and Energy Engineering

By Endeshaw Solomon

Advisor: Dr. Baseem Khan

Hawassa, Ethiopia

May, 2022

Hawassa University

Institute of Technology

Department of Electrical and Computer Engineering

School of Postgraduate Studies

ADVISOR'S APPROVAL SHEET

This is to certify that the thesis entitled "Damping of Low Frequency Oscillation through Optimal Sizing of Unified Power Flow Controller and Power System Stabilizer Employing Antlion Optimization'' (Case study: Tana Beles 400kV Transmission Line) submitted in partial fulfilment of the requirements for the degree of masters of science in Electrical engineering with specialization in Power system and energy engineering, the Graduated program of department of Electrical and Computer engineering, has been carried out by Endeshaw Solomon under my supervision. Therefore, I recommended that the student has fulfilled the requirements and hence hereby submit the thesis to the department.

Dr. Baseem khan	_____	_____
Advisors	Signature	Date
Mr. Mulualem Tesfaye	_____	_____
Co - advisors	Signature	Date

Hawassa University

Institute of Technology

Department of Electrical and Computer Engineering

School of Postgraduate Studies

APPROVED BY BOARD OF EXAMINERS

We the under signed Board of examiners of the final open defense by Endeshaw Solomon have read and evaluated thesis entitled ‘‘Damping of Low Frequency Oscillation through Optimal Sizing of Unified Power Flow Controller and Power System Stabilizer Employing Antlion Optimization’’ (Case study: Tana Beles 400kV Transmission Line) and examined the candidate. Therefore, to certify that the thesis has been accepted in partial fulfilment of the requirements for the degree.

Dr. Baseem Khan	_____	_____
Advisor	Signature	Date
_____	_____	
Internal Examiner	Signature	Date
_____	_____	
External Examiner	Signature	Date
_____	_____	_____
Chair holder	Signature	Date
_____	_____	_____
Faculty Dean	Signature	Date
_____	_____	_____
SGS Approval	Signature	Date

Final approval and acceptance of the thesis is contingent upon the submission of the final copy of the thesis to the school of graduate studies (SGS) through the department Graduate Committee (DGC) of Electrical and Computer Engineering.

Stamp of SGS: _____

Declaration

I undersigned, hereby declare that this thesis is my original work and has not been presented for a degree in this or any other university, and all sources of materials used for the thesis have been fully acknowledged.

All examiners' comments are duly incorporated.

Endeshaw Solomon _____ _____

Name Signature Date

Place: Hawassa Institute of Technology, Hawassa University

Hawassa, Ethiopia

This is to certify that the statement made above by the candidate is true to best of my knowledge and this thesis has been submitted for examination with my approval as university advisor.

Dr. Baseem Khan _____ _____

Advisor Name Signature Date

Mr. Mulualem Tesfaye _____ _____

Co-advisor Name Signature Date

Acknowledgment

First and foremost, I would like to thank you almighty of God and his mother Virgin Mary for giving strength to complete this work. Next I would like to express my sincere gratitude and appreciation to Dr. Baseem Khan for his continuous constructive comment, advice, suggestions, patience and encouragement throughout the thesis. His valuable support, understanding and expertise have been very important in completing this thesis work.

Next I would like to thanks to my co-advisor Mr. Mulualem Tesfaye for giving his comment, advice and help to accomplish this thesis work. Then I would like to appreciate and thanks to Mr. Walelign who is Tana Beles power plant operation manager for his willingness in providing the appropriate data and information necessary for my thesis work. I have received a very keen support from the office during my data collection period.

And I want to thank my wife, W/ro Mekdes Damtie for her continuous support and advice. Lastly I want to say thank you to all my families and friends who took part in this work directly or indirectly and wish good for me.

Abstract

Low frequency oscillations are an inevitable phenomena of power system. Integration of unified power flow controller (UPFC) and power system stabilizer (PSS) can considerably improve the stability by damping out of low frequency oscillation (LFO). This thesis had presented the damping out of LFO through optimal sizing of PSS and UPFC using an Antlion optimization (ALO) approach to improve the transfer capability of North West region of Ethiopian electric network from Tana Beles to Bahirdar 400kV line. The obtained results (minimal damping ratio, eigenvalues and time domain simulation) of the proposed ALO approach were compared with the results of conventional existing system, teaching learning based optimization (TLBO), particle swarm optimization (PSO) and genetic algorithm (GA) to investigate the efficiency of the proposed approach for various operating conditions of the considered electric network. In this thesis UPFC had been compared and selected from various flexible alternating current transmission system (FACTS) devices and filters to show the robustness of the proposed system. Further, the proposed ALO approach had improved the tuning time to estimate the key parameters of PSS and power oscillation damper (POD). Consequently, the settling time, controller gain and time constants of ALO to attain steady state system is small as compared with teaching learning based optimization, genetic algorithm and particle swarm. The nonlinear equation which describes the system had linearized and then placed in state space form to study and analyze the performance of the system by damping out of LFO problems. System eigenvalues obtained from ALO tuned UPFC-PSS and conventional existing system are compared to study the efficiency of the proposed method for various operating conditions. Besides, time domain simulation comparison proves the superiority of the proposed method over the existing system. Finally using PSS only improves the maximum overshoot by 42.2% and settling time of 63.7% but the proposed optimally sized UPFC-PSS employed with ALO method had improved the maximum overshoot by 56.06% and settling time by 78.7% as compared with conventional existing system (base case). Thus, this thesis addressed the mechanism regarding low frequency oscillation in the electric network by incorporating optimal sizing of PSS equipped with UPFC to the system.

***Key words**: Eigenvalues, LFO, minimum damping ratio, ALO, PSS, UPFC, POD*

Contents

List of Figures

List of Tables

Abbreviations

List of Acronyms

AC	Alternating current
AI	Artificial intelligence
AL	Antlion
ALO	Antlion optimization
ANN	Artificial Neural Network
AVR	Automatic voltage regulator
BPF	Band pass filter
CDC	Capacitance of direct current link
CENS	Cost of energy not supplied
CUPFC	Cost of Unified power flow controller
DC	Direct current
EEP	Ethiopian Electric power
EES	Energy storage systems
ETB	Ethiopian Birr
FACTS	Flexible AC transmission systems
FLC	Fuzzy logic controller
FLPSS	Fuzzy logic power system stabilizer
GA	Genetic Algorithm
HPF	High pass filter
HVDC	High voltage direct current
IEEE	Institute of Electrical and Electronics Engineers
IPFC	Interline power flow controller
kV	Kilo volt
kVA	Kilo Volt Ampere
kVAr	Kilo Volt Ampere reactive
LCL	Inductor capacitor Inductor
LFO	Lows frequency oscillation
LFS	Low-frequency swing
LPF	Low pass filter

MATLAB	Matrix Laboratory
MSFLA	Modified shuffled frog leaping algorithm
MVA	Mega Volt Ampere
MVAr	Mega Volt Ampere reactive
MW	Mega watt
MWh	Megawatt hour
NP	Number of operating point,
NPV	Net Present Value
NWR	North West region
OCC	Opportunity Cost of Capital
PLL	Phase locked loop
PSS	Power system stabilizer
PSO	Particle swarm optimization
POD	Power oscillation Damper
PV	Present Value
RC	Resistor Capacitor
RLC	Resistor Inductor Capacitor
RWs	Random walks
SFLA	Shuffled frog leaping algorithm
SMIB	Single machine infinite bus system
SSSC	Static series synchronous compensator
STATCOM	Static Synchronous compensator
SVC	Static VAR compensator
TCPS	Thyristor controlled phase shifter
TCSC	Thyristor controlled series capacitor
TLBO	Teaching learning based optimization
UPFC	Unified power flow controller
VAR	Volt Ampere Reactive
VDC	Voltage at dc link
VSC-B, VSC-E	Voltage source converters of boosting and excitation transformer

List of Symbols

Hz	Hertz
IC	Installation Cost
IT	Current iteration
IT_{max}	Maximum number of iteration
Td0	Open Circuit Time Constant of Generator for d-Axis
XB	Reactance for the Boosting Transformer
KB, KE	Gains of mB and δE based Controller
XE	Reactance for Excitation Transformer
x_{tE}	Reactance of the Transformer
x_{BV}	Reactance of the Transformer
Pe, Pm	Electrical and Mechanical Input Power of the Generator
pu	Per unit
M, D	Inertia Constant, Damping Coefficient
ω_b	Synchronous Speed of the Generator
δ, ω	Rotor Angle, Rotor Speed
E'_q	Generator Internal Voltage
E_{fd}	Field Voltage
ET, BT	Excitation and Boosting Transformer
T'_{d0}	Open Circuit Field Time Constant
x_d	Generator Reactance in the d-Axis
x'_d	d-Axis Transient Reactance
x_q	q-Axis Generator Reactance
V_{ref}	AC Bus Reference Voltage
u_{pss}	Control Signal of PSS
C0	Initial Investment
Vd, Vq	d–q axes Generator Terminal Voltages
Id, Iq	dq axes Generator Armature Current
Vt	Generator Terminal Voltage
Ie, Ib	Current in the Shunt and Series Transformer
mE, δE	Modulation Index and Angle of Shunt Converter

mB, δB	Modulation Index and Angle of Series Converter
KA, TA	Gain and Time Constant of Exciter and Regulator
KD	Damping Torque Coefficient
Eq	Internal Voltage of Generator
Vb	Infinite Bus Voltage
λ_i	Eigenvalues
σi, ωi	Eigenvalue's Real Part and Imaginary Part
$Q_{lineref}$	Transmission Line Reactive Power Flow
ξ	Damping ratio of mth Eigenvalue
T1, T2, T3, T4	Time Constants
K, Tw	Controller Gain and Washout Time Constant
X, Y, U	System State, Output Vectors, Input Vectors
Ybus	Bus Admittance Matrix
V_s	Stabilized Voltage
φ	Right Eigenvector

Chapter One

Introduction

1.1 Background

Low frequency oscillation (LFO) is a phenomenon in which oscillation continues for a relatively long period of time that leads to system instability. Low frequency oscillation (LFO) becomes the main cause of power system stability that limits the steady state transmission capacity of power system and affects normal operation of power system security and economics in Ethiopian electric transmission system. The range of frequency for LFO is from 0.1-3Hz and it is difficult to detect. If these oscillations are left untreated, it sustain and keep increasing to the level which may lead for system instability or complete blackout of the electric power system. Although PSS improves transmission system stability by damping of LFO, it is not effective for strong disturbance like three-phase fault near generator terminal. However, the development and use of UPFC in power system have discovered favorable results for enhancement of electric network stability, voltage stability and optimal power flow.

General advancement of FACTS device can solve such kind of problem. Along with primary function of FACTS device, the real power flow can be regulated to diminish LFO and increase power system stability. This recommends that FACTS will find new application as electric utilities merge and as a sale large power between distant and hostile interconnected partners become more wide spread.

Currently several FACTS device have been implemented and installed in practical power system like UPFC, Interline power flow controller (IPFC), Static VAr compensator (SVC), thyristor controlled series capacitor (TCSC), Static synchronous compensator (STATCOM) and many others. The organized application of PSS and UPFC ensures stability of the system and suppresses LFO during disturbance. The appropriate tuning of optimal parameters of UPFC and power system stabilizer determines its efficiency for LFO damping in any electric network. In an electric power system many devices and controllers have been used to keep the balance between demand and generation in a reliable manner with high power quality [1]. Any small or large disturbance can affect the synchronous operation of power system and its stability determines whether the system can settle down to a new or original steady state after transient disappears [2]. LFO are generator rotor angle oscillation having a

frequency of 0.1-2Hz. The main reasons of power system oscillation are the unbalance between demand and generation. Nowadays, large demand of power to the furthest end of the system that forces to transmit huge amount of power through a long transmission line and results an increasing power oscillations [3].

1.2 Statement of the Problem

The low frequency oscillation is a one type of stability problem in Tana Beles 400kV transmission line which is concerned with the behavior of the synchronous machines after disturbance due to a rapid change in load. There are different causes of low frequency oscillation for Tana Beles 400kV network, these are unbalance between supply and demand which is created by a change in load, generation or in network conditions. In any case the synchronous machine should remain in synchronism with other machines and they should operate in parallel as well as at the same speed. All the daily frequency, real power and reactive power data are presented on the appendix D.

Low frequency oscillation in Tana Beles 400kV power system network is one causes of power system instability, if adequate damping is not available as early as possible these frequencies may sustain and grow to cause system separation; blackout or partial load shedding. The range of low frequency variations in Tana Beles 400kV line is from 0.1-0.8Hz which may be created by large disturbance and small signal disturbance, such as change in load, use of high gain exciters in AVR and connection of poorly tuned generator excitations of Tana Beles power station. Further, sometimes the frequency had dropped beyond ±2.5Hz permissible range which is multiple contingency event or system separation event and finally lead to complete blackout throughout Ethiopia. Tana Beles 400kV electric transmission network must be stable to ensure continuity of supply throughout Ethiopia since LFO stability problem leads to partial load shedding or full system interruption. Therefore, it has always been traditional to use automatic voltage regulator (AVR) to improve system damping but in this thesis sizing of PSS and UPFC is proposed to damp out LFO problems.

1.3 Objective

1.3.1 General Objective

The general objective of this thesis is damping out of low-frequency oscillation through optimal sizing of PSS and UPFC using Antlion optimization.

1.3.2 Specific Objective

- Obtain synchronous machine rotor angle value, rotor speed deviation and DC link voltage.
- Sizing of Power Oscillation Damping controller
- Improve dynamic power system stability using PSS and UPFC.
- Compare conventional existing system with new integrated PSS and UPFC system
- Compare Ant lion algorithm with other existing techniques such as conventional fixed gain model, PSO, GA, TLBO.
- Perform eigenvalue analysis and time domain analysis.
- Simulate the overall system model using MATLAB/Simulink

1.4 Thesis Organization

For successful completion of the study some methods, steps, procedures and tasks must be conducted.

- **Introduction**: Some general introductions about LFO damping has been discussed.
- **Literature Review**: A number of published papers about low frequency oscillation damping and enhancement of dynamic stability of power system have been reviewed in different books, papers, articles, journals, lectures and materials.
- **Data collection**: Collect all the input data required for mathematical analysis and data required for simulation test.
- **Data Analysis**: Based on data collection, mathematical analysis takes place with and without controller for LFO damping of power system for SMIB network.
- **Component modeling**: Modeling of synchronous generator and Controllers like excitation system, power system stabilizer, unified power flow controller and POD controller.
- **System Modeling**: Modeling and simulation of single machine infinite bus system using MATLAB Simulink.
- **System simulation result and discussion**: Evaluate the proposed method achieves its general objective of the study or not.
- **Conclusion** based on the performance of the system relative effectiveness of PSS, UPFC and ALO based POD controller for overall system performance improvement is compared.

1.5 Significance of the Study

This thesis has an advantages of damping low frequency oscillation using PSS and FACTS to improve power system stability in power system network. Instability may occur due to different reasons that happen at the generation station, transmission or at the distribution when a large load is connected to the system. The main effect of low frequency oscillation causes interruption of power from generation to end user and may cause to break down electrical equipment due to oscillation generators. Enhancing dynamic power system stability by damping out of LFO helps to minimize the failure of electrical equipment as well as the whole power system network. So, to overcome such problems a solution is required which leads to the introduction of optimal sizing of UPFC and PSS using Antlion algorithm.

1.6 Scope of the Study

This study is concerned on the damping out of low frequency oscillation of electric networks through optimal design of UPFC and PSS which enhances the dynamic stability of a power system network. This problem would be solved by maintaining rotor angle of a synchronous machine under stable or optimum condition or minimizing low frequency oscillation by employing ALO. This study is limited to simulation of Tana Beles 400kV transmission network with optimally placed UPFC using MATLAB/Simulink following to the sizing of system components, power system stabilizer and make mathematical analysis. Also this thesis provides eigenvalue analysis and time domain analysis to determine the maximum overshoot and settling time of system states.

1.7 Thesis Layout

This thesis is composed of five chapters with detailed explanations. Chapter one presents a general introduction to the power system stability, low frequency oscillations, power system stabilizer, filters and UPFC, research objectives, statement of problem, significant and scope of the study and Methodology. Chapter two includes literature review and some general theoretical background of the research. Chapter three describes the linearization of non-linear SMIB system, power system stabilizer sizing, UPFC sizing and ALO technique. Chapter four represent the Simulation results and discussion of the eigenvalue analysis and time domain simulation of Tana Beles 400kV electric network and LFO damping, and PSS optimized parameters and UPFC controller. Chapter five represents the conclusion, recommendations and future work of the study.

Chapter Two

Literature Review

2.1 Introduction

This thesis presents the studies that would conduct on damping out of low frequency oscillation by using PSS and UPFC to improve dynamic stability of a power system network. Related research works published in the technical literature are described and the concepts of small signal and large signal disturbance of power systems are analyzed.

2.2 Summary of Literature Review

Al-Hinai, A. and Al-Hinai, S. (2009) investigated that dynamic stability enhancement using particle swarm optimization power system stabilizer. In this work the damping out of LFO for single machine infinite bus power system is analyzed. Such analysis needs a certain level of mathematical modeling and simulation. The major components of the mathematical models are synchronous machine, excitation systems and power system stabilizer. In general MATLAB Simulink is used for system modeling. According to system performance a proper design for PSS using PSO has been carried out. Then the sized power system stabilizer is implemented in the model and dynamic system response is analyzed. Since the simulation results without PSS shows unacceptable system response the response of the system with PSS has successfully stabilize the system [4].

In December 2010, Datta and Roy recommend damping out of power system oscillations for SMIB system using STATCOM in combination with power system stabilizer controller. It has been observed that Lead-Lag controllers have better capability in damping power system oscillations than that of proportional controllers. Simulation result was obtained using MATLAB/Simulink software. The damping capability of power system stabilizer controller is superior to Lead-Lag controller designed model by damping low frequency oscillation with less overshoot and shorter settling time [5].

Rout and Panda (2010) investigated the performance of FLC based adaptive PSS for SMIB system stability enhancement. Power system stabilizer is used to generate additional excitation control signals to damp out LFO of the electric network. In this case speed deviation and accelerated power are used as input for FLC. The inference mechanism of FLC is represented by If-Then rules. The performance of fuzzy logic power system stabilizer

and the result of the system with PSS were obtained. The simulation was tested under different types of condition [6].

Linda, et al. (2010) investigated a novel non-traditional optimization approach for designing fuzzy based PSS for a SMIB has been presented. The level of robustness to system load deviation is better than conventionally tuned power system stabilizer. When the number of energy deliverers connected to the system increases this research can be directed to develop systematic techniques of design and analysis of fuzzy based stabilization control like PSO, Ant Colony Optimization. The simulation results of both parameter optimization techniques can be compared for single machine infinite bus systems and its effectiveness can also be studied [7].

Kushwaha, et al. (2013) emphasize particle swarm optimization optimized PSS to increase the dynamic stability of the entire power system using linearized state space model for SMIB system. Many input and output parameters of PSS controllers are optimized using PSO to achieve good result and enhance stability. Out of the various choices for input to the PSS controller, the rotor speed deviation $\Delta\omega$ and acceleration α are considered as the input to power system stabilizer controller. Moreover the behavior of the conventional controller, power system stabilizer controller and PSO optimized PSS is obtained for various parameters [8].

In March 2014, Arizadayana et al. proposed that a linearized model of SMIB power system installed with UPFC is presented to study power system oscillation. The proposed model is then simulated using MATLAB-SIMULINK and compared with the conventional system with PSS. The simulation results indicated that by incorporating FLPSS with UPFC, the damping of low frequency oscillation shown a better performance than conventional PSS thus improving the dynamic power system stability [9].

Gupta et al. (2014) proposed that normal operating voltage stability enhancement of power system using FACTS devices. This work leads towards the main issues of the power system to enhance voltage stability of the system and to decrease real power loss in the system. The analysis has been done on IEEE 14 bus system using two FACTS devices namely thyristor controlled series compensator and static synchronous compensator for power system stability under different loading conditions. The simulation has been done using MATLAB Simulink and optimal location is obtained by calculating voltage collapse proximity index and line stability index to locate the critical line with respect to bus [10].

Morteza et al. (2016) proposed that controller design of STATCOM using modified shuffled frog leaping algorithm (MSFL) for LFO damping. In this work, a new MSFL algorithm is proposed for optimal selection of STATCOM damping controller parameters to shift eigenvalues to the left hand side of the plane. m. A SMIB system had been considered to examine the operation of proposed controllers. Sudden change in the input power of generator is taken as a disturbance. The robustness of the controller for damping of LFO is tested at various operating conditions and results are compared to particle swarm optimization and SFLA methods. Simulation results show the potential and superiority of the proposed MSFLA over the SFLA and PSO [11].

Jalali et al. (2016) prove recent technologies in ESS have initiated a global interest to harness their potential in enhancing reliability and robustness of power system. The advantages of integrating STATCOMs with ESSs acts as a dynamic compensation device for voltage stability enhancement are demonstrated. In this regard, the issues of placement and operation of these devices are addressed. It is shown that a desired level of voltage stability margin for a power system with embedded wind farm can be attained efficiently, regardless of variations of wind power generation and loading condition. The approach is to test on IEEE 30-bus test system [12].

Vigneysh, and Kumarappan, (2017) assume adaptive fuzzy proportional-integral controller is proposed to improve the dynamic performance of the inverter interfaced autonomous micro-grid. For this purpose, an accurate small signal state space model of the micro-grid with electronically interfaced distributed generation units is developed. The developed model includes the network dynamics, controller dynamics, dynamics of LCL filter and load dynamics [13].

Vladimir et al. (2018) proposed method on enhancement of dynamical characteristics of a fuzzy control system by using unstable subsystem controller synthesis ensures the placement of roots in the right half-plane, when the output signal of the system is in the area of large deviations. This approach provides a further increase in system transients. The use of hodograph of roots that is different from the circular ones (for a system with two roots in the right half- plane) allows for slight improving of the properties of the system. However, it requires a significant complication of the control system. The MATLAB SOS Toolbox was applied to synthesize a control action for a nonlinear polynomial fuzzy system while providing Lyapunov stability [14].

2.2.1 Methods or Techniques Point of View for damping out of LFO

Table 2.1: Techniques and number of literature for different purpose

Methods/Techniques	Total No. of literatures reviews out of 45 literatures
Optimization based methods	[4],[11],[16],[27],[36],[37],[38],[42]
AI-based techniques	[5],[6],[7],[11],[13],[14],[21],[25],[26],[33],[40],[43]
Other method	[1],[2],[3],[8],[9],[10],[12],[15],[16],[17],[18],[19],[20],[22],[23],[24],[26],[28],[29],[30],[31],[32],[34],[35],[39],[41],[44],[45]

2.2.2 Operating Parameters Point of View

Table 2.2: Operating Parameters point of view

Operating Parameters of power systems	Total No. of literatures reviews out of 45 literatures
Voltage stability	[10],[12],[17],[28]
Coordination of FACTS Controllers	[2],[5],[18],[27][29][30][31][33][34],[35],[36],[38],[39],[41][42],[44]]
Low frequency oscillation	[3],[4],[11],[19],[24],[26],[36],[40],[43]
Power system stability	[1],[4],[5],[6],[7],[8],[15],[16],[17],[21],[22],[25],[32],[37]
Other parameters point of view	[9],[13],[14],[20],[23]

Table 2.3: Literature review summary

Authors	**Titles**	**Advantages**	**Limitations**
Al-Hinai, and Al-Hinai	Dynamic stability enhancement using particle swarm optimization power system stabilizer	Uses tuned PSS by employing PSO	For any strong disturbance PSS does not make the system stable, FACTs device must be utilized to get accurate result
Datta, Subir and Roy, A. K	Damping of power system oscillation for SMIB system using STATCOM in combination with power system stabilizer controller	Uses both STATCOM and PSS to damp out LFO	Its controller was conventionally sized and poor, it does not use any techniques to optimally tune controller parameters

Rout, and Panda	Performance of fuzzy logic based adaptive power system stabilizer for SMIB system	Uses AI based supplementary controller	It is not effective for any strong disturbance like three-phase fault
Linda, et al	Novel non-traditional optimization approach for sizing fuzzy based power system stabilizer for SMIB system	Compares AI techniques with optimization techniques	It does not use any controller and FACTs controller. Also it does not consider various operating conditions
Kushwaha, et al	PSO optimized PSS to enhance the dynamic stability of power system	Uses optimized PSS to make the system stable	It does not have supplementary controller and does not use any FACTS device to make system more stable
Arizadayana, Z. et al	SMIB power system installed with UPFC to study power system oscillation	It uses AI based PSS and UPFC	It does not have any supplementary damping controller for a UPFC and does not consider various operating conditions
The Proposed thesis	Damping low frequency oscillation in electric network through optimal sizing of PSS and UPFC employing ALO	It uses both PSS and UPFC with effective POD controller. It uses efficient technic to effectively tune POD parameter	It is costly

2.2.3 Research Gaps and limitations

The weakness of the above literatures are summarized as follows:

- Dynamic stability of power system is improved by using poorly tuned power system stabilizer and conventional unified power flow controller.
- The performance index of the response to attain steady state system takes large settling time and maximum overshoot to converge.

- The techniques utilized in the above papers could not be coordinated and stability is not improved effectively within short time.

Ref [36] had presented dynamic power system but it does not consider different operating conditions to test the robustness of the controller utilized. Also the analysis done is for only rotor speed deviation and angle deviation it does not compare other power system states to test its effectiveness. Furthermore it does not coordinate the PSS and UPFC together and hence the system is not effective for any strong disturbance like three phase fault near generator terminal. Ref [41] presented stability enhancement of PSS-UPFC installed power system, in this case the statistical performance measures for training and testing dataset are used to test the robustness of the system but it did not consider various operating condition in time domain simulation analysis. Ref [43] presented coordinated design of PSS and UPFC controller but it does not use any supplementary damping controller for the UPFC. Also Power system stabilizer parameters was estimated to treasure the optimum values of two key PSS parameters (K &T1) by keeping constant values to other three parameters (T2, T3, &T4) but the result may not accurate since three out of five parameters are setting to be constant to optimize K &T1. Ref [45] presented optimal multi objective design of robust PSS using GA, in this paper a conventional lead-lag PSS is developed to damp out LFO in multi machine system. However, the objective function is the same due to the behavior of employed algorithm and effectiveness of the developed PSS, it is not effective for any strong disturbance near generator terminal.

This thesis fills the gaps of past researchers by using excitation system control, power system stabilizer, unified power flow controller, and Antlion optimization techniques to improve low frequency oscillations of a power system. Comparisons of the controller are held based on performance index and proper installation of the devices system.

2.2.4 Improvements and Contribution of the proposed work

The main contribution of the proposed method is that the controllers are properly sized and coordinated optimally by ALO to damp out low frequency oscillation. The power oscillation damping controller have low controller gain, time constants and small settling time to attain steady state stability. Also the controller is optimally sized and installed with its proper place. For the objective functions presented in ref [36] only UPFC parameters are optimally tuned without any damping controller and the damping torque is low due to absence of damping controller. The power system stabilizer is also conventional. In ref [41], ref [43] and ref [45]

the parameters of the controller are sized with training and testing data sheet by setting (K and T1) manually and finding the remaining parameters and the parameters may not be brand optimal because some values are kept constant to estimate other parameters. The proposed technique utilizes different mathematical models to estimate the key parameters of the UPFC and PSS based on different techniques.

The evolved mathematical models were employed to estimate the respective values of the key parameters in real time depending on the operating conditions of the power system network. The superiority of the proposed ALO based UPFC-PSS system over the one described in ref [41], ref [43] and ref [45] was confirmed through presented minimum damping ratio and eigenvalue analyses along with the time domain representations of the power system states with properly sized damping controller. In the proposed system the power oscillation damping controller parameters are optimally sized by ALO to produce electrical torque in phase with speed deviation by phase compensation technique which meets the proposed objective function. Therefore ALO based optimal sizing of PSS and UPFC makes this thesis superior over the other papers due to the proper sizing and installation of power system oscillation damping controller on the UPFC.

2.3 Theoretical Background

2.3.1 Classification of Power System Stability

The basic considerations of classifying power system stability are based on the magnitude of disturbance considered which influences the techniques of calculation and estimation of stability; processes and the time span that must be taken to be considered for assessing stability [15].

i. Rotor angle stability: the ability of synchronous machine of an interconnected system to remain in synchronism after subjected to disturbance.

ii. Voltage stability: It is the ability of power system to keep normal operating voltages for all buses in the system after subjected to disturbance from the given initial operating condition.

iii. Frequency stability: It refers to the ability of power system to keep nominal frequency following a series system upset resulting in a significant imbalance between generation and demand. It maintains the equilibrium between generation and load with minimum loss. Instability results in the form of continued frequency swing leading to tripping of generating

units or loads. Power system stability can be classified in to three categories. Figure 2.1 [15] below presents the classification of power system stability with different categories.

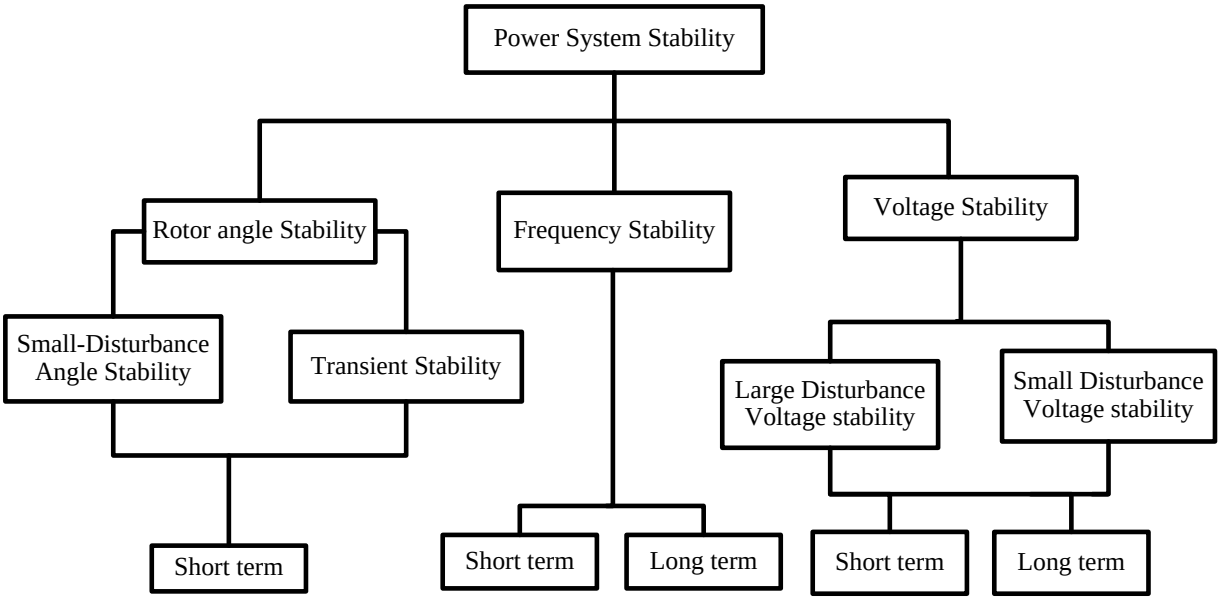

Figure 2.1: Classification of Power system Stability

1. **Steady state stability:** It is the study of power system, generators steady state condition and answering the question what is the maximum possible generator load that can be transmitted without loss of synchronism any one of generator. The maximum power transmitted during this state is said to be steady state stability limit.

2. Transient stability: It is the ability of power system to keep synchronism when a given system is subjected to a sudden and large disturbance with a small time such as loss of generation or load and a fault on transmission line is said to be transient stability. A large signal disturbance involves the system response of power flows, large excursions of synchronous generators rotor angle and bus voltages. Transient stability is a rapid phenomenon usually occurring within one second for a generator close to cause disturbance like three phases to ground fault, line to line fault and double line to ground fault [15].

3. Dynamic Stability: Dynamically stable system is a system that the oscillation does not obtain more than certain magnitude and this amplitude will die out quickly. In a power system a dynamic stability concept is used in the study of transient state conditions. The power balance of generating unit is always disturbed and there by mechanical oscillations of synchronous generator rotor follow the disturbance in addition to the electrical transient phenomena produced.

Table 2.4: Comparison between FACTS device for LFO damping

No.	Facts device	Power system stability enhancement	Load flow control	Voltage control	Transient stability	Damping of LFO
1	UPFC	YES	HIGH	HIGH	MEDIUM	HIGH
2	TCSC	YES	MEDIUM	LOW	HIGH	MEDIUM
3	SVC	YES	LOW	HIGH	LOW	MEDIUM
4	SSSC	YES	LOW	HIGH	MEDIUM	MEDIUM
5	HVDC	YES	MEDIUM	HIGH	MEDIUM	MEDIUM

2.4 Benefits of Utilizing UPFC

The main reasons why UPFC are recommended for damping of low frequency oscillation in electrical network can be determined as follows:

- UPFC increases transfer capability of lines and prevent blackouts.
- Boosting generation productivity, reduce circulating reactive power, improvement of system stability limit.
- Damping out of any range of LFO, guaranteeing system stability, security, reliability and system economic operation.
- It gives additional flexibility and perform both function of STATCOM and SSSC.
- It provides simultaneous or individual controls of transmission system parameters such as voltage, impedance and phase angle [16].

2.5 Classification of Power System Oscillations

Electromechanical oscillation of electrical generators in power system is considered as one of the disturbance of the power system network. These oscillations can be effectively damped to keep power system stability and the oscillation is named as power swings. Electromechanical oscillations are grouped in four categories [17].

a) Local oscillations: - This type of oscillation occurs between a single generator and rest of generating station as well as between the generating station and rest of power system. Under this oscillation frequency ranges from 0.2Hz to 2.5Hz.

b) Interplant oscillations: - It occurs between two electrically close generating plants and the range frequency can vary from 1Hz to 2Hz.

c) Inter area oscillations: - It occurs between two major groups of generating plants. Frequencies are typically in the range of 0.2Hz to 0.8Hz and generally called low frequency oscillation.

d) Global oscillations: - It is characterized by a common in phase oscillations of all generators on an isolated system and the frequency ranges are below 0.2Hz.

2.6 Low Frequency Oscillations

Using high gain exciters and poorly tuned generator excitation may create LFOs with negative damping; this is a small signal stability problem [18]. LFOs include local plant modes; control modes and torsional modes induced by the interaction between the mechanical and electrical modes of a turbine-generator system, and inter area modes, which may be caused by either high gain exciters or heavy power transfers across weak tie lines. LFO can be created by small disturbances, such as changes in the load and are normally analyzed through the small signal stability of the power system. These small disturbances lead to a steady increase or decrease in generator rotor angle caused by the lack of synchronizing torque, or to rotor oscillations of increasing amplitude due to a lack of sufficient damping torque. The most typical instability is the lack of a sufficient damping torque on the rotor's low frequency oscillations. There are several blackouts occurred in the past years caused by low frequency oscillations which are shown in table 2.5 [19] below:

Table 2.5: Different blackouts occurred due to low frequency oscillations.

Country	UK	Taiwan	Canada	China	US	Italian
Oscillating Frequency (Hz)	0.5	0.78-1.05	0.224	0.4	0.17	0.55

Low frequency oscillation phenomena can be harmful:

- It can narrow system security margin.
- It can make the original large power system slowly change in to system separation status.
- It has negative impacts on load side like long duration frequency instability which may reduce the yield rate of industries.
- It reduces power transmission capability of the existing interconnection lines.

Chapter Three

Methodology and Dynamic Modeling of Power System

3.1 Introduction

The flow chart of general methodology to accomplish this thesis work is represented as follows:

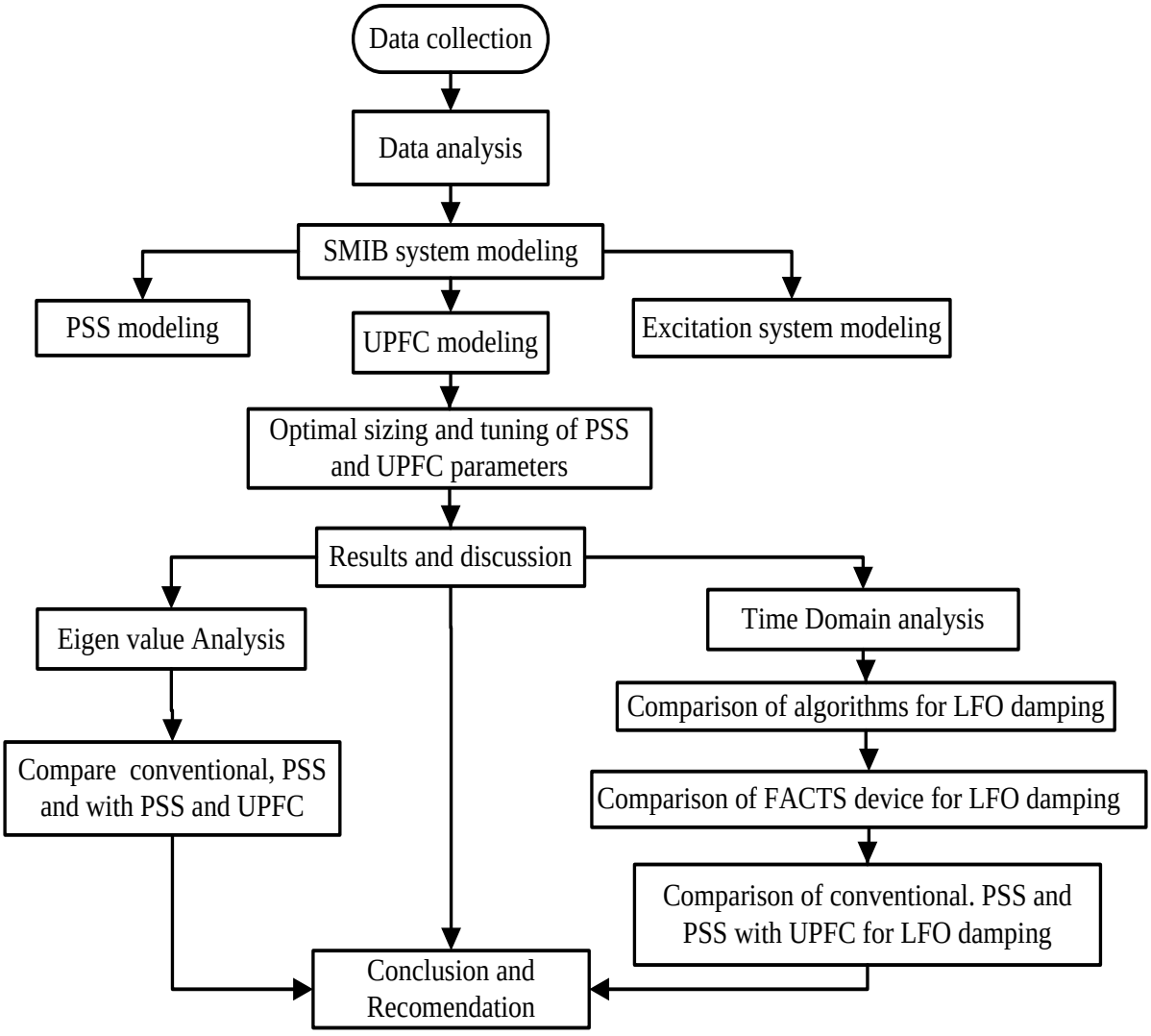

Figure 3.1: Basic flow chart of thesis methodology

3.1.1 Data Collection

The necessary data for this thesis is collected from different sources by asking question and receiving recorded data from Tana Beles and Bahirdar substation. The required data's are transmission line impedance, transformer impedance, and synchronous generator rated power factor, frequency, transient reactance, nominal power and voltage.

Table 3.1: Tana Beles hydropower plant data

Generator parameters of the system	$Voltage\ (kv) = 15kv$ M=8MJ/MVA $S = 133MVA, Inertia\ H(s) = 3.14$ $T'_{d0} = 9.2s, T''_{d0} = T''_{q0} = 0.1s$ $X_d = 1.03, X_q = 0.7, X'_d = 0.31$ $X''_d = X'' = X''_q = 0.25\ X_L = 0.2$ D=4
Exciter type EXST1 data	$T_R = 0.01;\ V_I \min = -0.3;\ V_I max = 0.2$ $T_C = 0;\ T_B = 0;\ K_A = 60$ $T_A = 0.002s;\ VR\ max = 5;\ VR\ min = -5$ $K_C = 0;\ K_F = 0.03;\ T_F(>0) = 1$ $E_{fd}max = 7.3\ pu, E_{fd}min = -7.3\ pu$ $K_e = 1, T_e = 0, K_f = 0.00008;\ T_f = 0.1$
Control parameters for generators with governor type UYGOV	$\mathrm{K_a} = 3.33; \mathrm{T_a} = 0.07, \text{beta} = 0, \mathrm{T_w} = 2,$ R, permanent droop $= 0.04$ r, temporary droop $= 0.5$ $\mathrm{T_r}(>$ $0)$, governor time constant $= 6, \mathrm{T_f}(>$ $0)$, filter time constant $= 0.05, \mathrm{T_g}(>$ $0)$Servo time constant $= 0.5$ At, Turbine gain $=$ 1.2, Dturb, tubine damping $= 0.3$
Transformer	$X_T = 0.1pu; X_{tE} = 0.1pu; X_{BV} = 0.1pu$
Transmission line	$X_L = 1pu$
Operating condition	$P = 0.8pu; V_t = 1\ pu;\ V_b = 1pu$
DC link parameter	$V_{DC} = 2pu; C_{DC} = 1pu$
UPFC parameter	$X_E = X_B = 0.1;\ m_B = 0.08;\ \delta_B = -78.21;\ \delta_E = 85.35;$ $m_E = 0.4; K_{s1} - K_{s4} = 1; T_{s1} - T_{s4} = 0.05$ $\mathrm{K_{dcp}} = -5, \mathrm{K_{dcI}} = 0, \mathrm{K_{dp}} = -5, \mathrm{K_{dI}} = -60$ $K_{I-Vdc} = 20, K_{P-Vdc} = 10, K_{I-VEt} = 40, K_{P-VEt} = 2, K_{I-QEt} = 3, K_{I-QEt} = 0.4$

Table 3.1 above shows the parameters of Tana Beles generator, transformer and transmission line system but detail data were presented in appendix C and appendix D.

3.2 Single Machine Infinite Bus Model

The mathematical model for small signal analysis of synchronous machine, excitation system, power system stabilizer and UPFC are briefly discussed. This thesis also includes mathematical analysis and modeling of synchronous generator, modeling of transmission line, modeling of PSS and modeling of UPFC. Antlion optimizer, POD controller, PSS and UPFC techniques are developed to improve low frequency oscillation for SMIB system. The ability of power system to maintain stability depends to a large extent on the controllers

available on the developed system to damp low frequency oscillations. Figure 3.2 presents the overall diagrams of single machine infinite bus power system network of the whole system [20].

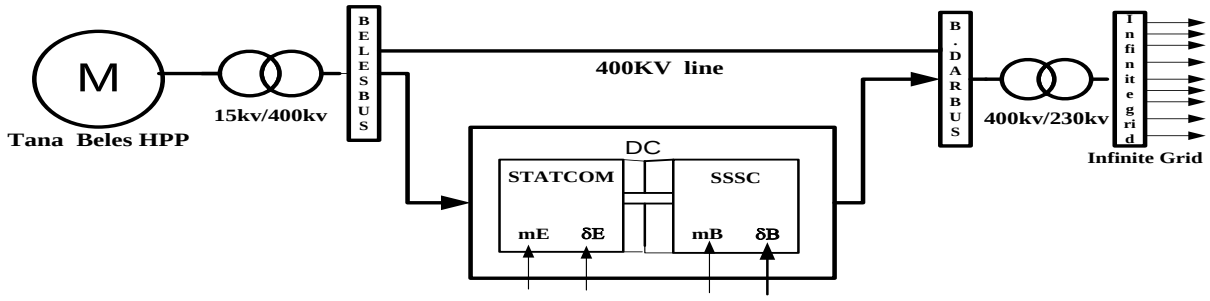

Figure 3.2: Single line diagram of the overall power network equipped with UPFC

3.2.1 Mathematical Modeling of Synchronous Generator

The general system configuration of single synchronous generator represented by the classical model with all resistance included is represented in figure 3.3 [21] below. Here E' is the voltage behind X'_d and its magnitude is assumed to remain constant at the pre-disturbance value.

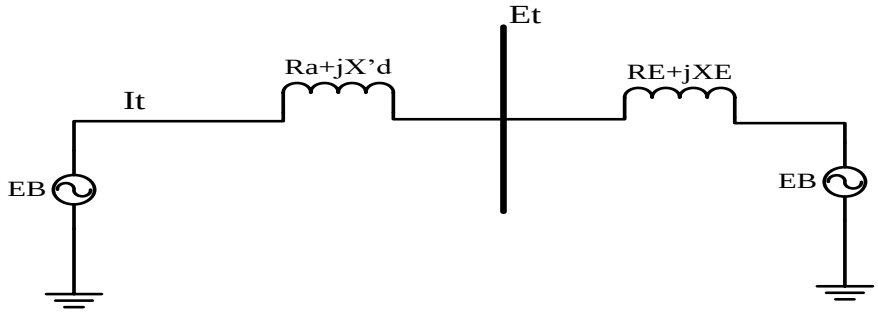

Figure 3.3: Mathematical model representation of generator

The terminal current flowing through the classical model representation of the generator is determined between terminal voltage and infinite bus voltage.

$$\tilde{I_t} = \frac{\widetilde{E_t} - \widetilde{E_B}}{R_E + jX_E} \tag{3.1}$$

$$\widetilde{E}' = \widetilde{E_t} + (R_a + jX'_d)\widetilde{I_t} \tag{3.2}$$

The complex power behind the transient reactance is given by the equation (3.3) as shown below.

$$S' = P + jQ' = \widetilde{E}'\widetilde{I_t}^{*} \tag{3.3}$$

$$S' = \frac{E'E_B}{X_T}\sin\delta + j\frac{E'(E' - E_B\cos\delta)}{X_T} \tag{3.4}$$

In per unit, the air-gap torque is equal to the air-gap power. With stator resistance included, the air-gap power is equal to the terminal power.

$$T_e = p = \frac{E'E_B}{X_T}\sin\delta \tag{3.5}$$

In order to linearize the equation (3.5) the initial operating condition is assumed and the partial derivative of the equation with respect to the rotor angle of the system equation gives the new representation of the equation (3.6) as expressed. Linearizing about an initial loading conditions given by $\delta = \delta 0$ yields

$$\Delta T_e = \frac{\partial T_e}{\partial \delta}\Delta\delta = \frac{E'E_B}{X_T}\cos\delta_0(\Delta\delta) \tag{3.6}$$

The equations of motion in per unit are represented in equation (3.7) and (3.8) below.

$$p\Delta\omega_r = \frac{1}{2H}(T_m - T_e - K_D\Delta\omega_r) \tag{3.7}$$

$$p\delta = \omega_0\Delta\omega_r \tag{3.8}$$

Linearizing equation and substituting for equations (3.7) and (3.8) in above equation (3.6) the new equation is obtained as follows:

$$p\Delta\omega_r = \frac{1}{2H}(\Delta T_m - K_s\Delta\delta - K_D\Delta\omega_r) \tag{3.9}$$

$$K_s = (\frac{E'E_B}{X_T})\cos\delta_0 \tag{3.10}$$

Writing the above equation in vector-matrix form equation (3.11) and (3.12) are obtained as follows:

$$p\Delta\delta = \omega_0\Delta\omega_r \tag{3.11}$$

$$\frac{d}{dt}\begin{bmatrix}\Delta\omega_r \\ \Delta\delta\end{bmatrix} = \begin{bmatrix}\frac{-K_D}{2H} & -\frac{K_s}{2H} \\ \omega_0 & 0\end{bmatrix}\begin{bmatrix}\Delta\omega_r \\ \Delta\delta\end{bmatrix} + \begin{bmatrix}\frac{1}{2H} \\ 0\end{bmatrix}\Delta T_m \tag{3.12}$$

This is the form $\dot{x} = Ax + bu$

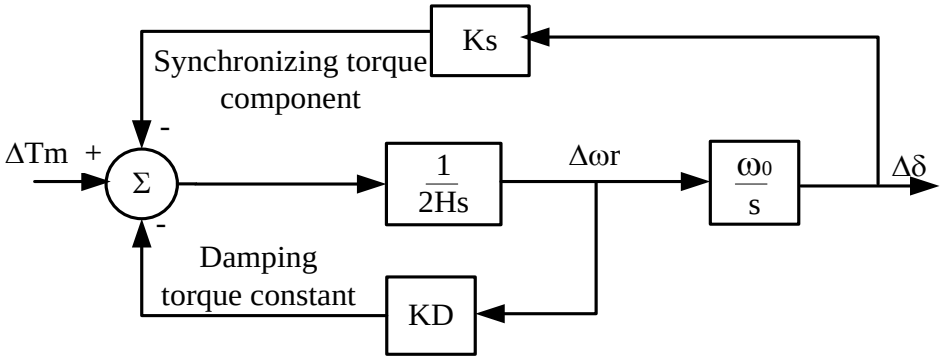

Figure 3.4: Block diagram of SMIB system with generator model

The elements of the state matrix A are seen to be dependent on the system parameters KD, H, XT, and the initial operating condition represented by the values of E' and δ_0. The block diagram representation shown in figure 3.4 [21] above describes SMIB system for small-signal performance. From the block diagram this change of rotor angle to initial operating condition of rotor speed and the rest parameters are represented as shown in equation (3.13) below.

$$\Delta\delta = \frac{\omega_0}{S}\left[\frac{1}{2HS}(-K_s\Delta\delta - K_D\Delta\omega_r + \Delta T_m)\right]$$

$$\Delta\delta = \frac{\omega_0}{S}\left[\frac{1}{2HS}\left(-K_s\Delta\delta - \frac{K_D S\Delta\delta}{\omega_0} + \Delta T_m\right)\right] \quad (3.13)$$

By rearranging equation (3.13) the new equation can be obtained as follow;

$$S^2(\Delta\delta) + \frac{K_D}{2H}S(\Delta\delta) + \frac{K_s}{2H}\omega_0(\Delta\delta) = \frac{\omega_0}{2H}\Delta T_m \quad (3.14)$$

Therefore, by simplifying equation (3.14) the characteristic equation is given by:

$$S^2 + \frac{K_D}{2H}S + \frac{K_s}{2H}\omega_0 = 0 \quad (3.15)$$

This is the general form of the formula with s-operator

$$S^2 + 2\zeta\omega_n S + {\omega_n}^2 = 0 \quad (3.16)$$

The simplified mathematical analysis of un damped natural frequency can be represented as:

$$\omega_n = \sqrt{K_s\frac{\omega_0}{2H}}\ \text{rad/s} \quad (3.17)$$

The damping ratio is obtained as:

$$\zeta = \frac{1}{2}\frac{K_D}{2H\omega_n} = \frac{1}{2}\frac{K_D}{\sqrt{K_s 2H\omega_0}} \quad (3.18)$$

When synchronizing torque coefficient increases then the natural frequency increases but damping ratio can decreases. An increase in damping torque coefficient increases the damping ratio. From the equation (3.16) above eigenvalues can be obtained as follow:

$$\lambda_1, \lambda_2 = -\zeta\omega_n \pm j\omega_n\sqrt{1-\zeta^2} \quad (3.19)$$

The damped frequency is:

$$\omega_d = \omega_n\sqrt{1-\zeta^2} \quad (3.20)$$

Where, Ks is synchronizing torque coefficient in pu torque/rad, KD= is damping torque coefficient in pu torque/pu, H= inertia constant in MW.s/MVA, $\Delta\omega_r$, is the speed deviation in pu=$(\omega_r - \omega_0)/\omega_0$, $\Delta\delta$ is rotor angle deviation in rad, S is Laplace operator and ω_0 is the rated speed in rad/s=$2\pi f_0$, $f_0 = 50Hz$. Eigenvectors are determined from the simultaneous

equation of the system in which the two equations are linearly dependent and the equation can be:

$$\begin{bmatrix} \frac{-K_D}{2H} - \lambda_i & -\frac{K_S}{2H} \\ \omega_0 & 0 - \lambda_i \end{bmatrix} \begin{bmatrix} \emptyset_{1i} \\ \emptyset_{2i} \end{bmatrix} = 0 \tag{3.21}$$

The time response of SMIB system variables speed deviation and rotor angle deviation is represented in matrix form as follows:

$$\begin{bmatrix} \Delta\omega_r(t) \\ \Delta\delta(t) \end{bmatrix} = \begin{bmatrix} \emptyset_{11} & \emptyset_{12} \\ \emptyset_{21} & \emptyset_{22} \end{bmatrix} \begin{bmatrix} c_1 e^{\lambda_1 t} \\ c_2 e^{\lambda_2 t} \end{bmatrix} \tag{3.22}$$

The constant coefficients of exponential function, c_1 and c_2 are obtained from equation (3.23)

$$\begin{bmatrix} c_1 \\ c_2 \end{bmatrix} = \begin{bmatrix} \psi_{11} & \psi_{12} \\ \psi_{21} & \psi_{22} \end{bmatrix} \begin{bmatrix} \Delta\omega_r(0) \\ \Delta\delta(0) \end{bmatrix} \tag{3.23}$$

3.2.2 Mathematical Model of Synchronous Machine Field winding

The rotor windings have axes 120 electrical degrees apart and assumed to have an equivalent sinusoidal distribution, the following windings are depicted which is the three stator windings denote a, b, and c, field winding denoted F. This winding carries the field current which gives rise to the field flux. This rotating flux induces the voltages in the stator windings. Short circuited damper winding in the d-axis denoted by D. Short circuited damper winding in the q-axis denoted by Q.

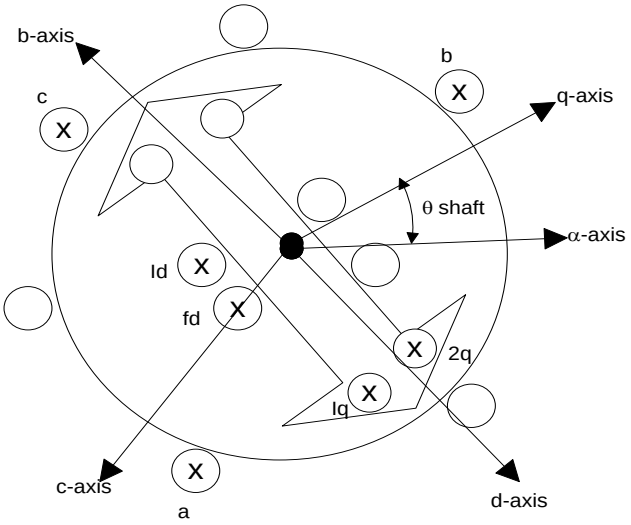

Figure 3.5: Windings in the synchronous generator and their axes.

The basic voltage Equations which descript the machine in a-b-c reference system are:

3.2.3 Stator and rotor Equations of synchronous machine

$$v_{ai} = i_{ai} r_{ai} + \frac{d}{dt}\psi_{ai} \qquad i = 1, \ldots\ldots n \tag{3.24}$$

$$v_{bi} = i_{bi}r_{bi} + \frac{d}{dt}\psi_{bi} \qquad i = 1, \ldots\ldots\ldots..n \tag{3.25}$$

$$v_{ci} = i_{ci}r_{ci} + \frac{d}{dt}\psi_{ci} \qquad i = 1, \ldots\ldots\ldots\ldots.n \tag{3.26}$$

$$v_{fdi} = i_{fdi}r_{fdi} + \frac{d}{dt}\psi_{fdi} \qquad i = 1, \ldots\ldots\ldots\ldots n \tag{3.27}$$

Where, ψ is the flux linkage, v, I and r is winding voltage, current and resistance in the a-b-c reference system respectively.

3.2.4 Park's transformation

It is convenient to transform all synchronous machine stator and network variable into a reference frame that converts three-phase sinusoidal variations into constant. Such a transformation is:

$$v_{dqo} \triangleq T_{dqo}v_{abc}, i_{dqo} \triangleq T_{dqo}i_{abc}, \psi_{dqo} \triangleq T_{dqo}\psi_{abc} \tag{3.28}$$

Where, $v_{abc} \triangleq [v_a \;\; v_b \;\; v_c]^t, i_{abc} \triangleq [i_a \;\; i_b \;\; i_c]^t, \psi_{abc} \triangleq [\psi_a \;\; \psi_b \;\; \psi_c]^t$

$v_{dqo} \triangleq \left[v_d \;\; v_q \;\; v_o\right]^t, i_{dqo} \triangleq \left[i_d \;\; i_q \;\; i_o\right]^t, \psi_{dqo} \triangleq [\psi_d \;\; \psi_q \;\; \psi_o]^t$

$$T_{dqo} = \frac{2}{3}\begin{bmatrix} cos\omega_s t & \cos(\omega_s t - \frac{2\pi}{3}) & \cos(\omega_s t + \frac{2\pi}{3}) \\ -sin\omega_s t & -\sin(\omega_s t - \frac{2\pi}{3}) & -\sin(\omega_s t + \frac{2\pi}{3}) \\ \frac{1}{2} & \frac{1}{2} & \frac{1}{2} \end{bmatrix} \tag{3.29}$$

$$T_{dqo}^{-1} = \frac{2}{3}\begin{bmatrix} cos\omega_s t & -\sin(\omega_s t) & 1 \\ \cos(\omega_s t - \frac{2\pi}{3}) & -\sin(\omega_s t - \frac{2\pi}{3}) & 1 \\ \cos(\omega_s t + \frac{2\pi}{3}) & -\sin(\omega_s t + \frac{2\pi}{3}) & 1 \end{bmatrix} \tag{3.30}$$

Applying kirchhoff and Faradays law are

$v_{abc} = r_s i_{abc} + \frac{d}{dt}\psi_{abc}$ and $v_{dqo} = r_s i_{dqo} + T_{dqo}\frac{d}{dt}T_{dqo}^{-1}\psi_{dqo}$

$$\begin{bmatrix} V_{Di} \\ V_{Qi} \\ V_{Oi} \end{bmatrix} = T_{dqo}\, T_{dqo}^{-1} \begin{bmatrix} V_{di} \\ V_{qi} \\ V_{Oi} \end{bmatrix} = \frac{1}{\sqrt{2}} T_{dqo} \begin{bmatrix} V_{ai} \\ V_{bi} \\ V_{ci} \end{bmatrix} \qquad i = 1, \ldots\ldots\ldots n \tag{3.31}$$

$$\begin{bmatrix} I_{Di} \\ I_{Qi} \\ I_{Oi} \end{bmatrix} = T_{dqo}\, T_{dqo}^{-1} \begin{bmatrix} I_{di} \\ I_{qi} \\ I_{Oi} \end{bmatrix} = \frac{1}{\sqrt{2}} T_{dqo} \begin{bmatrix} I_{ai} \\ I_{bi} \\ I_{ci} \end{bmatrix} \qquad i = 1, \ldots\ldots\ldots n \tag{3.32}$$

$$\begin{bmatrix} \psi_{Di} \\ \psi_{Qi} \\ \psi_{Oi} \end{bmatrix} = T_{dqo}\, T_{dqo}^{-1} \begin{bmatrix} \psi_{di} \\ \psi_{qi} \\ \psi_{Oi} \end{bmatrix} = \frac{1}{\sqrt{2}} T_{dqo} \begin{bmatrix} \psi_{ai} \\ \psi_{bi} \\ \psi_{ci} \end{bmatrix} \qquad i = 1, \ldots\ldots\ldots n \tag{3.33}$$

Where, T_{dqo} the machine transformation. After the system in dqo coordinates has the forms

3.2.5 Stator and rotor equations

$$\frac{\mathrm{d}}{\mathrm{dt}}\psi_{\mathrm{Di}} = \mathrm{i_{Di}r_{si}} + \omega_{\mathrm{i}}\psi_{\mathrm{Qi}} + \mathrm{V_{Di}} \quad i = 1, \ldots\ldots\ldots..n \tag{3.34}$$

$$\frac{d}{dt}\psi_{Qi} = i_{Qi}r_{si} - \omega_i\psi_{Di} + V_{Qi} \quad i = 1, \ldots..n \tag{3.35}$$

$$\frac{d}{dt}\psi_{Oi} = i_{Oi}r_{si} + V_{Oi} \qquad i = 1, \ldots\ldots\ldots..n \tag{3.36}$$

Where, V_{Di}, V_{Qi}, V_{Oi}, i_{Di}, i_{Qi}, i_{Oi}, ψ_{Di}, ψ_{Qi}, and ψ_{Oi} are the stator voltage, current, and flux linkage in the dqo reference system, rsi is the stator resistance, where ω_i is the rotor speed.

$$v_{fdi} = i_{fdi}r_{fdi} + \frac{d}{dt}\psi_{fdi} \qquad i = 1, \ldots\ldots\ldots\ldots..n \tag{3.37}$$

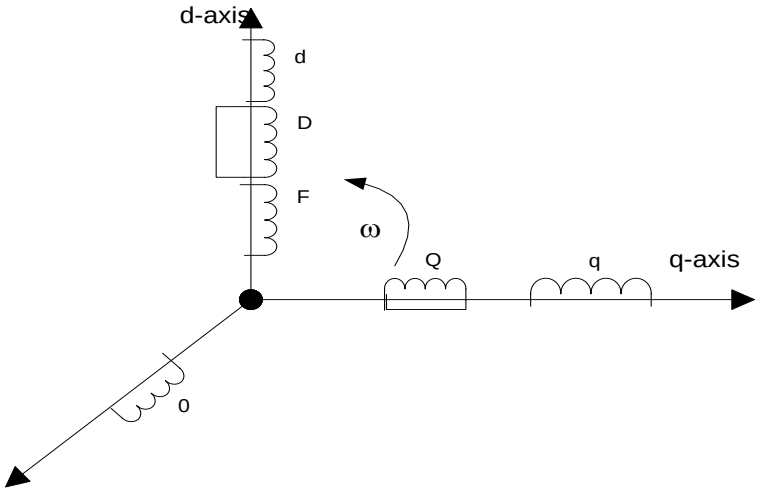

Figure 3.6: model of synchronous machine in dqo axis

Where, $v_{fdi}, i_{fdi}, r_{fdi}\ and\ \psi_{fdi}$ implies the field voltage, current, resistance and flux component in the dqo reference system respectively.

3.2.6 Motion Equation

$$\frac{d\delta}{dt} = \frac{d\theta_i}{dt} - \omega_s \quad i = 1, \ldots\ldots\ldots., n \tag{3.38}$$

$$\dot{\delta} = \omega_i - \omega_s \qquad i = 1, \ldots\ldots., n \tag{3.39}$$

$$\frac{2H_i}{\omega_s}\frac{d^2\delta}{dt^2} = \frac{2H_i}{\omega_s}\left(\frac{d\omega_i}{dt}\right) = \left(T_{mi} - T_{ei} - T_{fwi}\right) \quad i = 1, \ldots\ldots..n \tag{3.40}$$

$\dot{\omega}_\iota = \frac{\omega_s}{2H_i}\left(T_{mi} - T_{ei} - T_{fwi}\right) \quad i - 1, \ldots\ldots..n$ Where, H= the inertia time constant in seconds, T_{mi}=mechanical torque, T_{ei}= electrical torque, T_{fwi}=damping torque coefficient given in pu, δ=angular position of the rotor, ω_s=synchronous speed and ω_i= rotor speed.

3.3 Excitation System Model

Excitation system gives DC current to synchronous machine field winding. In addition, the excitation system carry out both control and protective functions needed to the satisfactory performance of power system by controlling field voltage and there by the filed current. The control function includes reactive power flow and control of voltage, and enhancement of

system dynamic stability. The protective function ensures the capability limit of synchronous machine excitation system, and other equipment are not exceeded [22].

3.3.1 Elements of Excitation System Model

1) Exciter: supplies DC power to synchronous machine field winding.

2) Regulator: Processes and amplifies input control signal to a level and form appropriate control of the exciter which includes both regulating and excitation system stabilizing function.

3) Terminal voltage transducer and load compensator: senses generator terminal voltage, rectifier and filters to DC quantity and compares with its reference.

4) Power system stabilizer: gives additional input stabilizing signal to the excitation system to damp out LFO.

5) Limiters and protective circuits: Provides both control and protective function which ensures capability limit of exciter and synchronous generator are not exceeded. The main block diagram of an excitation control system for a large synchronous generator are shown in figure 3.7 below.

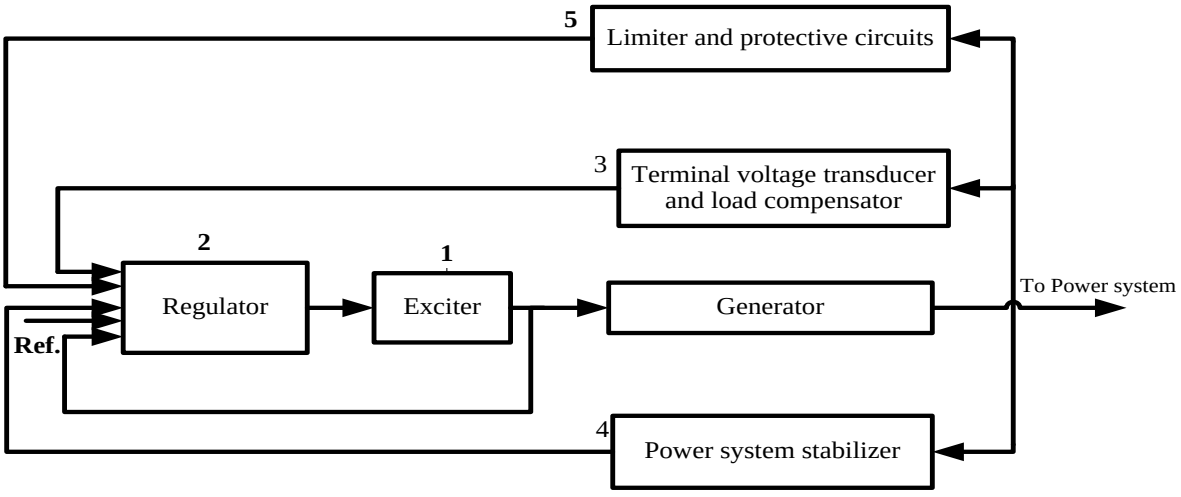

Figure 3.7: Block diagram of synchronous generator excitation control system

3.4 Transmission Line Modeling

Electrical power is transferred from generating stations to consumers through overhead lines and cables. Overhead lines are used for long distance in open country and rural areas, where as cables are used for underground transmission in urban areas and for underwater crossings. To transfer electric power transmission lines are modeled as nominal π circuit as shown in figure 3.8 [23].

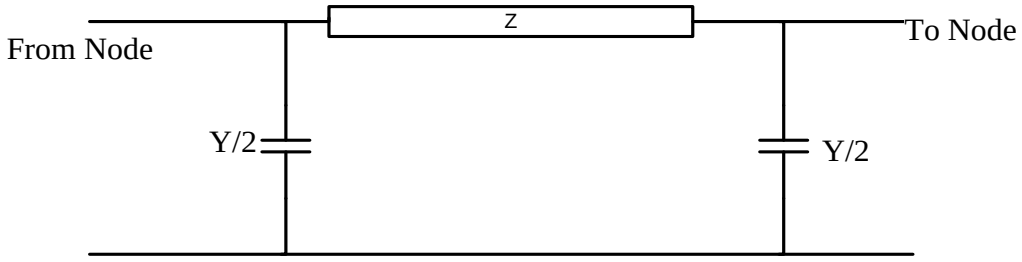

Figure 3.8: Transmission Lines as a nominal π circuit

Where, Z is the series impedance of the line, $\frac{y}{2}$ is half of total line charging y at each node,

A transmission line can be represented by series RLC circuit shown in figure 3.9. The differential equations for the circuit elements, after applying Park's transformation, can be expressed in the d-q reference frame by the following matrix expressions.

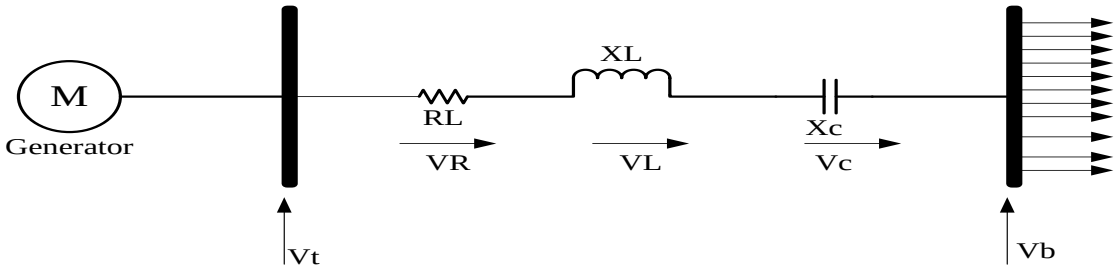

Figure 3.9: A series RLC transmission line

The voltage across the resistance

$$\begin{bmatrix} V_{Rd} \\ V_{Rq} \end{bmatrix} = \begin{bmatrix} R_L & 0 \\ 0 & R_L \end{bmatrix} \begin{bmatrix} i_d \\ i_q \end{bmatrix} \tag{3.41}$$

The voltage across the inductance

$$\begin{bmatrix} V_{Ld} \\ V_{Lq} \end{bmatrix} = \begin{bmatrix} 0 & -\frac{\omega}{\omega_0} X_L \\ \frac{\omega}{\omega_0} X_L & 0 \end{bmatrix} \begin{bmatrix} i_d \\ i_q \end{bmatrix} + \begin{bmatrix} \frac{X_L}{\omega_0} & 0 \\ 0 & \frac{X_L}{\omega_0} \end{bmatrix} \begin{bmatrix} \frac{di_d}{dt} \\ \frac{di_q}{dt} \end{bmatrix} \tag{3.42}$$

The voltage across the capacitor:

$$\begin{bmatrix} \frac{dV_{cd}}{dt} \\ \frac{dV_{cq}}{dt} \end{bmatrix} = \begin{bmatrix} \omega_0 X_c & 0 \\ 0 & \omega_0 \end{bmatrix} \begin{bmatrix} i_d \\ i_q \end{bmatrix} + \begin{bmatrix} 0 & \omega_0 \\ \omega_0 & 0 \end{bmatrix} \begin{bmatrix} V_{cd} \\ V_{cq} \end{bmatrix} \tag{3.43}$$

The overall equation of the transmission line can be written as

$$\begin{bmatrix} \frac{dV_{cd}}{dt} \\ \frac{dV_{cq}}{dt} \\ V_{td} \\ V_{tq} \end{bmatrix} = [Att] \begin{bmatrix} V_{cd} \\ V_{cq} \end{bmatrix} + [Rt1] \begin{bmatrix} \frac{di_d}{dt} \\ \frac{dt_q}{dt} \end{bmatrix} + [Rt2] \begin{bmatrix} i_d \\ i_q \end{bmatrix} + [Btt][V_b] \tag{3.44}$$

Where, $[Att] = \begin{bmatrix} 0 & \omega \\ -\omega & 0 \\ 1 & 0 \\ 0 & 1 \end{bmatrix}$, $[\mathrm{Rt1}] = \begin{bmatrix} 0 & 0 \\ 0 & 0 \\ \frac{X_L}{\omega_0} & 0 \\ 0 & \frac{X_L}{\omega_0} \end{bmatrix}$, $[\mathrm{Rt2}] = \begin{bmatrix} \omega_0 X_c & 0 \\ 0 & \omega_0 X_C \\ R_L & -\frac{\omega}{\omega_0} X_L \\ \frac{\omega}{\omega_0} X_L & R_L \end{bmatrix}$, $[Btt] = \begin{bmatrix} 0 \\ 0 \\ sin\delta \\ cos\delta \end{bmatrix}$

3.5 Transformer Modeling

Transformers are modeled to step up or step down the given voltage to the required level which enables utilization of different voltage levels across the system. Transformers are with off nominal turns ratio and are modeled as equivalent π circuit as shown in figure 3.10 [23].

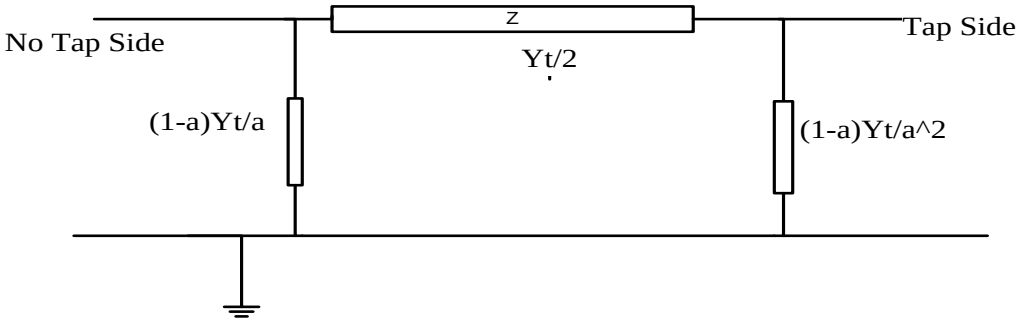

Figure 3.10: Transformer as equivalent π circuit

Where, $\mathrm{y_t} = \frac{1}{z_t}$

z_t: represents the series impedance at nominal turn ratio, α: represents per unit off-nominal tap position. The transmission network represented by algebraic equation:

$\bar{I} = Y_{bus}\bar{V}$

Where, $\bar{I}$: Vector of bus currents, Y_{bus}: Bus admittance matrix and $\bar{V}$: Vector of bus voltages

3.6 Power System Stabilizer

Power system stabilizer is used to enhance damping of LFO through excitation control. PSS provides an additional signal to increase damping torque of the generator excitation system. This control signal can provide positive damping effect, without affecting voltage regulation function of voltage regulator and the ability of maintaining generator terminal voltage level and also known as additional excitation control. To increase capability of preventing power system from low-frequency oscillation, PSS can use generator rotor speed ($\Delta\omega$), system frequency (Δf), accelerating power ($\mathrm{Pm} - \mathrm{Pe}$), electrical power ($\Delta Pe$), and combination of these signals as input signals. In this study the input signal for single input generic PSS model is synchronous machine rotor speed deviation ($\Delta\omega$) while the output signal of PSS is stabilized voltage (V_s). T_w, is the washout time constant and shows the stabilizer gain of PSS. T1-T4 are representing the two stages of lead-lag compensation time constants [24]. System

separation occurs if no adequate damping is available to compensate for the insufficiency of damping torque in synchronous generator unit. This insufficiency of damping is mainly due to AVR exciter's high speed, gain and system's loading. In order to solve the problem, PSS parameters have been successfully tuned to damp out unwanted low frequency oscillations.

3.6.1 Optimal Parameter Sizing of PSS

There are two main types of PSS such as generic PSS and multiband PSS. In this study generic type PSS is used because it is commonly applicable for damping of electrical torque and LFO. The block diagram of generic type PSS is shown in figure 3.11 [25] below which involves a gain block (K_{PSS}), washout time block with time constant Tw, two lead-lag blocks with time constant T1, T2, T3 and T4 [25]. Generic PSS could generate torque on the rotor of electrical machines and hence phase lag between exciter input and machine electrical torque is compensated.

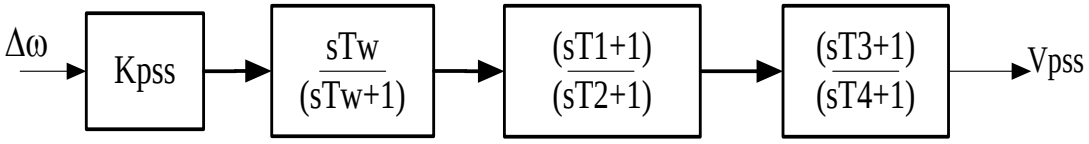

Figure 3.11: General Power system stabilizer lead-lag structure

The value of time constant is taken between 0.01 to 1 seconds. Phase compensation block with time constant T1, T2, T3 and T4 supplies the appropriate phase lead characteristics to compensate phase lag between input and output signals. The five optimal parameters of generic PSS are four time constants T1-T4 and gain K_{PSS} which is optimally selected by ALO algorithm to guarantee optimal system performance under various system configuration and disturbances [25].

3.7 Modeling of Power System Stabilizer

The method of incorporating excitation system models into a LFO damping by considering excitation system model is shown in figure 3.12 below.

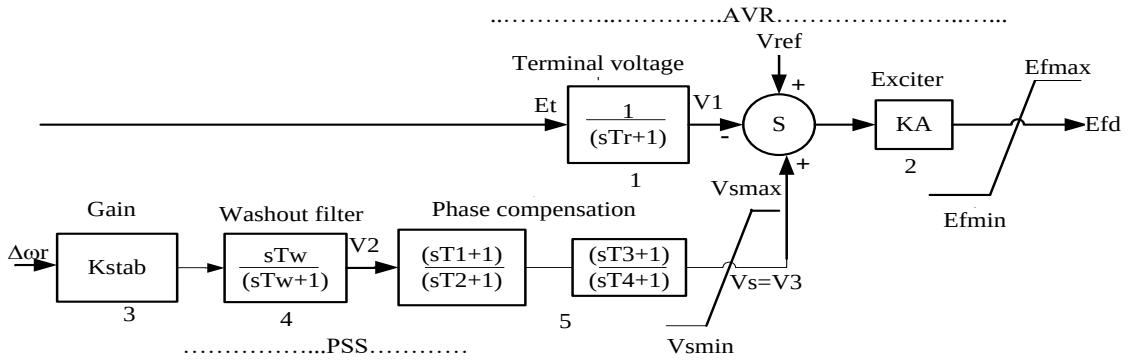

Figure 3.12: Power system stabilizer with AVR block

The AVR regulator model (block 1) shown in figure 3.12 [26] has the parameter Tr that represents the terminal voltage transducer time constant. A high exciter gain (block 2), without transient gain reduction or derivate feedback, is used. The non-linearity associated with the model is due to the ceiling on exciter output voltage represented by ($\mathrm{EF_{max}}$ $\mathrm{EF_{min}}$) and PSS output voltage (V_{Smax} V_{Smin}). The PSS model in figure 3.12 consists of three blocks a phase compensation block, signal washout block and gain block. The phase compensation block (block 5) provides suitable phase lead characteristics to compensate for phase lag between exciter input and generator electrical torque. The signal washout block (block 4) acts as a high pass filter with time constant Tw and allows signals associated with oscillations. Without it, steady changes in speed modifies the terminal voltage. The stabilizer gain K_{STAB} (block 3) determines the amount of damping introduced by PSS. From block 1 of figure 3.12

$$\mathrm{pv_1} = \frac{1}{\mathrm{T_r}}(\mathrm{E_t} - \mathrm{v_1}) \tag{3.45}$$

From blocks 3 and 4

$$\mathrm{pv_2} = \mathrm{K_{STAB}} p\Delta\omega_\mathrm{r} - \frac{1}{\mathrm{T_w}}\mathrm{v_2} \tag{3.46}$$

With, $p\Delta\omega_r$ from block 5

$$\mathrm{pv_3} = \frac{1}{\mathrm{T_2}}(\mathrm{T_1 pv_2} + \mathrm{v_2} - \mathrm{v_3}) \tag{3.47}$$

With pv_2 is given by equation (3.31). The stabilizer output V_s is

$$\mathrm{V_s} = \mathrm{v_3}$$

With $V_Smin \leq V_s \leq V_smax$ from block 2, the exciter output voltage is

$$\mathrm{E_{fd}} = \mathrm{K_A}[\mathrm{V_{ref}} - \mathrm{v_1} + \mathrm{v_s}] \tag{3.48}$$

With $\mathrm{E_{F\,min}} \leq \mathrm{E_{fd}} \leq \mathrm{E_{F\,max}}$

Initial value of excitation system variables

$v_1 = E_t, v_2 = 0, V_s = 0$

The AVR reference is

$$V_{ref} = \frac{E_{fd}}{K_A} + v_1 \quad (3.49)$$

Thus V_{ref} takes a value appropriate to the generator loading condition prior to disturbance. The power system stabilizer is composed of phase compensation block which consists of first order lead lag system with gain and reset block. The signal is provided to the excitation control unit to balance the speed of the rotor based on the rotor speed variation. Hence for PSS, time constant and gain of compensation block acts as control parameters to damp out system oscillations.

3.8 Unified Power Flow Controller (UPFC)

A UPFC is a versatile controller in FACTS concept. It has the ability to tune three control parameters like voltage, reactance and phase angle between two buses either simultaneously or independently. It has two voltage source converters (VSC), series converters and shunt converters that are coupled with a common DC link capacitor which provides bidirectional flow of real power between series connected SSSC and shunt STATCOM respectively. The series controller SSSC is used to add controlled voltage magnitude and phase angle in series with the line whereas the shunt converter STATCOM is used to obtain reactive power to AC system. The UPFC model can be incorporated to power flow equations by including the impedances of the converters transformers into the bus admittance matrix and adding the UPFC injection powers at specific buses. The schematic diagram of UPFC used for SMIB system is shown figure 3.13 below.

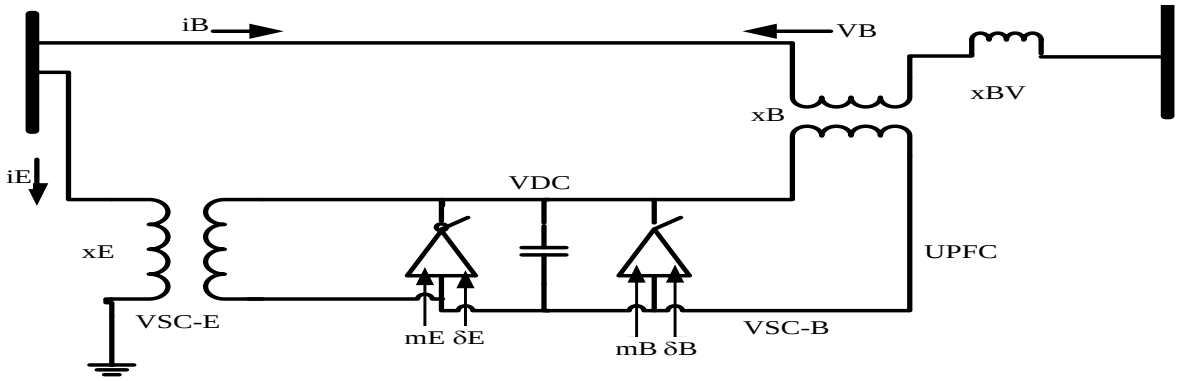

Figure 3.13: Single line diagram of UPFC

Excitation and boosting transformers (ET and BT) are used to connect the UPFC with transmission line. The major components of UPFC are two VSCs which are VSC-B and VSC-E coupled with a common DC link capacitor. The parts of UPFC are a bidirectional AC-to-AC converter. The VSC-B or static synchronous series compensator (SSSC) injects the series voltage with the help of boosting transformer that is connected in series with TL whereas the VSC-E (STATCOM) supplies or absorbs real power to support VSC-B according to the requirement. Due to the series voltage injection at DC link of the UPFC, it could be needed to support the real power exchange. Reactive power generation is another task of VSC-E if it is desired that ensures the shunt reactive compensation independently for the transmission line. The four input control parameters of UPFC are m_E, m_B, δ_E & δ_B where δ_E & δ_B are the phase angles of E_T and B_T, respectively and m_E and m_B are the amplitude modulation ratio of E_T and B_T, respectively.

3.9 Controlling mechanism of UPFC

3.9.1 Shunt Converter Control Mechanism

The shunt converter takes a controlled current from the network. The shunt inverter is operated to absorb or generate reactive power to regulate bus voltage at which UPFC is connected. The shunt converter is used to inject a controllable current, into the transmission line. This current has two component I_p and I_q. The first component of this current is Ip, which is automatically calculated by the requirement to balance the active power gone to the series converter via DC link. The other part of the current in shunt converter is the reactive current, Iq that can be controlled with the same method as STATCOM. The shunt converter controls UPFC bus voltage and the DC link capacitor voltage. UPFC bus voltage is controlled by q-axis shunt inverter voltage. The DC link capacitor voltage is controlled by the d-axis shunt inverter voltage (V_{shd}).

There are two modes of operating control for shunt converter (STATCOM) which are [27]:-

i. Reactive Power (VAR) Control Mode: - In this case capacitive or inductive VAr request is taken as a reference input. Shunt converter control translates VAr reference into equivalent shunt request and tunes gating of converter to establish the desired current. In this mode a feedback signal representing dc bus voltage, V_{dc} is also required [27,28].

ii. Automatic Voltage Control Mode: - In this mode, the shunt converter is regulated to keep transmission line voltage to a reference value. So, voltage feedback signals are obtained from the sending end bus feeding the shunt-coupling transformer [27, 28].

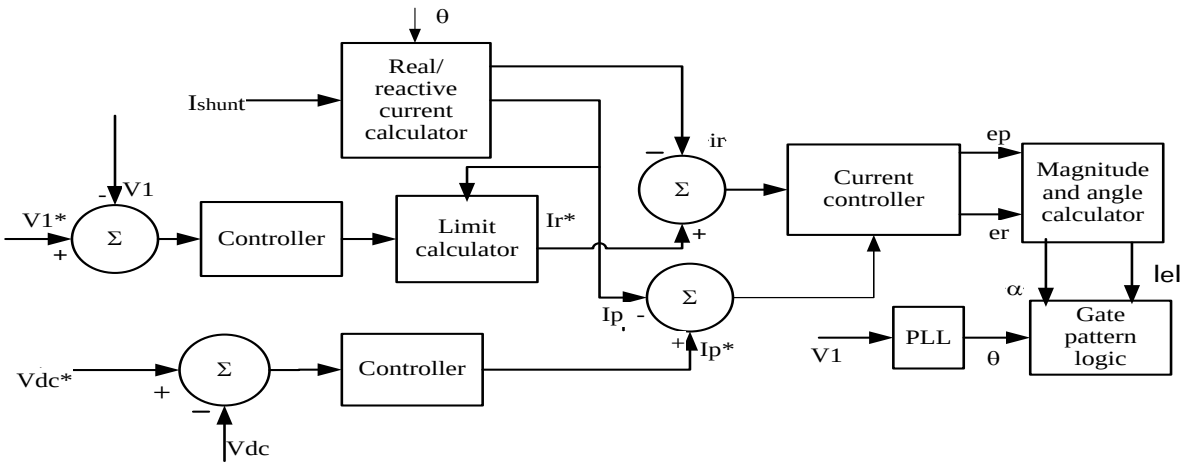

Figure 3.14: Block diagram of shunt converter

3.9.2 Series Converter Control Mechanism

The series converter controls the magnitude and angle of series injected voltage, V_{se} in series with the transmission line [27], [28],[29]. This voltage injection is directly or indirectly intended to influence the flow of power on the line. However, V_{se} depends on the operating mode chosen for UPFC to control power flow. The series inverter injected voltage is split into two components, one in-phase (V_d) and the other in quadrature (V_q) with UPFC bus voltage. The series converter controls real power flow in the transmission line by injecting a voltage in quadrature (V_q) with the UPFC bus voltage. The in-phase component (V_d) of the series injected voltage controls the transmission line side bus voltage (V_{line}). By regulating the transmission line side bus voltage reference ($V_{linere f}$), transmission line reactive power flow ($Q_{linere f}$) can be controlled.

The principal operating modes of series converter are:

i. Direct Voltage Injection Mode: - series converter simply generates the voltage vector, V_{se} with the magnitude and phase angle requested by reference input. A direct voltage injection is when the injected voltage vector, V_{se} is maintained in phase with the system voltage for voltage magnitude control or in quadrature with it for controlled quadrature boosting, or in quadrature with line current vector, IL to provide controllable reactive series compensation.

ii. Line Impedance Compensation Mode: - in this case the magnitude of series injected voltage vector, V_{se} is controlled in proportion to the magnitude of the line current, IL so that the series insertion emulates impedance when viewed from the line. The desired impedance is specified by reference input and in general it may be complex impedance with resistive and reactive components of either polarity. A special case of impedance compensation occurs when the injected voltage is maintained in quadrature with respect to the line current to emulate purely reactive.

iii. Phase Angle Regulation Mode: - in this case the injected voltage vector, V_{se} is controlled with respect to the input bus voltage vector, V_s so that the output bus voltage vector, V_o is phase shifted without any magnitude change. One special case of phase shifting occurs when V_{se} is maintained in quadrature with V_s to emulate the quadrature booster [30].

iv. Automatic Power flow Mode: - in this case the magnitude and phase angle of injected voltage vectors, V_{se} is controlled so as to force such a line current vector that results in the desired real and reactive power flow in the line. Also the series injected voltage is determined automatically and continuously by a closed-loop control system to ensure the desired P and Q are maintained despite power system changes. The general block diagram of series converter controller is shown in figure 3.15 below.

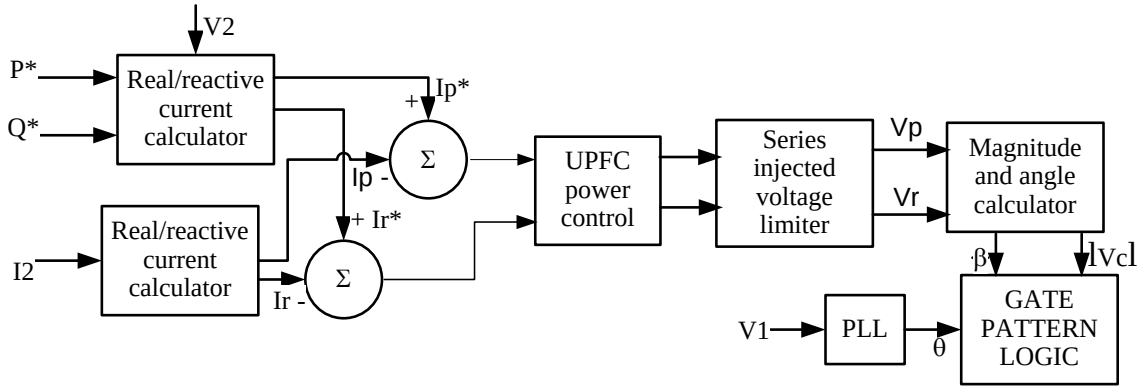

Figure 3.15: Block diagram of series controller

3.10 Mathematical Model of SMIB equipped with UPFC

Synchronous generator is supplying electric power to infinite bus through transmission line and UPFC. The structure of the UPFC with damping controller is shown in figure 3.16 [31] below where, N can be m_E, m_B, δ_E, and δ_B which is input parameter to UPFC.

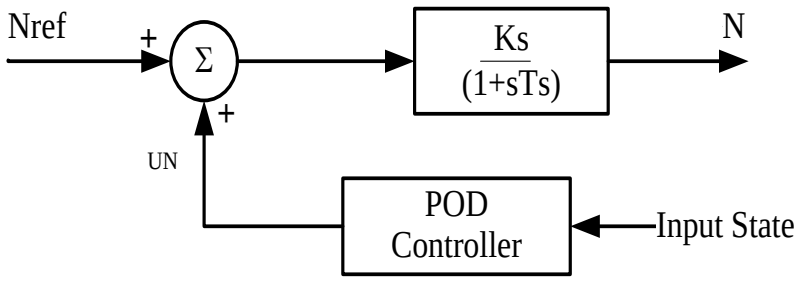

Figure 3.16: UPFC with damping controller

To keep the power flow between series and shunt converters, a DC voltage regulator must be incorporated. The DC voltage is controlled through modulating phase angle of ET voltage δE. The figure 3.17 [32] represents UPFC with dc voltage regulator together with damping controller which is most robust to properly tune UPFC input parameters.

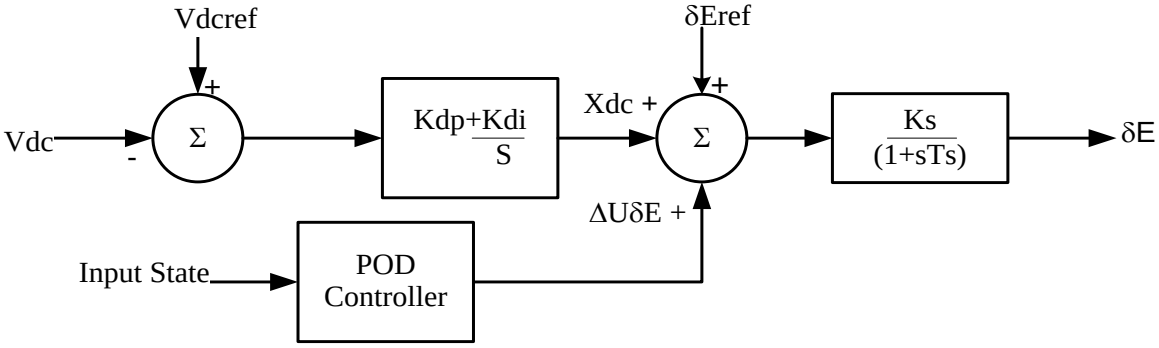

Figure 3.17: UPFC with dc voltage regulator and damping controller

3.10.1 Non-linear Dynamic Modeling of UPFC

Referring to figure 3.17 shown above, the nonlinear differential equation describes the dynamic behavior of UPFC, three phase excitation current, three phase boosting current, and DC link voltage which can be written as follows [33]:

Modeling shunt converter three-phase current equation is described as:

$$\begin{bmatrix} \frac{di_{Ea}}{dt} \\ \frac{di_{Eb}}{dt} \\ \frac{di_{Ec}}{dt} \end{bmatrix} = \begin{bmatrix} -\frac{r_E}{l_E} & 0 & 0 \\ 0 & -\frac{r_E}{l_E} & 0 \\ 0 & 0 & -\frac{r_E}{l_E} \end{bmatrix} \begin{bmatrix} i_{Ea} \\ i_{Eb} \\ i_{Ec} \end{bmatrix} - \frac{m_E V_{dc}}{2l_E} \begin{bmatrix} \cos(\omega t + \delta_E) \\ \cos(\omega t + \delta_E - 120^0) \\ \cos(\omega t + \delta_E + 120^0) \end{bmatrix} + \begin{bmatrix} \frac{1}{l_E} & 0 & 0 \\ 0 & \frac{1}{l_E} & 0 \\ 0 & 0 & \frac{1}{l_E} \end{bmatrix} \begin{bmatrix} V_{Eta} \\ V_{Etb} \\ V_{Etc} \end{bmatrix} \quad (3.50)$$

Modeling series converter three-phase current equation is described as:

$$\begin{bmatrix} \frac{di_{Ba}}{dt} \\ \frac{di_{Bb}}{dt} \\ \frac{di_{Bc}}{dt} \end{bmatrix} = \begin{bmatrix} -\frac{r_B}{l_B} & 0 & 0 \\ 0 & -\frac{r_B}{l_B} & 0 \\ 0 & 0 & -\frac{r_B}{l_B} \end{bmatrix} \begin{bmatrix} i_{Ba} \\ i_{Bb} \\ i_{Bc} \end{bmatrix} - \frac{m_B V_{dc}}{2l_B} \begin{bmatrix} \cos(\omega t + \delta_B) \\ \cos(\omega t + \delta_B - 120^0) \\ \cos(\omega t + \delta_B + 120^0) \end{bmatrix} + \begin{bmatrix} \frac{1}{l_B} & 0 & 0 \\ 0 & \frac{1}{l_B} & 0 \\ 0 & 0 & \frac{1}{l_B} \end{bmatrix} \begin{bmatrix} V_{Bta} \\ V_{Btb} \\ V_{Btc} \end{bmatrix} \quad (3.51)$$

Modeling DC-link Capacitor Voltage equation can be:

$$\frac{dv_{dc}}{dt} = \frac{m_E}{2C_{dc}}\begin{bmatrix}\cos(\omega t + \delta_E)\\ \cos(\omega t + \delta_E - 120^0)\\ \cos(\omega t + \delta_E + 120^0)\end{bmatrix}^T\begin{bmatrix}i_{Ea}\\ i_{Eb}\\ i_{Ec}\end{bmatrix} + \frac{m_B}{2C_{dc}}\begin{bmatrix}\cos(\omega t + \delta_B)\\ \cos(\omega t + \delta_B - 120^0)\\ \cos(\omega t + \delta_B + 120^0)\end{bmatrix}^T\begin{bmatrix}i_{Ba}\\ i_{Bb}\\ i_{Bc}\end{bmatrix} \quad (3.52)$$

Where, $V_{Et}, i_E, r_E, and\ l_E$ are the excitation transformer voltage, current, resistance and inductance respectively; $V_{Bt}, i_B, r_B, and\ l_B$ are the boosting voltage, current, resistance, and inductance respectively; C_{dc}, V_{dc} are the dc link capacitance and voltage respectively. To consider the effects of UPFC in damping of low-frequency swing (LFS), the dynamic model of UPFC is employed, while resistance and transient of the transformers of UPFC can be disregarded. The equation describing the dynamic performance of UPFC can be written as [33].

Modeling of shunt converter voltage equation is described as:

$$\begin{bmatrix}v_{Etd}\\ v_{Etq}\end{bmatrix} = \begin{bmatrix}0 & -x_E\\ x_E & 0\end{bmatrix}\begin{bmatrix}i_{Ed}\\ i_{Eq}\end{bmatrix} + \begin{bmatrix}\frac{m_E\, v_{dc}cos\delta_E}{2}\\ \frac{m_E v_{dc}sin\delta_E}{2}\end{bmatrix} \quad (3.53)$$

Modeling of series converter voltage equation is described as:

$$\begin{bmatrix}v_{Btd}\\ v_{Btq}\end{bmatrix} = \begin{bmatrix}0 & -x_B\\ x_B & 0\end{bmatrix}\begin{bmatrix}i_{Bd}\\ i_{Bq}\end{bmatrix} + \begin{bmatrix}\frac{m_B\, v_{dc}cos\delta_B}{2}\\ \frac{m_B v_{dc}sin\delta_B}{2}\end{bmatrix} \quad (3.54)$$

Modeling of DC-link voltage equation is described as:

$$\frac{dvDC}{dt} = \frac{3m_E}{4C_{DC}}[cos\delta_E \quad sin\delta_E]\begin{bmatrix}i_{Ed}\\ i_{Eq}\end{bmatrix} + \frac{3m_B}{4C_{DC}}[cos\delta_B \quad sin\delta_B]\begin{bmatrix}i_{Bd}\\ i_{Bq}\end{bmatrix} \quad (3.55)$$

Where, V_E, X_E and i_E are voltage, reactance and current of excitation transformer respectively; V_B, X_B and i_B are voltage, reactance and current of boosting transformer respectively. V_{DC}, and C_{DC} are the voltage and capacitance of DC-link. Equations (3.56), (3.57), (3.58), and (3.59) below represents the non-linear dynamic model of UPFC for SMIB system [33]:

$$\dot{\delta} = \omega b(\omega - 1) \quad (3.56)$$

$$\dot{\omega} = \frac{1}{M}(p_m - p_e - D(\omega - 1)) \quad (3.57)$$

$$\dot{E'_q} = \frac{1}{T'_{do}}(E_{fd} - E'_q - i_d(x_d - x'_d)) \quad (3.58)$$

$$\dot{E}_{fd} = \frac{1}{T_a}(k_a(\dot{v}_{ref} - v_t) - E_{fd}) \quad (3.59)$$

$$\dot{V_{dc}} = \frac{3m_E}{4C_{dc}}\left(I_{Ed}sin\delta_E + I_{Eq}cos\delta_E\right) + \frac{3m_B}{4C_{dc}}(I_{Bd}sin\delta_B + I_{Bq}cos\delta_B) \quad (3.60)$$

The equation of real power balance between shunt and series converters can be shown below:

$\mathrm{Re}(\mathrm{V_B I_B^* - V_E I_E^*}) = 0$

From the above equations δ is the rotor angle, ω and ωb are the rotor speed and synchronous speed, Pm is the input mechanical power, Pe is output electrical power, D and M are damping coefficient and machine inertia, $\mathrm{E_{fd}}, \dot{\mathrm{E}}'_{\mathrm{q}}$ and E'_q are the generator field, internal voltage of generator and transient generator, respectively, T'_{do} is the time constant of field circuit, the reference voltage is $\mathrm{V_{ref}}. \mathrm{K_a}, \mathrm{T_a}$ are gain and time constant of excitation system respectively.

$$\mathrm{P_e = V_{td} i_d + V_{tq} i_q} \tag{3.61}$$

The generator output power is written in terms of the q-axis as well as d-axis components of the armature current i and terminal voltage Vt as:

$$\mathrm{V_t = \sqrt{V_{td}^2 + V_{tq}^2}} \tag{3.62}$$

$\mathrm{V_{tq} = E'_q - x'_d i_d}, \mathrm{V_{td} = v_d - x_t i_q = x_q i_q}, \mathrm{V_{tq} = v_q + x_t i_d = E_q - x_d i_d = E'_q - x'_d i_d}$

Where $\mathrm{v_d = Vb\ sin\delta}$; $\mathrm{v_q = Vbcos\delta}$

$\mathrm{i_d = \frac{E'_q - V_b cos\delta}{x'_{d\Sigma}}}$, $\mathrm{i_q = \frac{V_b sin\delta}{x'_{d\Sigma}}}$, $\mathrm{i_d = i_{Ed} + i_{Bd} + i_{TLd}}$ and $\mathrm{i_q = i_{Eq} + i_{Bq} + i_{TLq}}$

Where, $\mathrm{v_{td}}$; $\mathrm{v_{tq}}$ and $\mathrm{i_d}$; $\mathrm{i_q}$ $\mathrm{v_d}$; $\mathrm{v_q}$ are the d and q components of the terminal voltage of generator, $\overline{V_t}$, line current, $\overline{I_t}$, and the voltage at infinite bus bar V_b respectively. All the network currents are presented in Appendix A.

3.10.2 Linear Modeling of UPFC

The model of linear dynamic by linearization of non−linear model for the operating condition [34].

$$\Delta\dot{\delta} = \omega_b \Delta\omega \tag{3.63}$$

$$\Delta\dot{\omega} = \frac{1}{\mathrm{M}}(\Delta \mathrm{p_m} - \Delta \mathrm{p_e} - \mathrm{D}\Delta\omega) \tag{3.64}$$

$$\Delta\dot{\mathrm{E}}'_{\mathrm{q}} = \frac{1}{\mathrm{T'_{do}}}\left(\Delta \mathrm{E_{fd}} - \Delta \mathrm{E'_q} - \Delta \mathrm{i_d}(\mathrm{x_d} - \mathrm{x'_d})\right) \tag{3.65}$$

$$\Delta\dot{\mathrm{E}}_{\mathrm{fd}} = \frac{1}{\mathrm{T_a}}(-\mathrm{k_a}\Delta \mathrm{v_t} - \Delta \mathrm{E_{fd}}) \tag{3.66}$$

$$\Delta\dot{\mathrm{V}}_{\mathrm{dc}} = \mathrm{K_7}\Delta\delta + \mathrm{K_8}\Delta \mathrm{E'}_{\mathrm{q}} - \mathrm{K_9}\Delta \mathrm{V_{dc}} + \mathrm{K_{ce}}\Delta \mathrm{m_E} + \mathrm{K_{c\delta e}}\Delta\delta_{\mathrm{E}} + \mathrm{K_{cb}}\Delta \mathrm{m_B} + \mathrm{K_{c\delta b}}\Delta\delta_{\mathrm{B}} \tag{3.67}$$

The terminal voltage is [34]:

$$\Delta \mathrm{V_t} = \mathrm{K_5}\Delta\delta + \mathrm{K_6}\Delta \mathrm{E'_q} + \mathrm{K_{vd}}\Delta \mathrm{V_{dc}} + \mathrm{K_{ve}}\Delta \mathrm{m_E} + \mathrm{K_{v\delta E}}\Delta\delta_{\mathrm{E}} + \mathrm{K_{vb}}\Delta \mathrm{m_B} + \mathrm{K_{v\delta b}}\Delta\delta_{\mathrm{B}} \tag{3.68}$$

Where, $\Delta P_e = K_1\Delta\delta + K_2\Delta E'_q + K_{pd}\Delta v_{DC} + K_{pe}\Delta m_E + K_{p\delta e}\Delta\delta_E + K_{pb}\Delta m_B + K_{p\delta b}\Delta\delta_B$

$\Delta E'_q = K_4\Delta\delta + K_3\Delta E'_q + K_{qd}\Delta v_{DC} + K_{qe}\Delta m_E + K_{q\delta e}\Delta\delta_E + K_{qb}\Delta m_B + K_{q\delta b}\Delta\delta_B$

$\Delta v_t = K_5\Delta\delta + K_6\Delta E'_q + K_{vd}\Delta v_{DC} + K_{ve}\Delta m_E + K_{v\delta e}\Delta\delta_E + K_{vb}\Delta m_B + K_{v\delta b}\Delta\delta_B$

$\Delta\dot{V}_{dc} = K_7\Delta\delta_E + K_8\Delta E'_q - K_9\Delta v_{DC} + K_{ce}\dot{\Delta m}_E + K_{c\delta e}\Delta\delta_E + K_{cb}\Delta m_B + K_{c\delta b}\Delta\delta_B$

$K_{pd}, K_{pe}, K_{p\delta e}, K_{pb}, K_{p\delta b}, K_{qd}, K_{qe}, K_{q\delta e}, K_{qb}, K_{q\delta b}, K_{vd}, K_{ve}, K_{v\delta e}, K_{vb}, K_{v\delta b}, K_{ce}, K_{c\delta e}, K_{cb}, K_{c\delta b}$, and the constants K_1 *to* K_9, are function of the system coefficients and the initial operating coefficients. In state space exemplification, these equations can be expressed as:

$$\Delta\dot{X} = A\Delta X + B\Delta U \tag{3.69}$$

Where, the state vector x, the control vector u, and the matrices A and B are shown $\Delta X = [\Delta\delta\ \Delta\omega\ \Delta E_q\ \Delta E_{fd}\ \Delta V_{dc}]^T$, and $\Delta U = [\Delta U_{Pss}\ \Delta m_E\ \Delta\delta_E\ \Delta m_B\ \Delta\delta_B]^T$

Then, the construction of the matrix A and B are shown as follows [34]:

$$A = \begin{bmatrix} 0 & \omega_b & 0 & 0 & 0 \\ -\frac{K_1}{M} & -\frac{D}{M} & -\frac{K_2}{M} & 0 & -\frac{K_{pdc}}{M} \\ -\frac{K_4}{T'_{do}} & 0 & -\frac{K_3}{T'_{do}} & \frac{1}{T'_{do}} & -\frac{K_{qdc}}{T'_{do}} \\ -\frac{K_A K_5}{T_A} & 0 & -\frac{K_A K_6}{T_A} & -\frac{1}{T_A} & -\frac{K_A K_{Vdc}}{T_A} \\ K_7 & & K_8 & 0 & -K_9 \end{bmatrix}$$

$$B = \begin{bmatrix} 0 & 0 & 0 & 0 & 0 \\ 0 & -\frac{K_{PE}}{M} & -\frac{K_{P\delta E}}{M} & -\frac{K_{PB}}{M} & -\frac{K_{P\delta B}}{M} \\ 0 & -\frac{K_{qE}}{T'_{do}} & -\frac{K_{q\delta E}}{T'_{do}} & -\frac{K_{qB}}{T'_{do}} & -\frac{K_{q\delta B}}{T'_{do}} \\ \frac{K_A}{T_A} & -\frac{K_A K_{VqE}}{T_A} & -\frac{K_A K_{V\delta E}}{T_A} & -\frac{K_A K_{VB}}{T_A} & -\frac{K_A K_{V\delta B}}{T_A} \\ 0 & K_{CE} & K_{C\delta E} & K_{CB} & K_{C\delta B} \end{bmatrix}$$

Where Δm_E, Δm_B, $\Delta\delta_E$ and $\Delta\delta_B$ are a linearization of the input control signal of the UPFC and the equations related to the K parameters have been presented in Appendix B. All the design parameters of UPFC were presented in appendix B1 at the end of this thesis. The voltage across the DC link capacitor was controlled by POD controller during δ_E as [34]:

$$\delta_E = \left\{\left(K_{dp} + \frac{K_{dI}}{s}\right)\Delta\omega + \left(K_{dcp} + \frac{K_{dcI}}{s}\right)(V_{dcrf} - V_{dc})\right\}\left(\frac{K_s}{1+sT_s}\right) \tag{3.70}$$

Where, K_{dp} is proportional gain of controller and k_S is proportional gain of SSSC controller

3.10.3 Rating of UPFC

Improper sizing is bad for UPFC itself and for the power system network. Sizing includes shunt converter rating, series converter rating and capacitor rating. Input to UPFC primary

side transformers of both converters are the line voltage and power where UPFC is connected. The primary side voltage of the transformers of shunt and series converters are equal to the bus bar voltage, which is 400kV. The secondary side voltage of the shunt and series transformers are around 10% of the primary side voltage of the two transformers according to IEEE standards of UPFC details. This is true for both shunt and series converter of UPFC transformers. Other transformer parameters like transformer reactance X and resistance R are selected from EEP catalogue. Capacitor sizing is determined from energy storage of capacitors principle which states energy stored in a capacitor is proportional to capacitance of the capacitor and the supply voltage to it. The rating of the capacitor can be found as;

$$S = \frac{E}{t} = \frac{CV^2}{2*t} \tag{3.71}$$

Where, E is the energy stored on the capacitor $E = \frac{CV^2}{2}$ and C is the capacitance of the capacitor. V is the secondary side transformer of the shunt converter. S is the power rating on the capacitor

3.10.4 Modeling of DC-link Capacitor

For maintaining the power flow in the capacitor, controlling the net input power should instantaneously meet the charging and discharging rate of energy in the capacitor. The input power to capacitor comes through shunt converter and output power pass through series converter. The power maintained in the capacitor is given by:

$$P_{dc} = P_{sh} - P_{se} \tag{3.72}$$

Where, the shunt and series power are written as:

$P_{sh} = V_{shd}i_{shd} - V_{shq}i_{shq}$, $P_{se} = V_{sed}i_{sed} - V_{seq}i_{seq}$ and $P_{dc} = I_{DC} * V_{dc}$

The current in the capacitor is calculated as:

$$i_{dc} = C\frac{d}{dt}V_{dc}$$

Where, P_{se} , P_{sh} and P_{dc} are active powers of the series converter, shunt converters and DC link capacitor respectively. Therefore, the dynamics of DC link capacitor is;

$$CV_{dc}\frac{d}{dt}V_{dc} = \left(V_{shd}i_{shd} - V_{shq}i_{shq}\right) - \left(V_{sed}V_{sed} - V_{seq}i_{seq}\right)$$

$$CV_{dc}\frac{d}{dt}V_{dc} = \frac{1}{2}C\frac{d}{dt}V_{dc}^2 = \left(V_{shd} * i_{shd} - V_{shq} * i_{shq}\right) - \left(V_{sed} * V_{sed} - V_{seq}i_{seq}\right)$$

$$CV_{dc}\frac{d}{dt}V_{dc} = \frac{d}{dt}V_{dc}^2 = \frac{2}{C}\{\left(V_{shd}i_{shd} - V_{shq}i_{shq}\right) - \left(V_{sed}V_{sed} - V_{seq}i_{seq}\right)\} \tag{3.73}$$

3.11 Constraints of UPFC Sizing and Placement

The optimization problem has both equality constraints and inequality constraints to be processed.

3.11.1 Equality Constraints

The equality constraints are the power balance equation that can be represented by:

$$P_{gi} - P_{di} - V_i \sum_{k=1}^{NPQ} V_j \left(G_{ij}\cos\theta_{ij} + B_{ij}\sin\theta_{ij}\right) = 0 \quad (3.74)$$

$$Q_{gi} - Q_{di} - V_i \sum_{k=1}^{NPQ} V_j \left(G_{ij}\cos\theta_{ij} + B_{ij}\sin\theta_{ij}\right) = 0 \quad (3.75)$$

Where P_{gi} is real power generation at bus i, P_{di} is the real power demand at bus i, Q_{gi} is the reactive power generation at bus i, Q_{di} is the reactive power demand at bus i.

3.11.2 Inequality Constraints

The inequality constraints are the ranges of bus voltage magnitudes, reactive power injection and variables of the UPFC device. The inequality constraint represents system operating limits:

- UPFC series injected voltage limits: $0 \leq V_{se} \leq V_{se}^{max}$
- UPFC reactive current limits: $I_q^{min} \leq I_q \leq I_q^{max}$
- Reactive power limits: $Q_{gi}{}^{min} \leq Q_{gi} \leq Q_{gi}{}^{max}$
- Bus voltage limits: $V_i^{min} \leq V_i \leq V_i{}^{max}$
- Line power flow limit: $S_l \leq S_l$ max
- Real power limit: $P_{gi}{}^{min} \leq P_{gi} \leq P_{gi}{}^{max}$

Where, P_{gi}^{min} and P_{gi}^{max} represents real power flow limits of n^{th} bus, Q_{gi}^{min} and Q_{gi}^{max}, are the reactive power flow limits of the n^{th} bus, and V_{gi}^{min} and V_{gi}^{max} are the voltage magnitude limits of the n_{th} bus. The power loss is given by:

$$P_L = \sum_{j=1}^{N} V_i V_j Y_{ij} \cos(\theta_{ij} - \delta_i + \delta_j) \quad (3.76)$$

Where, i=1, 2, 3……n. In this thesis, the contribution is to find the optimal location and sizing of UPFC devices for damping of LFO of the system.

3.12 Control Scheme of UPFC

For effective oscillation damping, the injected series voltage (V_{se}) should be properly controlled. Series injected voltage V_{se}, consists of V_p and V_q, which are in-phase and quadrature components in the UPFC control system. Vse can be calculated as:

$r = \sqrt{v_p^2 + v_q^2}$ And the angle $\gamma = \arctan(\frac{v_q}{v_p})$

The overall control scheme of the proposed POD controller based UPFC is shown in figure 3.18 [35] below.

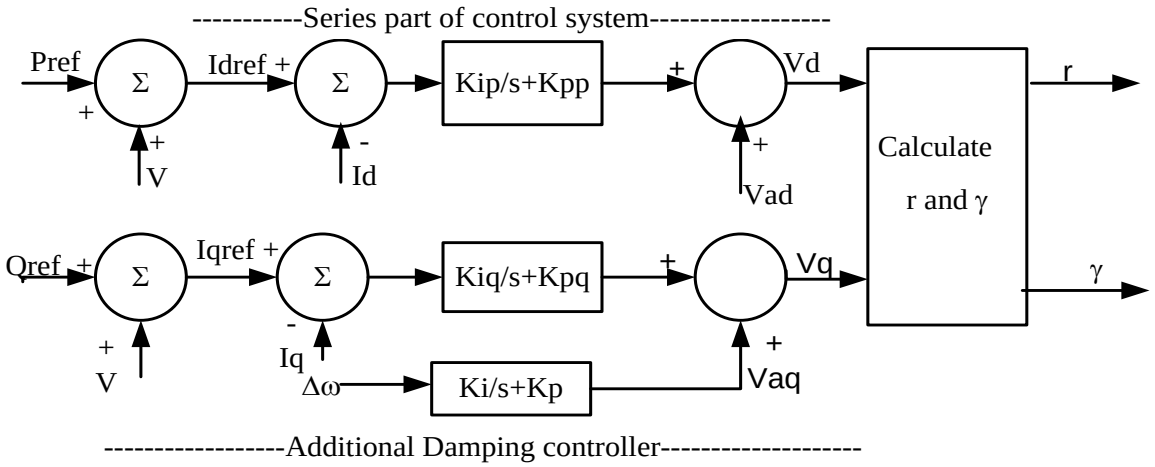

Figure 3.18: Control Scheme of UPFC

3.12.1 UPFC Supplementary Controller

For effective damping increase, supplementary control function helps UPFC via improving its UPFC control function [35]. In this block diagram, Tw is wash-out time constant, T1 and T2 are lead time constant, T3 and T4 are lag time constant, and K is controller gain. Controlling parameters should be selected so optimally that have maximum effect on damping power system oscillations. In this research, these parameters are optimally selected using ALO algorithm.

3.12.2 PSS and UPFC Controller

The structure of PSS to be considered and used is lead-lag controller and described as:

$$u_{pss} = K\frac{sT_w}{1+sT_w}\left(\frac{1+sT_1}{1+sT_2}\right)\left(\frac{1+sT_3}{1+sT_4}\right)\Delta\omega \quad (3.77)$$

The UPFC damping controller have the structure shown below in figure 3.19 where, u can be m_E, δ_E, m_B, or δ_B. To keep the power balance between series and shunt converter DC voltage regulator is used. The DC voltage is controlled by adjusting the phase angle of ET voltage δ_E controller to be considered as shown in figure 3.19.

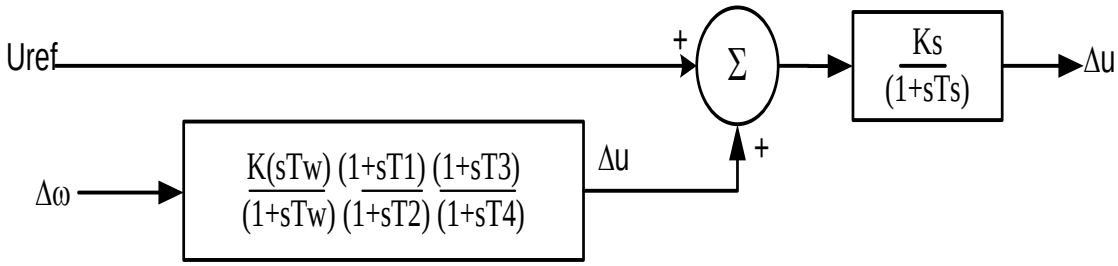

Figure 3.19: UPFC with POD controller

This Δu is the control signal of UPFC which can be any one of the four signals mE, mB, δE, and δB. In this case Δ δ_B is chosen as Δu, and then the ΔU_{ref} could be $\Delta\delta_{\mathrm{B}_{ref}}$. So, like this way reference signals are selected depending upon the value of Δu.

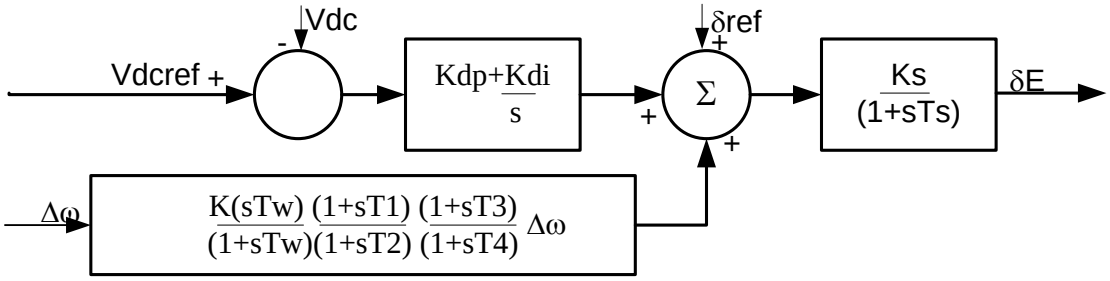

Figure 3.20: UPFC with POD and DC voltage regulator

3.12.3 Controllability Index for UPFC Location

The series converter of UPFC which is installed in series with the transmission line is represented by series voltage source, V_{cR} and the shunt converter of UPFC which is connected to the transmission line by the coupling transformer is represented by the shunt voltage sources, V_{vR}.

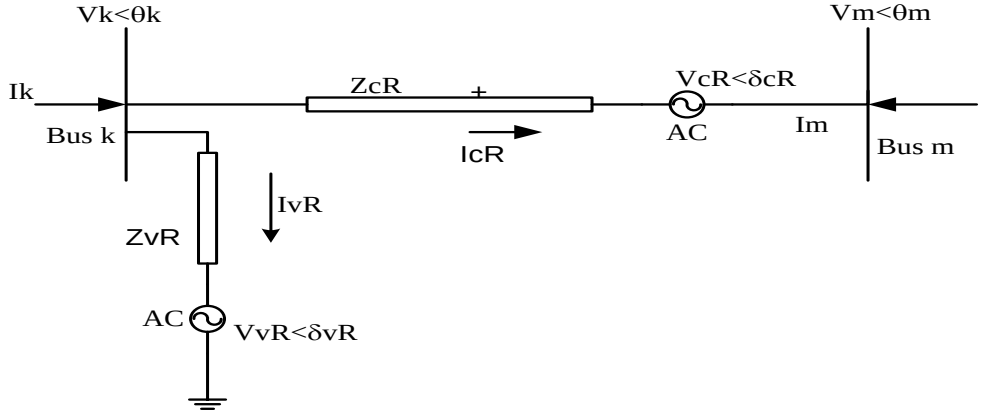

Figure 3.21: Voltage source equivalent circuit of UPFC

The UPFC voltage sources are:

$$E_{cR} = V_{cR}(\cos\delta_{cR} + j\sin\delta_{cR}) \quad (3.78)$$

$$E_{VR} = V_{vR}(\cos\delta_{vR} + j\sin\delta_{vR}) \quad (3.79)$$

Where, V_{cR} and V_{vR} are within the controllable magnitude.

$V_{cR}^{min} \leq V_{cR} \leq V_{cR}^{max}$, and phase angle, $0 \leq \delta_{cR} \leq 2\pi$ of the voltage source representing the series converter. The magnitude V_{vR} and phase angle δ_{vR} of the voltage source representing the shunt converter are controlled between limits $V_{vR}^{min} \leq V_{vR} \leq V_{vR}^{max}$and $0 \leq \delta_{vR} \leq 2\pi$ respectively. Assume UPFC is located between two buses k and m as demonstrated in figure 3.21.

In a series converter the active and reactive power should be:

$$P_{cR} = V_{cR}^2 G_{jj} + V_{cR}V_i(G_{jj}\cos(\delta_{cR} - \delta_i) + B_{ij}\sin(\delta_{cR} - \delta_i) + V_{cR}V_j(G_{jj}\cos(\delta_{cR} - \delta_i) + B_{jj}\sin(\delta_{cR} - \delta_i) \quad (3.80)$$

$$Q_{cR} = -V_{cR}^2 B_{jj} + V_{cR}V_i(G_{jj}\sin(\delta_{cR} - \delta_i) - B_{ij}\cos(\delta_{cR} - \delta_i) + V_{cR}V_j(G_{jj}\sin(\delta_{cR} - \delta_i) - B_{jj}\cos(\delta_{cR} - \delta_i) \quad (3.81)$$

In a shunt converter the active and reactive power should be:

$$P_{vR} = -V_{vR}^2 G_{vR} + V_{vR}V_i(G_{vR}\cos(\delta_{vR} - \delta_i) + B_{vR}\sin(\delta_{vR} - \delta_i)) \quad (3.82)$$

$$Q_{cR} = V_{vR}^2 B_{vR} + V_{vR}V_j(G_{vR}\sin(\delta_{vR} - \delta_j) - B_{vR}\cos(\delta_{vR} - \delta_j)) \quad (3.83)$$

In the above equations, admittance between bus k and m is represented as $Y_{km} = G_{jj} + jB_{jj}$.

3.13 Ant lion Optimization Problem

The recently developed Ant Lion Optimizer (ALO) algorithm is a new meta-heuristic optimization approach. The ALO was first introduced by Seyedali Mirjalili (2015). The inspiration of the Antlion optimization algorithm has come from the real life analysis of the Antlion hunting mechanism in nature. ALO technique mimics the hunting strategy of antlions in nature. The five steps of hunting mechanism are random walk of ants, building traps, entrapment of ants in traps, catching preys, and rebuilding traps.

3.13.1 Operators of ALO Algorithm

In order to represent such interactions, ants are required to move on the search space and antlions are allowed to hunt the ants and become fitter using traps. The random walk of ants are as follows:

$$X(t) = [0, \text{cumsum}(2r(t_1) - 1), \text{cumsum}(2r(t_2) - 1), \text{cumsum}(2r(t_n) - 1)] \quad (3.84)$$

Where, $cumsum$ represents the cumulative sum, n is maximum number of iteration, t represents the steps of random walk and r(t) is a stochastic function which is represented as:

$$\mathrm{r(t)} = \begin{cases} 1 & \text{if rand} > 0.5 \\ 0 & \text{if rand} \leq 0.5 \end{cases} \tag{3.85}$$

Where, t represents the random walk of ants and rand is a random number generated with uniform distribution in the interval of [0, 1]. Position of ants has the following matrix:

$$\mathrm{M_{Ant}} = \begin{bmatrix} \mathrm{A_{1,1}} & \mathrm{A_{1,2}} & \cdots & \mathrm{A_{1,d}} \\ \mathrm{A_{2,1}} & \mathrm{A_{2,2}} & & \mathrm{A_2, d} \\ \vdots & & \ddots & \vdots \\ \mathrm{A_{n,1}} & \mathrm{A_{n,2}} & \cdots & \mathrm{A_{n,d}} \end{bmatrix} \tag{3.86}$$

Where, M_{Ant} is the matrix for saving the position of each ant, $A_{i,j}$ shows the value of the j^{th} variable of i^{th} ant, n is the number of ants, and d is number of variables. Matrix M_{Ant} has been considered to save the position of all ants during optimization. The fitness value of all ants are:

$$\mathrm{M_{oA}} = \begin{bmatrix} \mathrm{f([A_{1,1}} & \mathrm{A_{1,2}} & \cdots & \mathrm{A_{1,d}]}) \\ \mathrm{f([A_{2,1}} & \mathrm{A_{2,2}} & & \mathrm{A_2, d])} \\ \vdots & & \ddots & \vdots \\ \mathrm{f([A_{n,1}} & \mathrm{A_{n,2}} & \cdots & \mathrm{A_{n,d}])} \end{bmatrix} \tag{3.87}$$

Where, MOA is the matrix for saving the fitness of each ant, A_{ij} shows the value of j^{th} dimension of i^{th} ant, n is the number of ants, and f is the objective function. In order save their positions and fitness values, the following matrices are utilized:

$$\mathrm{M_{Antlion}} = \begin{bmatrix} \mathrm{AL_{1,1}} & \mathrm{AL_{1,2}} & \cdots & \mathrm{AL_{1,d}} \\ \mathrm{AL_{2,1}} & \mathrm{AL_{2,2}} & & \mathrm{AL_{2,d}} \\ \vdots & & \ddots & \vdots \\ \mathrm{AL_{n,1}} & \mathrm{A_{Ln,2}} & \cdots & \mathrm{AL_{n,d}} \end{bmatrix} \tag{3.88}$$

Where, $M_{Antlion}$ is the matrix for saving the position of each antlion, $AL_{i,j}$ shows the j^{th}dimension's value of i^{th} antlion, n is the number of antlions, and d is number of variables.

$$\mathrm{M_{oAL}} = \begin{bmatrix} \mathrm{f([AL_{1,1}} & \mathrm{AL_{1,2}} & \cdots & \mathrm{AL_{1,d}])} \\ \mathrm{f([AL_{2,1}} & \mathrm{AL_{2,2}} & & \mathrm{AL_2, d])} \\ \vdots & & \ddots & \vdots \\ \mathrm{f([AL_{n,1}} & \mathrm{AL_{n,2}} & \cdots & \mathrm{AL_{n,d}])} \end{bmatrix} \tag{3.89}$$

Where, MOAL is the matrix for saving the fitness of each ant lion, ALi,j shows the j^{th}dimension's value of i^{th} antlion, n is the number of antlions, and f is the objective function.

3.13.2 Random Walk of Ants

To keep the random walks inside the search space, they are normalized using the following equation:

$$X_i^t = \frac{(X_i^t - a_i) \times (d_i - c_i^t)}{d_i^t - a_i} + c_i \quad (3.90)$$

Where, a_i is the minimum of random walk of i^{th} variable, b_i is the maximum of random walk in i^{th} variable, c_i^t is the minimum of i^{th} variable, and d_i^t indicates the maximum of i^{th} variable.

3.13.3 Trapping in Ant lion's Pit

In order to mathematically model this assumption, the following equations are proposed:

$$c_i^t = \text{Antlion}_j^t + c^t \quad (3.91)$$

$$d_i^t = \text{Antlion}_j^t + d^t \quad (3.92)$$

Where, c^trepresents the minimum of all variables at t^{th} iteration, d^t indicates the vector including maximum of all variables at t^{th}iteration, c_j^t represents the minimum of all variables for i^{th} ant, d_i^t is the maximum of all variables for i^{th}ant, and Antlion_j^t shows the position of the selected j^{th} antlion at t^{th}iteration.

3.13.4 Sliding Ants towards Antlion

This behavior slides down the trapped Ant that is trying to escape. The following equations are proposed in this regard:

$$c^t = \frac{c^t}{I} \quad (3.93)$$

$$d^t = \frac{d^t}{I} \quad (3.94)$$

3.13.5 Catching Prey and Rebuilding Pit

The last stage of hunt is when an ant reaches the bottom of the pit and is caught in the Antlions jaw. The following equation is proposed:

$$\text{Antlion}_j^t = \text{Ant}_i^t \text{ if } f(\text{Ant}_i^t) > f(\text{Antlion}_i^t) \quad (3.95)$$

Where, t shows the current iteration, Antlion_j^t shows the position of selected j^{th} Antlion at t^{th}iteration, and Ant_j^t indicates the position of i^{th} Ant at t^{th} iteration.

3.13.6 Elitism

Elitism is a characteristics of evolutionary algorithm which allows them to keep the best solution obtained at any stage of optimization process since the elite is the fittest antlion, it should affect the movement of all ants during iteration. The elite is:

$$\mathrm{Ant}_i^t = \frac{R_A^t + R_E^t}{2} \tag{3.96}$$

Where, R_A^t is random walk around the antlion selected by roulette wheel at t^{th}iteration, R_E^t is random walk around the elite at t^{th} iteration, and Ant_i^t indicates position of i^{th}ant at t^{th} iteration.

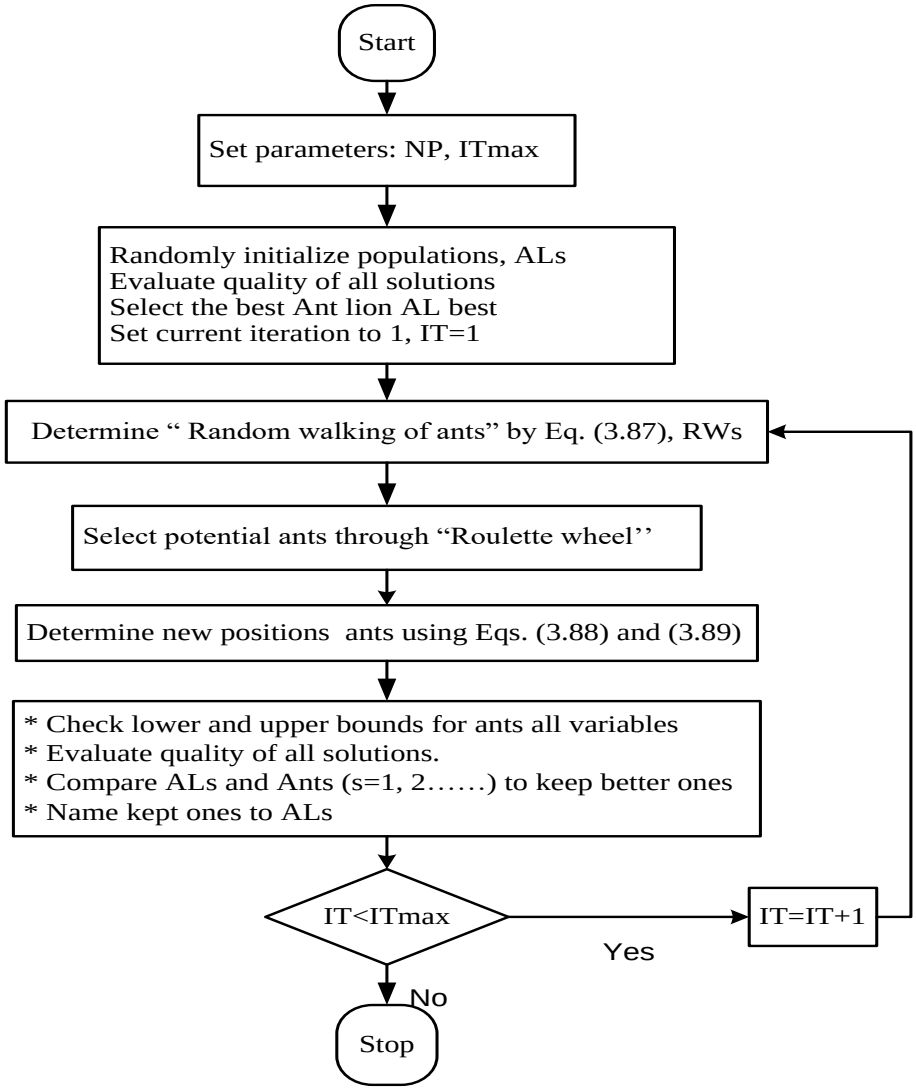

Figure 3.22: General flow chart diagram of Antlion optimization algorithm

3.14 Problem Formulation

ALO optimization is characterized as the way towards finding the conditions that gives good and most extreme condition of a function, where the function expresses the effort required. Basically optimization refers to maximizing or minimizing an objective function subjected to some specific constraints. In this thesis the main goal of employing ALO algorithm is to select the optimal parameters of PSS and UPFC among the different options to operate system in optimal conditions. So, ALO algorithm has been selected and used for optimal tuning method for the proposed thesis. To select the best stabilizer parameters that enhance LFO damping, the problem is formulated to optimize a selected objective function J subjected to gain and time constant inequality constraints.

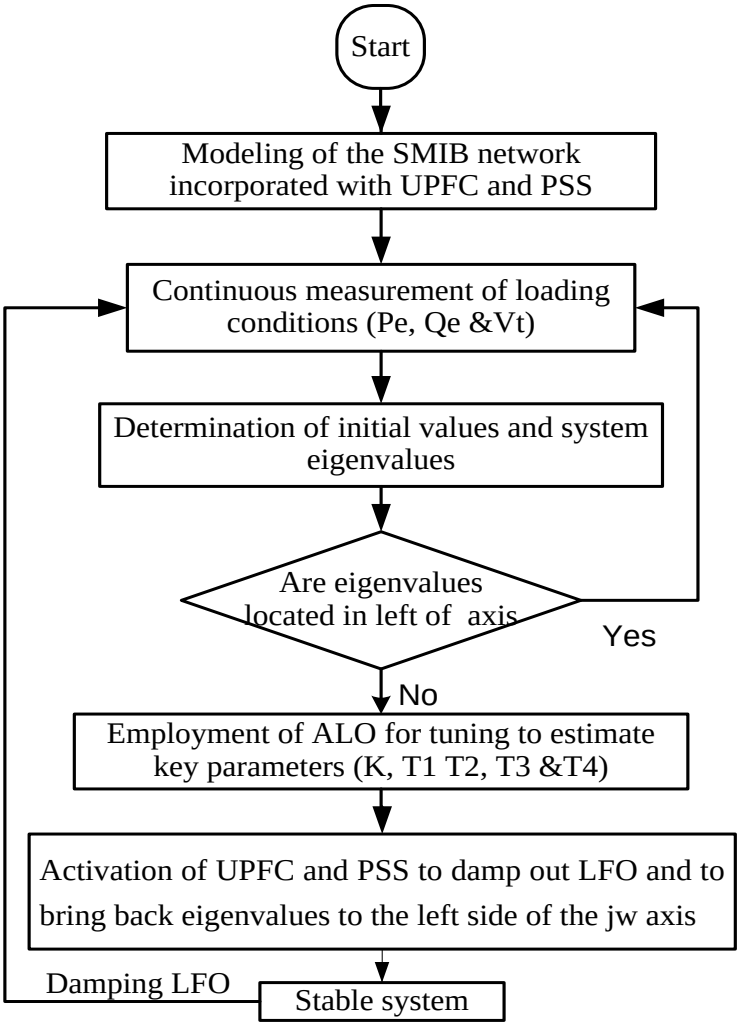

Figure 3.23: Flowchart of implementing ALO applicable for LFO

Table 3.2: Parameter initialization of implemented ALO based UPFC parameter setting

Parameters	**Settings**
Number of Search agent	40
Maximum number of iteration	100
Number of variables to be optimized	5

3.14.1 Finding Eigenvalues and Minimum Damping Ratio

The number of states and eigenvalues depend on the dimension of the system matrix.

$$[A - \lambda_i I]\emptyset = 0 \tag{3.97}$$

Where λ_i represents eigenvalues and ϕ represents right eigenvector. For non-trivial solution determinant of $A - \lambda_i I$ equals to zeros and the eigenvalues can be calculated.

The controllability of a system is determined by left eigenvector. The eigenvalues of the system matrix must lie in the left half plane to make the system stable. This indicates that the real part of complex conjugate must be placed in the left half plane. For unstable system the real part of complex conjugate always lies in the right half plane. Assume an eigenvalue in complex format $\lambda_i = \sigma_i \pm j\omega_i$, where i =1, 2,...,k and k denotes the total number of eigenvalues. The oscillation frequency (f) and damping ratio (ζ_i) can be calculated using the following expressions.

Damping factor σi = real (λi)

$$\zeta_i = -\frac{\sigma_i}{\sqrt{\sigma_i^2+\omega_i^2}} \tag{3.98}$$

Where, i=1, 2…… N, in which N is the total of state variables.

3.14.2 Objective Function

For LFO damping the appropriate input signal is speed deviation and the primary objective is to minimize this speed deviation when subject to a disturbance. The objective function of the proposed problem is a combination of two separate objective functions and both of them are associated with system eigenvalues. The first objective function tries to improve system damping factor while the second one sets the damping ratio to a suitable value. For this optimization problem eigenvalue based multi-objective function reflecting combination of both damping factor (σ) and damping ratio is considered. The main objective function is to minimize speed deviation and maximize it damping ration when the system is subjected to disturbance. To minimize this speed deviation the problem is formulated in terms of damping factor and damping ratio. To have some degree of relative stability, the parameters of the

PSS and POD controller may be selected to minimize the following objective function. The objective function depends on the problem formulation of the system not on the type of technic utilized to optimize the problem and the objective function of this thesis is the same with different algorithms like PSO, FA, GA, TLBO and ALO. The only thing that the output of different algorithm is different is that the nature of the algorithm but the result is not far enough to each other. The first objective function is damping factor which can be described as (J1) [41, 45]:

$J_1 = \sum_{i=1}^{NP} (\sigma_0 - \sigma_i)^2$

The second objective function is damping ratio which can be described as (J2):

$J_2 = \sum_{i=1}^{NP} (\zeta_0 - \zeta_i)^2$

The overall objective function J3 by ALO is the combination of two functions [41, 43, 45]

$J_3 = J_1 + \alpha * J_2$ (3.99)

$J_3 = \sum_{i=1}^{NP} (\sigma_0 - \sigma_i)^2 + \alpha * \sum_{i=1}^{NP} (\zeta_0 - \zeta_i)^2$ (3.100)

3.14.3 Constraint Equations

The constraint equations are the controller gain K and phase compensating time constants, lead-lag time constants T1-T4.

Minimize J subject to

Controller gain:

$K^{min} \leq K \leq K^{max}$

Phase compensating time constants [41, 43, 45]:

$T_1^{min} \leq T_1 \leq T_1^{max}$

$T_2^{min} \leq T_2 \leq T_2^{max}$

$T_3^{min} \leq T_3 \leq T_3^{max}$

$T_4^{min} \leq T_4 \leq T_4^{max}$

Where, Np is number of operating point, σ_i and ζ_i are the real part and damping ratio of i^{th} eigenvalue respectively. In this thesis the value of α, σ_0, and ζ_0 are 10, -2 and 0.5 respectively. The value of σ0 determines the relative stability in terms of damping factor margin provided for constraining the location of eigenvalues during process of optimization. The objective of optimization is to maximize the minimum damping ratio. The parameters to be optimized are K, T_1, T_2, T_3 and T_4. In this study Tw is set as 10 sec.

Table 3.3: Typical range of constraint parameters of PSS and POD [45]

Parameters	T1	T2	T3	T4	K
Minimum	0.01	0.01	0.01	0.01	0.01
Maximum	1	1	1	1	100

Figure 3.24a shows the first objective function (J1) which enforces the closed loop eigenvalues towards the negative half plane and places them inside the indicated dashed region. Similarly figure 3.24b illustrates the second objective function (J2) that controls the maximum overshoot of the eigenvalues by limiting them with in a particular dashed region. Thus, the system eigenvalues are restricted to a specific D-shaped region as shown in figure 3.24c when both objective functions (J1&J2) are considered. This would ensure stability by forcing the real parts of the eigenvalues in the left hand side of the complex plane for a specific range of overshoot [43].

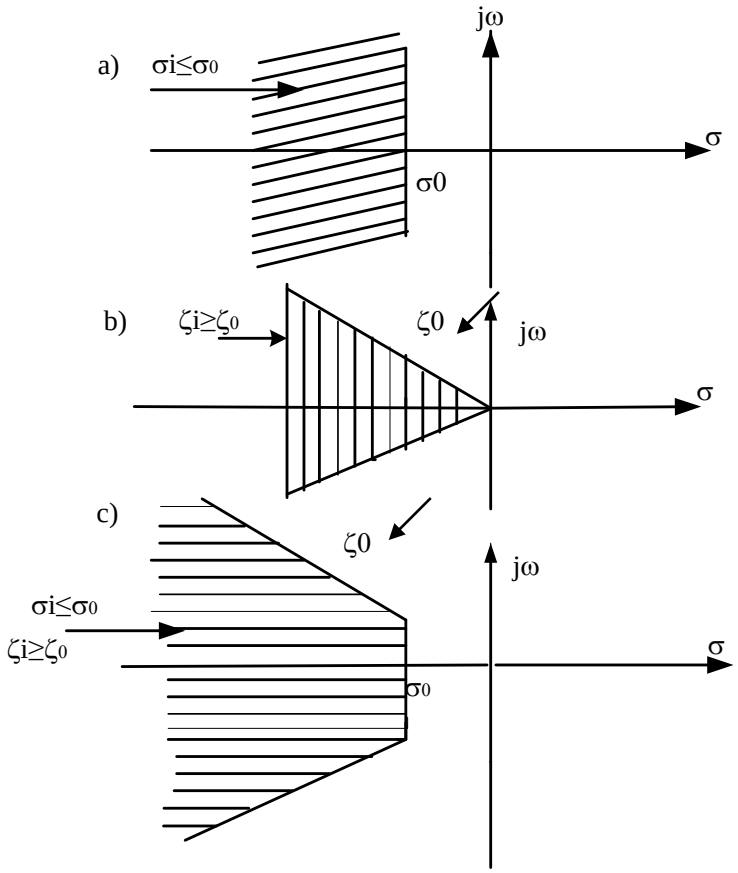

Figure 3.24: Region of eigenvalue location for objective functions

The application of ALO is used to enhance the terminal voltage and active power or to reduce the rotor speed deviation or losses occurring in a system depending on the designed objective function.

3.14.4 Controller Parameter Optimization

Four different optimization techniques such as ALO, PSO, TLBO and GA are compared to tune the POD damping controller for the enhancement of damping ratio. To determine T1 and T2 the phase angle lead ∅m to be provided by the compensator is related to T1 and T2 as:

$\sin(\emptyset_m) = \frac{1-\alpha}{1+\alpha}$ Where α is the ratio between T2 and T1

$\alpha = \frac{T_2}{T_1}$, $\omega_n = \frac{1}{\sqrt{\alpha}T_1}$, $T_2 = \frac{1}{\omega_n}$ typically, $\frac{T_1}{T_2}$ must be less than 10

Consequently, the objective function of this thesis transmutes into maximizing the minimum damping ratio.

3.14.5 Optimal Sizing of PSS Tuned by ALO

The five optimal parameters of PSS are four time constants T1-T4 and gain K_{PSS} which is optimally selected and sized by ALO algorithm to guarantee optimal system performance of the generator under various system configuration. The optimality intended in this thesis is that to find out the optimal parameter sizes of PSS. PSS could generate torque on the rotor of electrical machines and hence phase lag between exciter input and machine electrical torque is compensated. The main purpose of tuning PSS and POD parameters are to ensure appropriate phase lead to compensate the phase lag resulting from generator excitation system and the parameters are optimized to provide appropriate phase lead. Figure 3.25 and table 3.4 shows the optimal parameters of PSS tuned by ALO for exciter input.

Table 3.4: Optimal parameter values of power system stabilizer employing ALO

Parameters	K	Tw (s)	T1 (s)	T2 (s)	T3 (s)	T4 (s)
Optimal values	32.6712	10	0.0296813	0.560678	0.247449	0.63342

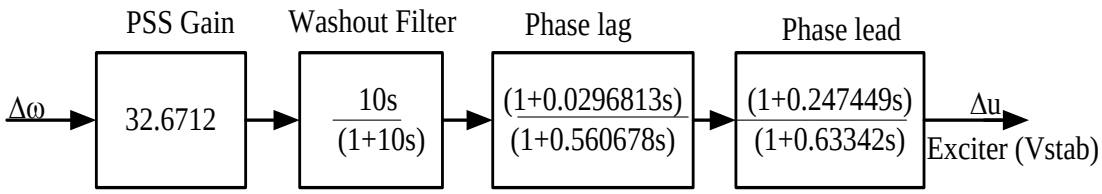

Figure 3.25: Optimally sized Power system stabilizer lead-lag structure

3.14.6 Controllable Parameter Region of UPFC Controllers

The installation of UPFC is used for LFO damping for normal operation of UPFC, the DC voltage across the DC link capacitor needs to be controlled by a DC voltage regulator. Therefore, there are total of four control functions to be fulfilled, i.e. active power flow control/LFO damping, reactive power flow control, AC voltage control and DC voltage control.

(1) DC voltage controller: $\delta_E = (K_{P-Vdc} + \frac{K_{I-Vdc}}{S})(V_{DC-ref} - V_{DC})$

(2) AC voltage controller: $m_E = (K_{P-VEt} + \frac{K_{I-VEt}}{S})(V_{Et-ref} - V_{Et})$

(3) Active power flow controller: $\delta_B = (K_{P-PEt} + \frac{K_{I-PEt}}{S})(P_{Et-ref} - P_{Et})$

(4) Reactive power flow controller: $m_B = (K_{P-QEt} + \frac{K_{I-QEt}}{S})(Q_{Et-ref} - Q_{Et})$

The UPFC active power flow controller, K_{I-PEt} and K_{P-PEt} are the vertical and horizontal coordinate. The other three UPFC controller parameters are set in appendix C.

3.15 Optimal Sizing of UPFC Supplementary Damping Controllers

To utilize UPFC devices for improving low frequency oscillation damping, a supplementary damping controller is required. The supplementary damping controller used as a lead-lag damping controller are called power oscillation damper (POD). The damping controllers are properly sized to produce an electrical torque in phase with speed deviation, that damp out LFO by phase compensation technique. The speed deviation, are considered as input to damping controllers. To damp LFO in power system, supplementary control action can be applied to UPFC devices to increase system damping.

3.15.1 ALO based Optimal Sizing of UPFC-POD Controller

The optimal sizing of POD controller is used to provide fast response of LFO damping and good steady-state accuracy of the system. It also increases the low frequency gain and system bandwidth, making the system response fast. The speed deviation $\Delta\omega$ is considered as the input to the damping controllers. This input passes through several transfer functions which adjusts gain and phase. The parameters of damping controller are optimized and obtained

using ALO technique [40]. The structure of POD controller is similar with PSS. The optimally sized block diagram of POD controller is illustrated in Figure. 3.26 [41]. Controlling parameters are selected so optimally that have maximum effect on damping low frequency oscillations which are optimally selected using ALO. The optimality intended in this thesis is that to find out the optimal parameter sizes of UPFC-POD controller [42]. The four control parameters of UPFC can be modulated in order to produce the damping torque [43]. The optimal tuned transfer function for power oscillation damper controller can be expressed as:

$$H(s) = 32.6712 * \frac{10s}{1+10s}\left(\frac{1+0.0296813s}{1+0.560678s}\right)\left(\frac{1+0.247449s}{1+0.63342s}\right)$$

The controller adjusts UPFC inputs by properly tuning and processing of the input error signal (speed deviation), and consequently provides an effective damping.

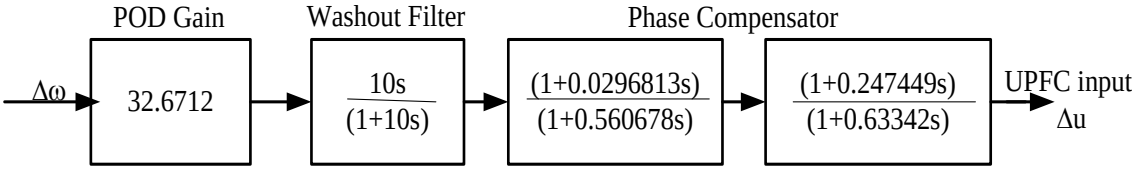

Figure 3.26: Structure of optimally sized UPFC-POD controller

3.15.2 Sizing and Location of UPFC

UPFC acts as a load and as a source hence, it should have optimal placement. If it were improperly placed, it would have negative impacts on LFO and stability as a whole. Its placement determines the effectiveness of controlling of low frequency oscillation of the power system. The optimal location is selected by giving due consideration for reduction in real power generation cost, reduction in LFO, reduction in UPFC installation cost, reduced disturbance losses and improved power flow. Because of higher cost of UPFC device, the installation is not recommended at all possible bus. The criteria of selection is carried out by using ALO algorithm to identify the most critical bus during which UPFC could be placed and hence, system can be operated under stable condition [44].

Table 3.5: Optimal location and Sizing of UPFC using ALO

Loading condition	**Optimal line/bus**	**Rating (MVAR)**
Normal loading	3	26
Light loading	3	24
Heavy loading	3	28

Table 3.5 shown above presents the optimal location and sizing of UPFC obtained by ALO technique. The practical available sizes of UPFC are 28 MVAr for heavy loading condition and 24 MVAr for light loading condition but it is a single unit which is installed at bus three (Bahir dar substation) optimized by ALO technique. In this study single unit UPFC should be recommended for practical application because the installation cost and maintenance cost of UPFC device is lower than that of using multiple unit UPFC. Also based on ALO the optimal location of UPFC is at bus three so, if it is not placed at this bus it is bad for the power system and the UPFC itself.

3.16 Overall System Diagram with MATLAB Simulink

The considered electric network consists of Tana Beles power plant equipped with PSS and an infinite bus which are interconnected through a transmission line and installed with UPFC at Bahir dar substation. The parameters of damping controllers for individual and coordinated sizing are optimized utilizing ALO technique based on eigenvalue objective function. The proper selection of PSS parameters are the key to place the eigenvalues in the left half plane to improve system stability by damping of LFO. It consists of Tana Beles power plants, three buses B1 to B3 interconnected through two transmission lines L1 and L2, two transformer T1 and T2 and two loads connected at buses B2 and B3. The UPFC placed at the right end of the 65 km line L2, between the 400 kV buses at B3 is used to damp out LFO throughout the transmission network. To study the performance of UPFC controller, simulation result has been performed using MATLAB Simulink implementation system model in figure 3.27 shown below.

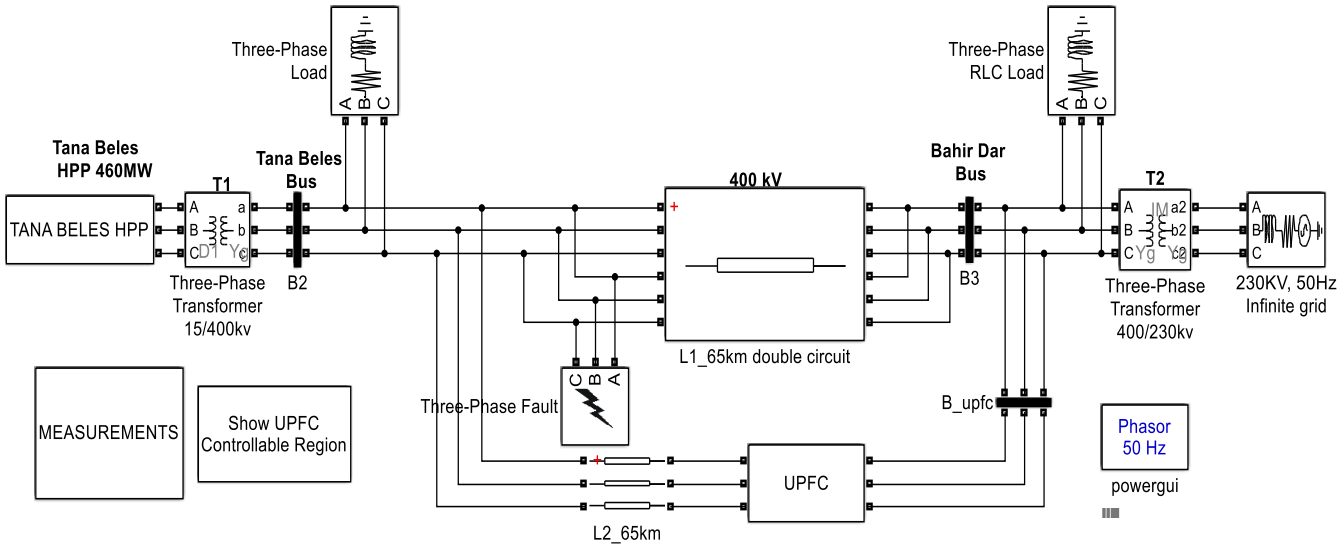

Figure 3.27: Overall power system network equipped with UPFC

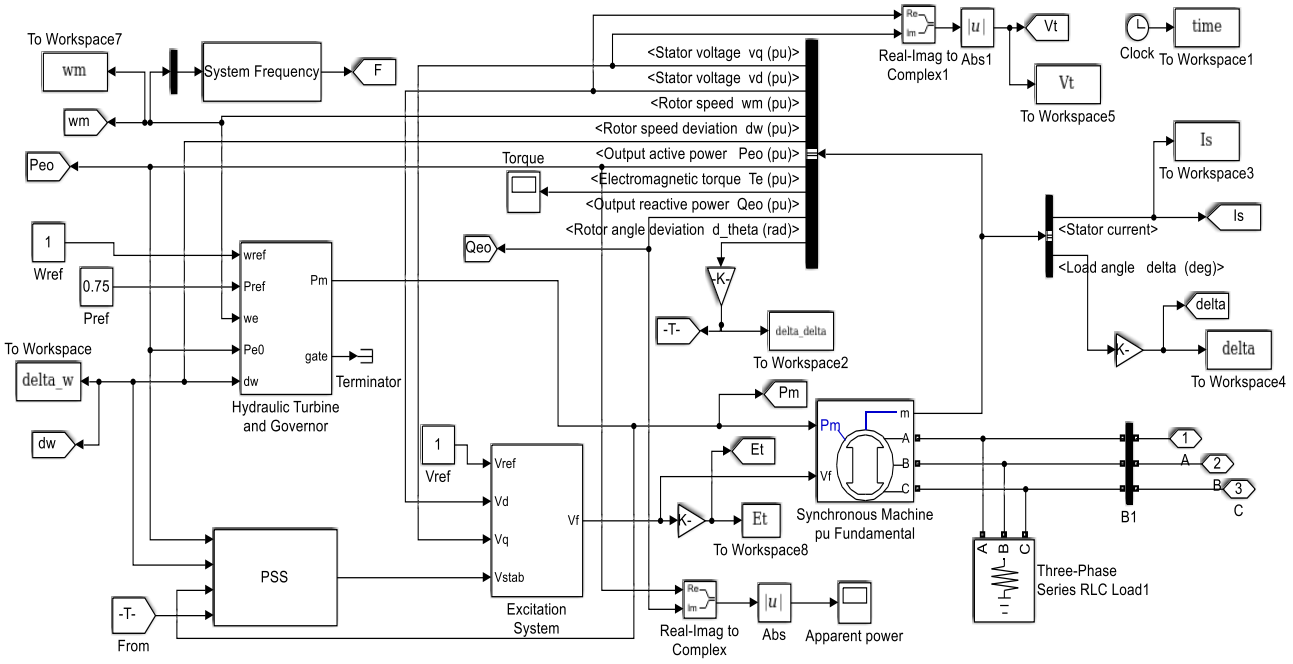

Figure 3.28: Circuit diagram of Tana Beles hydro power plant

Chapter Four

Simulation Result and Discussion

In this thesis damping of LFO for enhancement of Ethiopian power system dynamic stability for SMIB system with conventional existing system using optimized UPFC and PSS had been done. The required data for this work are standard data from different sources like EEP data from Tana Beles power station and transmission line data. The simulation result of the proposed ALO algorithm are compared with existing system, GA, PSO and TLBO. So, eigenvalue analysis and time domain simulation method has been performed for damping of LFO simulation results.

4.1 Eigenvalue Analysis and Minimum Damping Ratio

The system is stable if all eigenvalues has negative real parts. If any one of the eigenvalues have positive real part, then the system is unstable and if the eigenvalues have real part equal to zero, then the poles are complex with only the imaginary part and lies on the jω axis. The poles are conjugates of each other and response of the system is undamped. To obtain robust controllers, eigenvalue analysis and minimum damping ratio of three operating condition had been compared and discussed in table 4.1 below because of power system is a dynamic system. The synchronous machine variables like real power, reactive power and its terminal voltage (P0, Q0 and Ut) are considered as the loading conditions. Since the system is dynamic and the load is continuously varying then the range of values of the selected variables are taken between $0.2 \leq P0 \leq 1.2$, $0.01 \leq Q0 \leq 0.4$ and $0.6 \leq Ut \leq 1$.

Table 4.1: Eigenvalues and minimum damping ratio of different loading conditions

Operating Condition (pu)	Normal loading P0=0.8, Q0=0.114 Ut=1	Light loading P0=0.2, Q0=0.01 Ut=0.6	Heavy loading P0 = 1.20, Q0 = 0.4 Ut=1.4
Eigenvalues of conventional existing system (base case)	+0.1527+9.1627i +0.1527-9.1627i +1.4242+0.0000i -6.9972+0.0000i -2.8657+0.0000i	-7.0589+0.0000i +1.5345+0.0000i +0.1156+5.1410i +0.1156-5.1410i -2.8400+0.0000i	+0.1320+12.5527i +0.1320-12.5527i +1.5318+0.0000i -6.9952+0.0000i -2.9339+0.0000i

Eigenvalues for PSS only	-0.2123+8.4810i -0.2123-8.4810i -5.9644+4.8680i -5.9644-4.8680i +2.8079+0.0000i	+3.3395+0.0000i -1.3107+6.8592i -1.3107-6.8592i -6.9527+0.0000i -3.4574+0.0000i	-2.3738+10.6746i -2.3738-10.6746i -4.1923+5.8688i -4.1923-5.8688i +3.7656 + 0.0000i
Eigenvalues for ALO based PSS and UPFC Controller	-0.2655+7.2754i -0.2655-7.2754i -2.5097+2.447i -2.5097-2.447i -0.0154+0.000i	-0.2616 +4.1837i -0.2616-4.1837i -2.5210+2.4518i -2.5210-2.45181i -0.0007+0.0000i	-0.2701+10.1023i -0.2701-10.1023i -2.5038+2.4946i -2.5038-2.4946i -0.0182+0.0000i
Minimum damping ratio ζ for ALO based PSS and UPFC	0.03647 0.03647 0.7161 0.7161 1	0.0624 0.0624 0.7169 0.7169 1	0.02673 0.02673 0.7084 0.7084 1
Undamped natural frequency f_n (Hz)	1.1585 1.1585 0.3897 0.3897 0	0.6662 0.6662 0.3904 0.3904 0	1.6087 1.6086 0.3972 0.3972 0

The overall system for Tana Beles 400kV line is simulated for different loading conditions and tabulated in table 4.1 above. ALO based optimally tuned PSS and UPFC model describes good performance over conventional existing system and PSS only for each case in terms of minimum damping ratio. From table 4.1 shown above the eigenvalues for ALO based PSS and UPFC controller is more superior to conventional existing system. Damping ratio and eigenvalue comparison clearly shows better performance of ALO optimized PSS and UPFC controller over conventional existing system in real time operation of power system network. From table 4.1, with conventional existing system three of the eigenvalues are positive which lies on the right of $j\omega$ axis and the system is not stable while with PSS-UPFC controller all the eigenvalues are negative and damping ratio is positive which are located on the left of $j\omega$ axis and the system is stable.

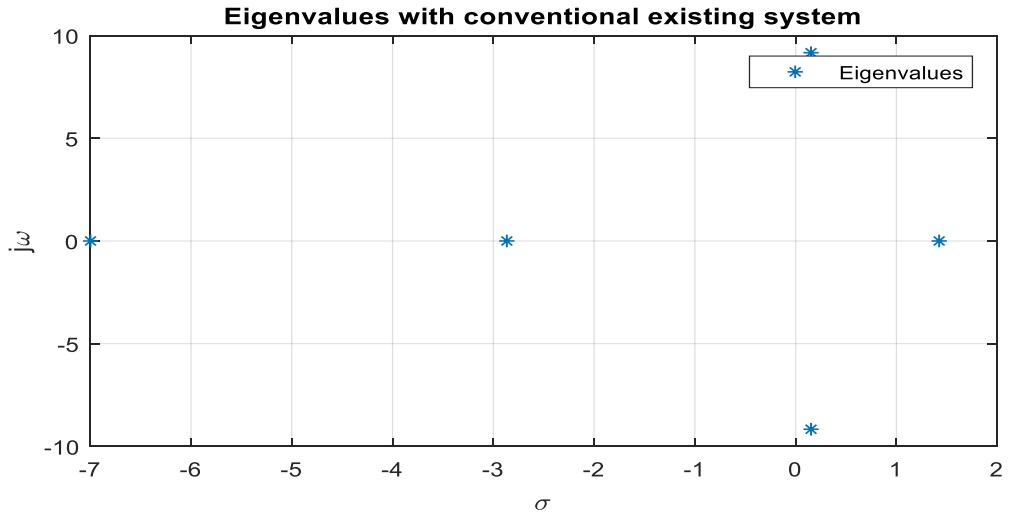

Figure 4.1: System eigenvalues with existing system at normal loading conditions

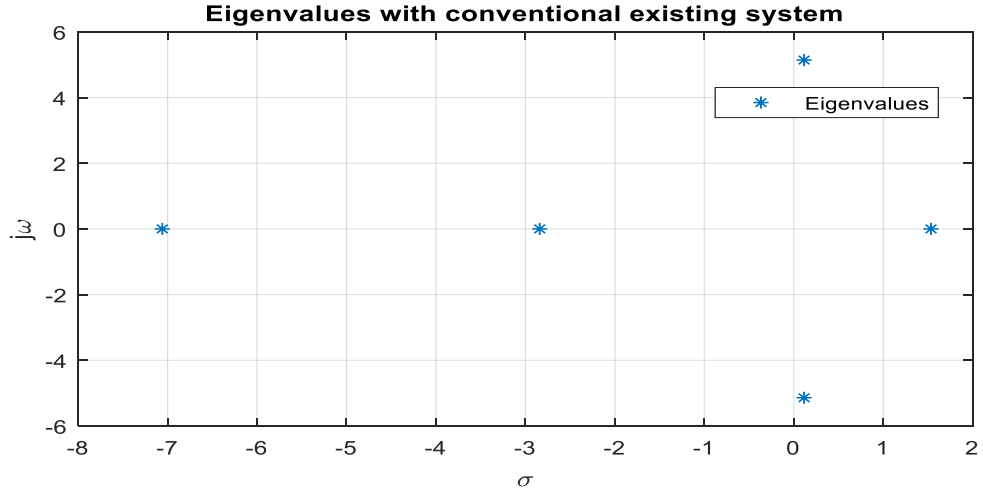

Figure 4.2: System eigenvalues with existing system at light loading conditions

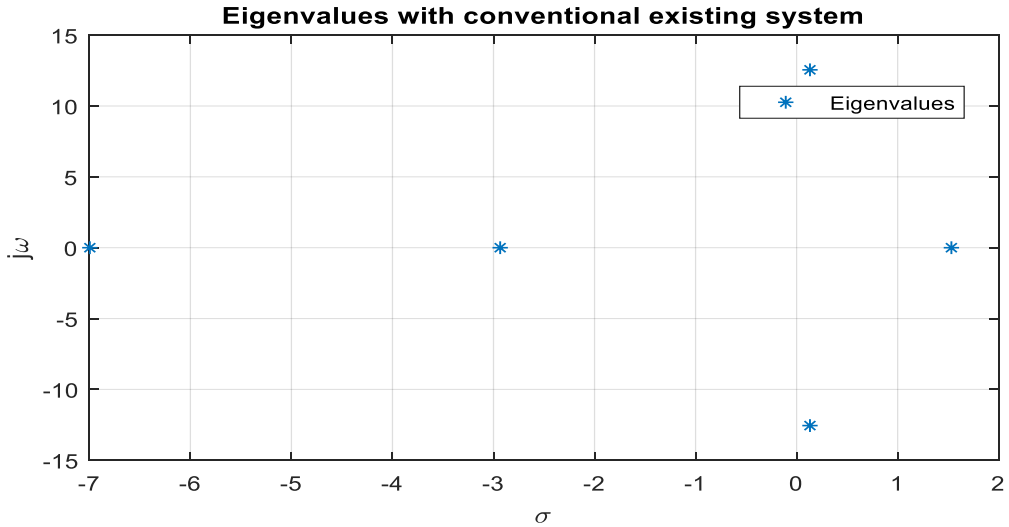

Figure 4.3: System eigenvalues with existing system at heavy loading conditions

Figure (4.1), (4.2) and (4.3) above shows the location of eigenvalues of conventional existing system at normal, light and heavy loading conditions respectively. The result shows that most of the eigenvalues have positive real part and negative damping ratio ($\zeta<0$) which lies on the right half plane of the $j\omega$ axis. Therefore, the system is unstable.

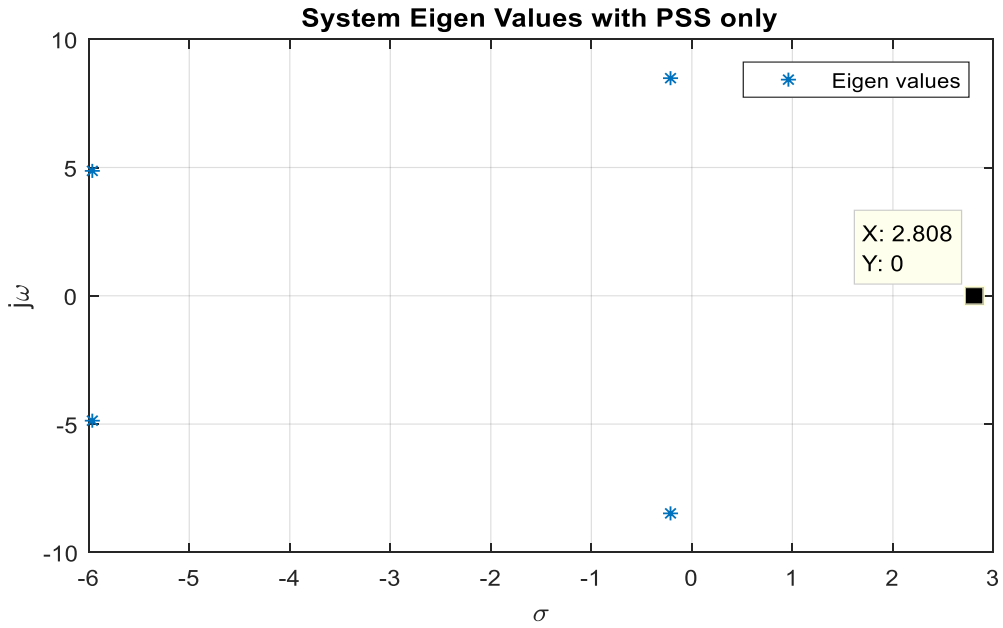

Figure 4.4: System eigenvalues with PSS only at normal loading conditions

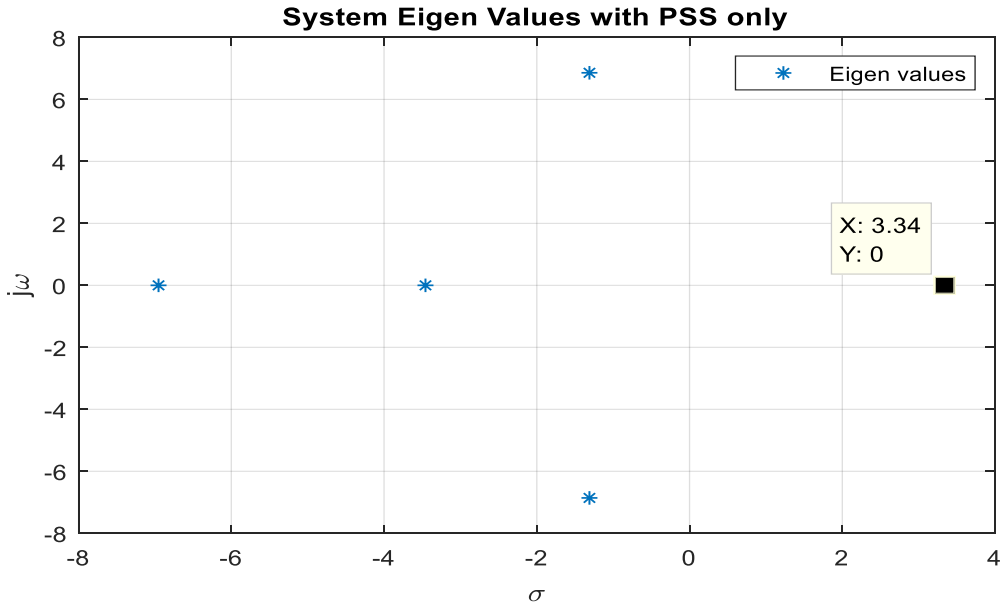

Figure 4.5: System eigenvalues with PSS only at light loading conditions

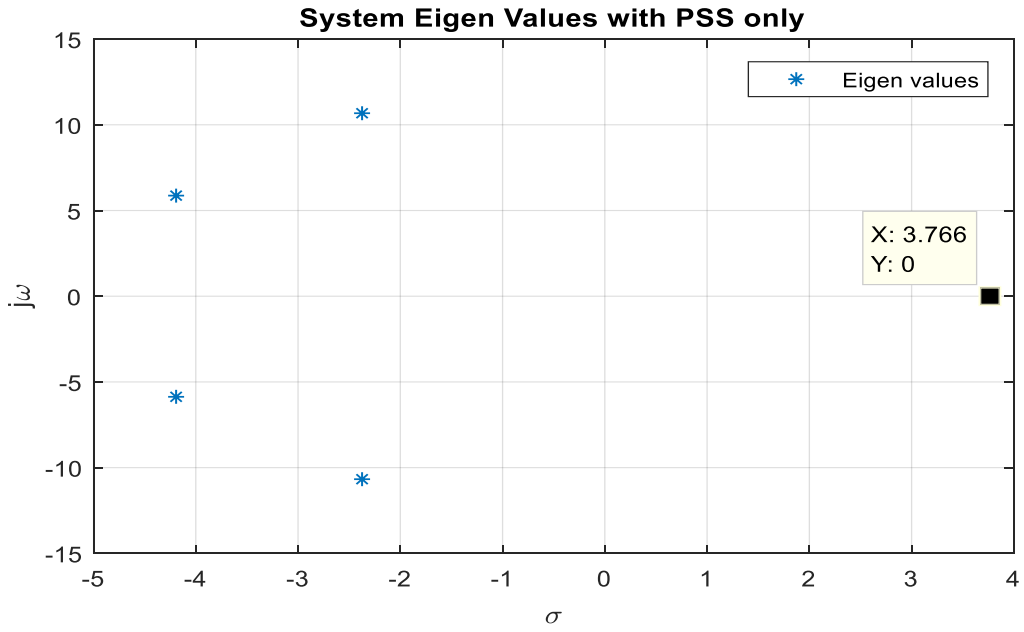

Figure 4.6: System eigenvalues with PSS only at heavy loading conditions

Figure (4.4), (4.5) and (4.6) shows the location of eigenvalues of the system with PSS only at normal, light and heavy operating conditions respectively. The above result shows that one of the eigenvalue has positive real part and negative damping ratio ($\zeta<0$) which lies on the right half plane of the $j\omega$ axis. So, the system is unstable.

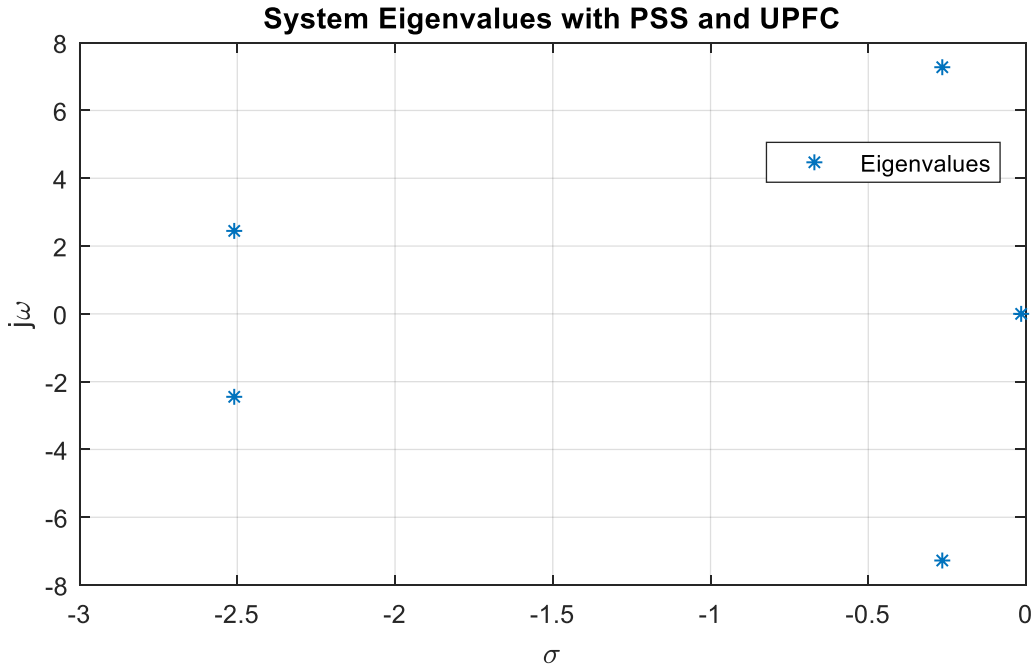

Figure 4.7: System eigenvalues with PSS and UPFC at normal loading condition

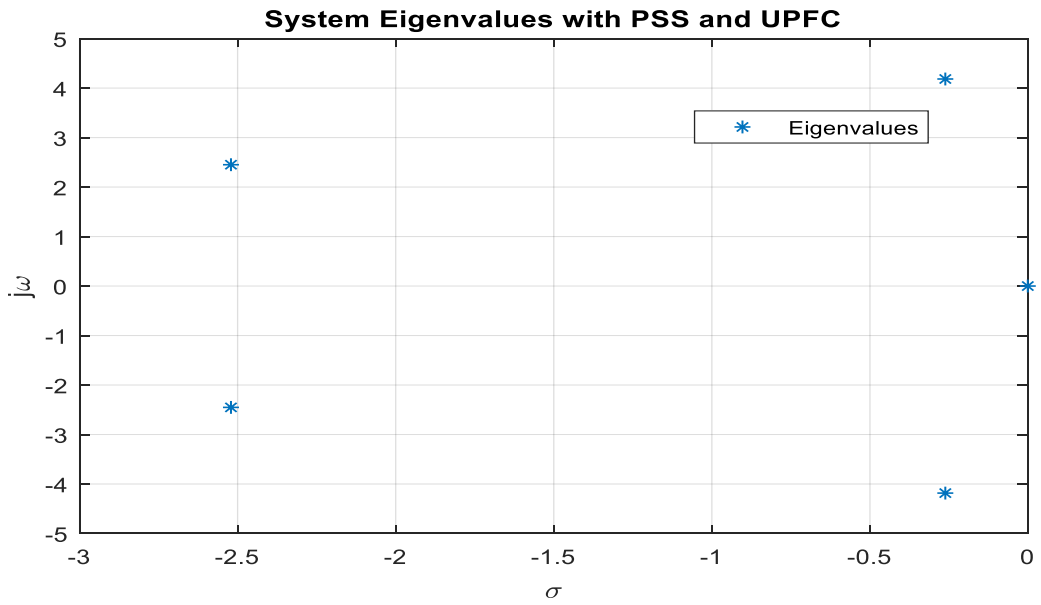

Figure 4.8: System eigenvalues with PSS and UPFC at light loading condition

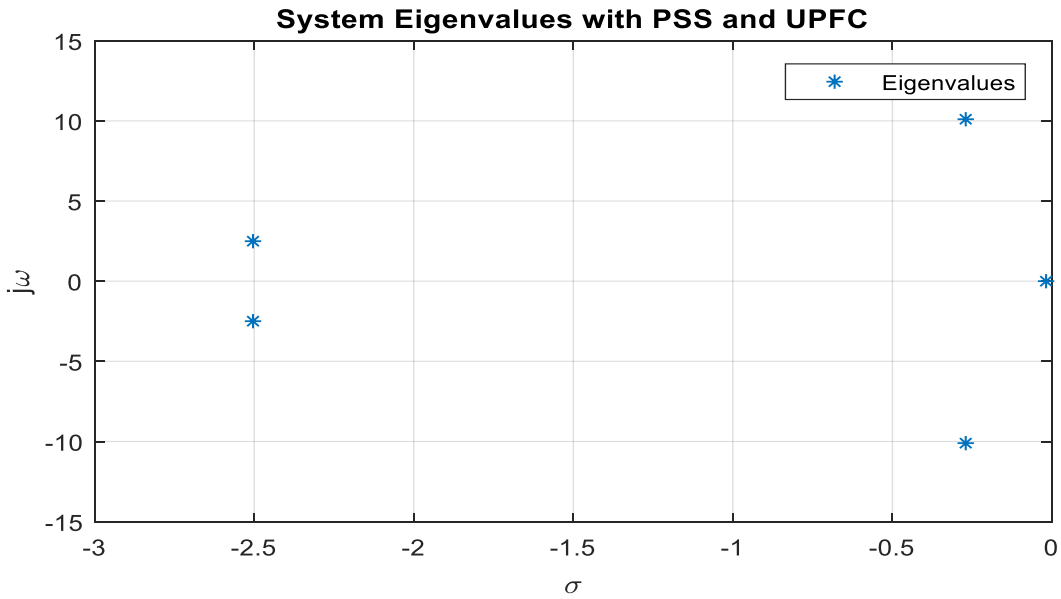

Figure 4.9: System eigenvalues with PSS and UPFC at heavy loading conditions

Figure (4.7), (4.8) and (4.9) shows the location of system eigenvalues with PSS and UPFC controller for normal, light and heavy loading conditions respectively. In these cases all eigenvalues have negative real part and positive damping ratio implies that the eigenvalue lies on the left of the $j\omega$ axis. Since damping ratio is between 0&1 ($0 < \zeta < 1$) and the poles are located on second and third coordinates due to existence of both real and imaginary parts and the response of the system is stable. The last eigenvalue has damping ratio $\zeta=1$ and the poles are real and equal which lies on the negative σ-axis and the response of the system is critically damped or stable.

4.2 Time Domain Simulation Analysis

4.2.1 Optimal parameters of PSS and UPFC

Low frequency oscillation damping mainly depends on controller gain (K) and time constants (T1-T4) and these parameters must be optimized and the mentioned objective function (J) fulfills the same requirement.

Table 4.2: Optimal parameters of PSS and UPFC-POD using different techniques

Parameters → / Algorithm ↓	K	Tw	T1	T2	T3	T4
ALO	32.6712	10	0.0296813	0.560678	0.247449	0.63342
GA	41.708	10	0.194398	0.212408	0. 148983	0.877625
PSO	41.708	10	0.4250	0.802737	0.107363	0.988972
TLBO	81.4742	10	0.166037	0.659183	0.708986	0.444357

The above table 4.2 shows that the optimal parameter values of the controller for different algorithms. The time constant and controller gain of ALO is small as compared with GA, PSO and TLBO optimization technique. The proposed ALO developed model in power system requires less time to attain steady state system and avoid adverse interaction with active power generation and amplification of high frequency noise as compared with above mentioned algorithms.

4.3 Simulation Results of UPFC

Figure (4.10) and (4.11) below shows the simulation results of UPFC control parameters.

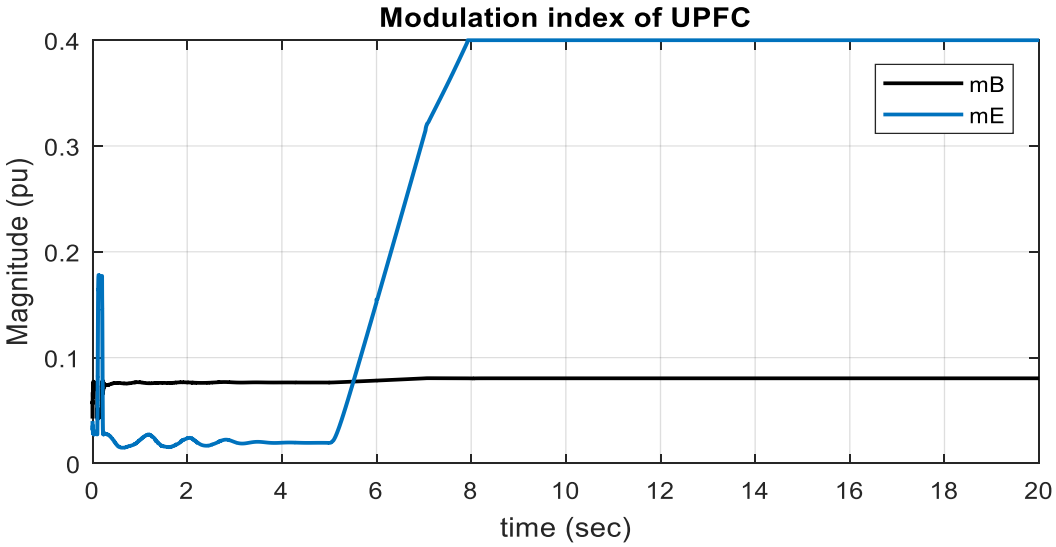

Figure 4.10: Modulation index of series (m_B) and shunt converter (m_E)

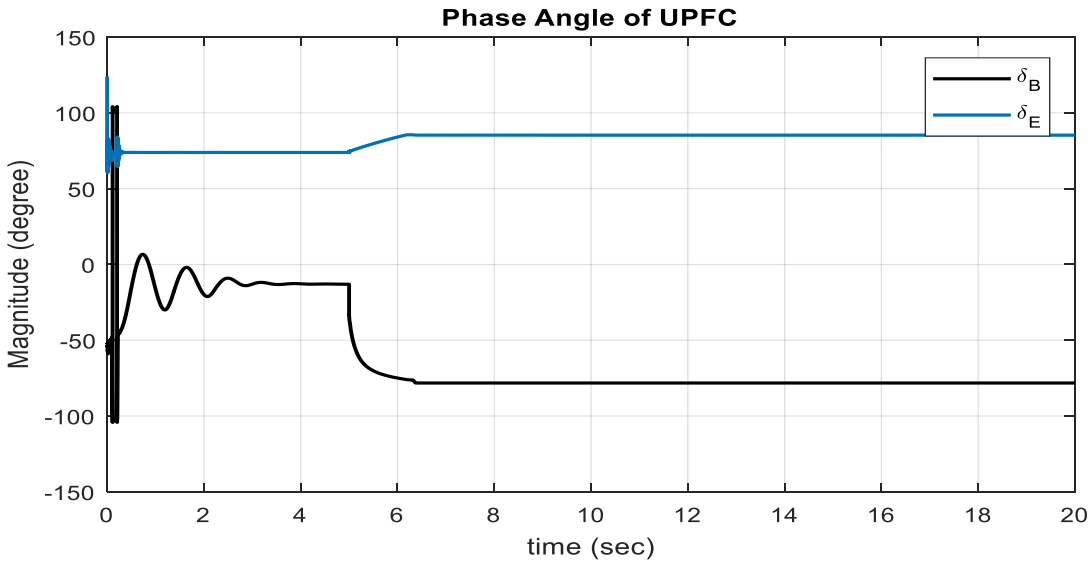

Figure 4.11: Phase angle of series converter (δ_B) and shunt converter (δ_E)

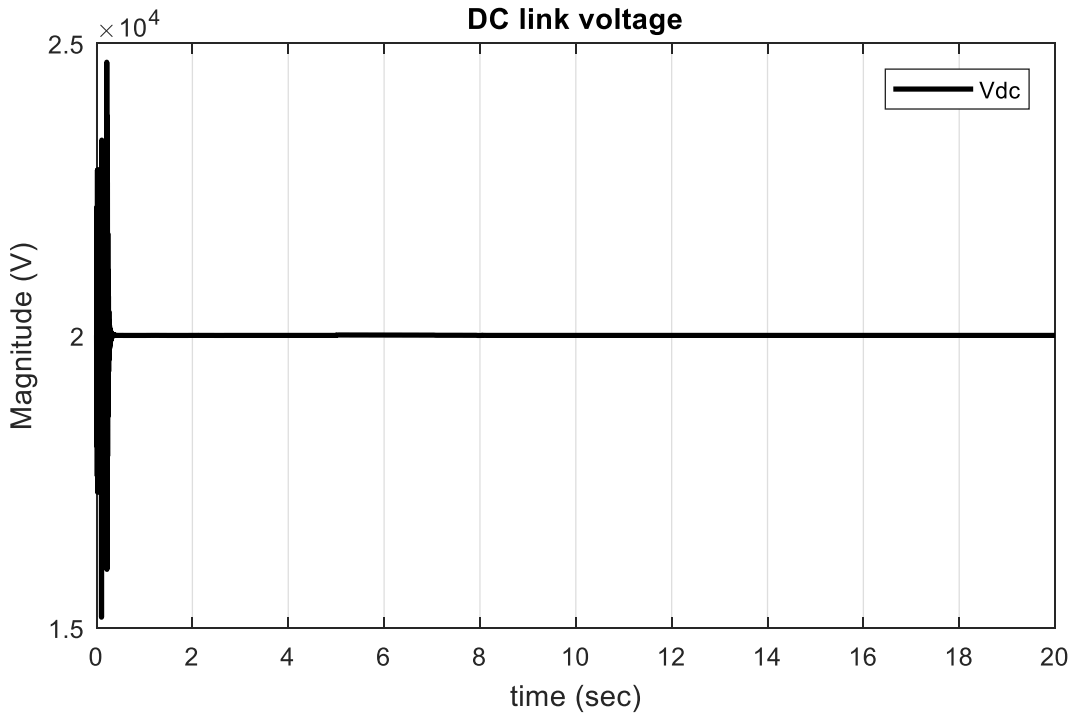

Figure 4.12: DC link capacitor voltage oscillations

From figure 4.12 the DC link capacitor voltage shows very little oscillations. This is because the shunt inverter controls the DC link capacitor voltage effectively. At the instant of fault occurrence, the DC link capacitor voltage drops as it supplies some of its stored energy to the fault. Subsequent to fault removal, the shunt inverter modulates its consumption of real power and controls the DC link capacitor voltage to its reference value. The objective of LFO study is to make certain that whether the designed system can damp out LFO and attains

steady value following clearance of disturbances. In this thesis simulation results have been done for the parameters like rotor angle deviation, rotor speed deviation, active power, reactive power, rotor angle, excitation voltage, rotor speed, terminal voltage, and positive sequence voltage. These parameters clearly shows that the damping out of low frequency oscillation and resulting power system stability enhancement.

However, when the system is disturbed, the output power of the generators either increases or decreases from their maximum output. Figure 4.13, below shows the positive sequence voltage (a), active power generation (b) and reactive power of each bus (c) and for this case the system oscillates and unstable for very short duration but UPFC can damp out those oscillations quickly and attains the system to a steady state value without interruption.

(a)

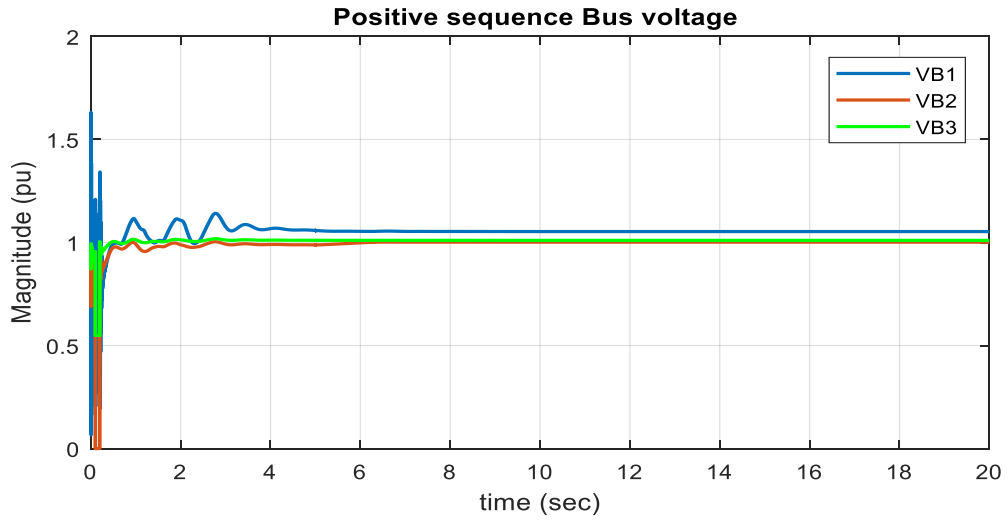

(b)

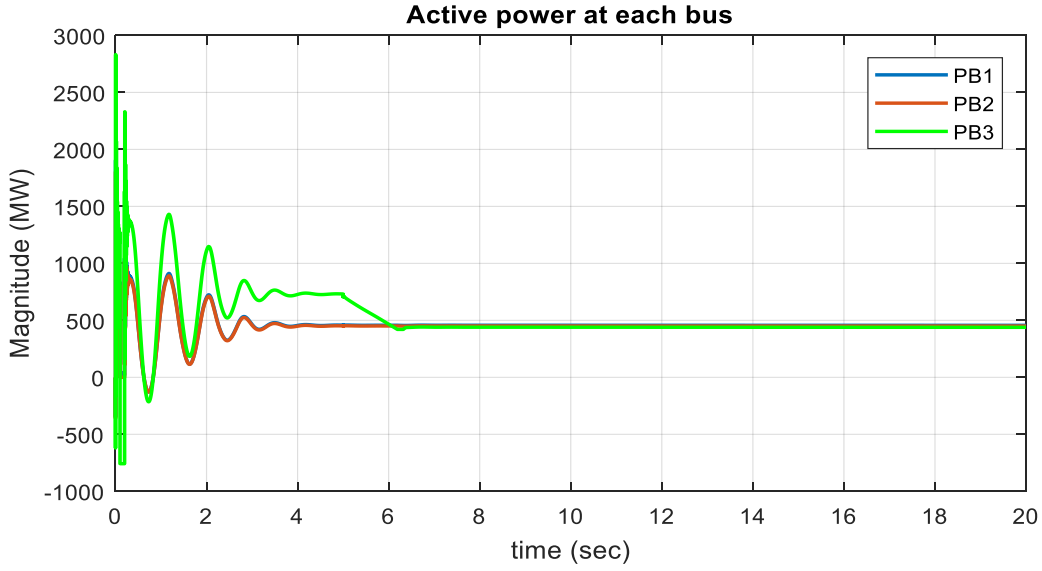

(c)

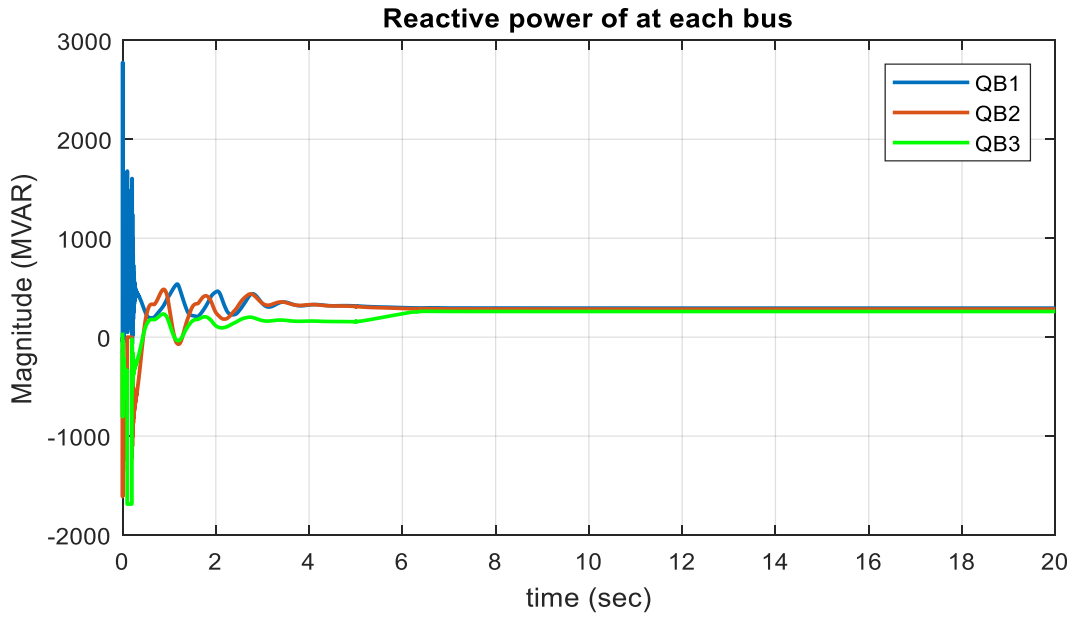

Figure 4.13: Positive sequence voltage (a), active (b) and reactive power (c) using UPFC

The positive sequence voltages, active power and reactive power at different buses could be obtained as shown in figure 4.13(a), (b) and (c). Although there are oscillations for very few seconds the system has been attained its steady state value because of UPFC damps out those oscillations from the system. It is clear from the results that UPFC controller can effectively damp out LFO. This thesis presents the robustness of PSS-UPFC on damping out of LFO and power system stability improvement. The time taken to damp out LFO is much reduced when UPFC is installed to the system and the system get stabilized with in small duration of time.

4.4 Comparison of Simulation Results with Different Algorithms

For comparative analysis of different algorithms (GA, PSO, TLBO and ALO) the objective function and constraint equation provided is the same for those mentioned algorithms. The parameters of the controllers are properly tuned for all algorithms but the result is different because of the characteristics of the algorithm and the compatibility of the technique with the proposed system. Simulation result illustrates that the proposed objective function based optimized PSS and UPFC controller with ALO has good performance in damping LFO and stabilizes the system quickly as compared to the conventional fixed gain model, GA, PSO and TLBO method. Table 4.3 clearly shows the tabular representation of power system states which are depicted from figure 4.14 to figure 4.18 shown below.

Table 4.3: Maximum overshoot and settling time of power system parameters

	Maximum overshoot					Settling time (sec)				
	Existing	GA	PSO	TLBO	ALO	Existing	GA	PSO	TLBO	ALO
$\Delta\omega$	0.0182	0.0181	0.0180	0.0180	0.0167	oscillatory	6.97	11.85	14.52	4.62
$\Delta\delta$	-2.165	-1.932	-1.935	-1.933	-1.865	oscillatory	6.27	9.78	12.23	3.95
δ	2.1509	2.1899	2.1939	2.1959	2.1937	oscillatory	3.2	4.87	7.8	2.75
ω	0.017	0.0173	0.0185	0.0180	0.016	oscillatory	7.04	11.32	13.6	4.68
F	0.87	0.89	0.90	0.89	0.84	oscillatory	7.02	11.63	14.35	4.28

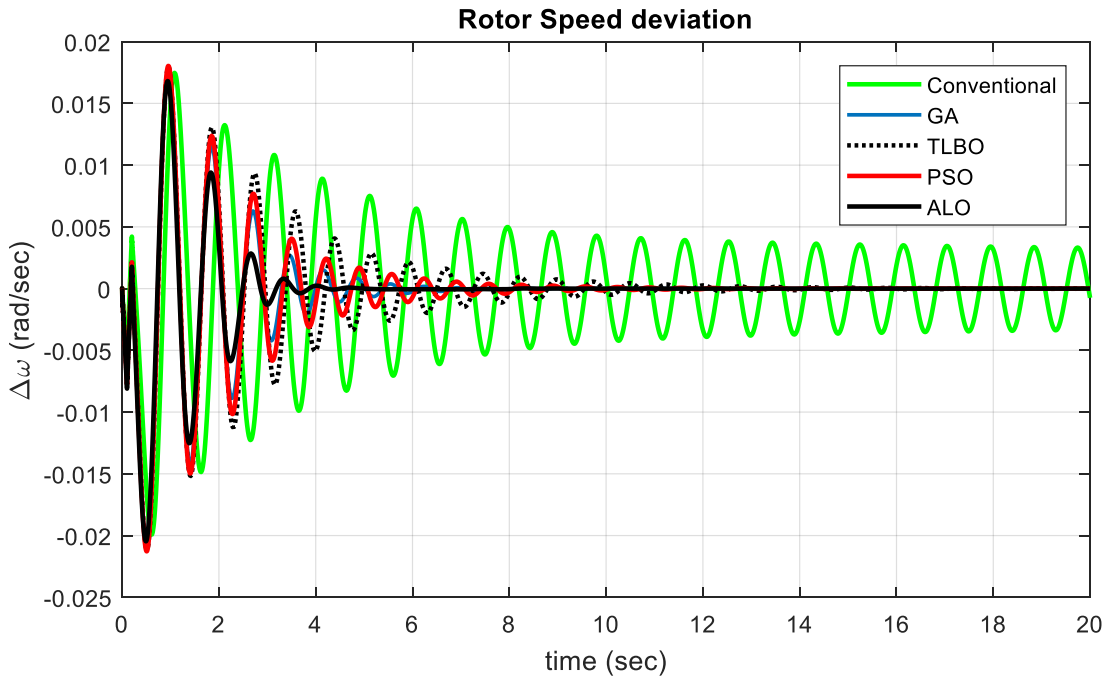

Figure 4.14: Rotor speed deviation of different algorithms with conventional fixed gain

From figure 4.14 above the rotor speed deviation of different algorithms with conventional fixed gain in which the maximum overshoot and settling time of ALO is less than other optimization algorithms. Generally ALO technique gives more accurate results than the rest of the techniques to damp out low frequency oscillation within shortest possible time. Simulation result demonstrated that the ALO technique is most effective for solving and damping out of LFO problem as the maximum overshoot and settling time of angular frequency deviations are relatively small compared to other techniques. The obtained results are promising and proves the potential of the proposed LFO control strategy based ALO algorithm to ensure power system stability.

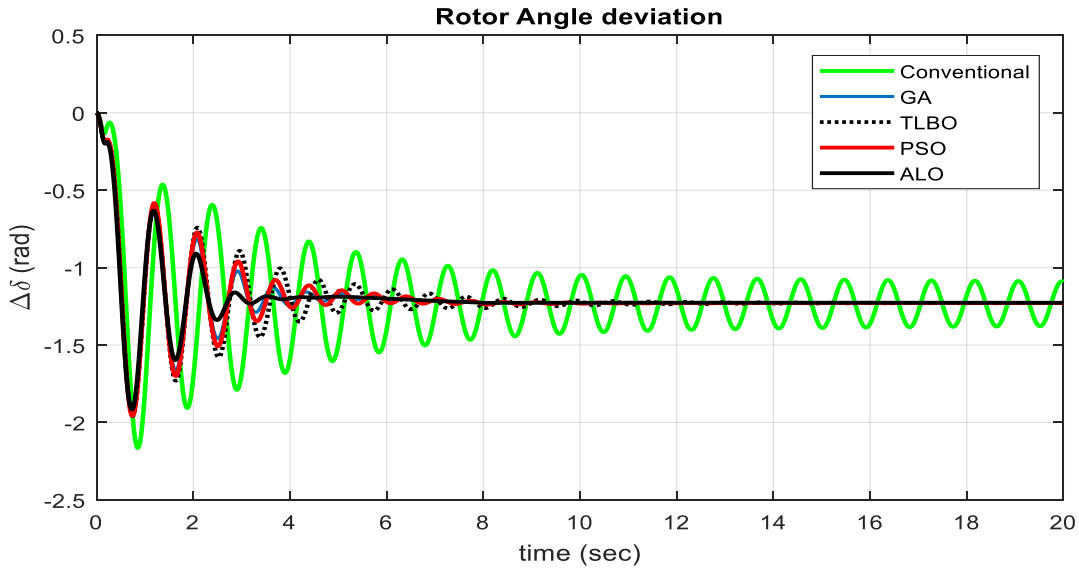

Figure 4.15: Rotor angle deviation of different algorithms with conventional fixed gain

From figure 4.15 above the rotor angle deviation of different algorithms with conventional fixed gain model in which the maximum overshoot and settling time of ALO is less than the remaining techniques. ALO gives more accurate results than the rest methods to damp out low frequency oscillation within shortest possible time.

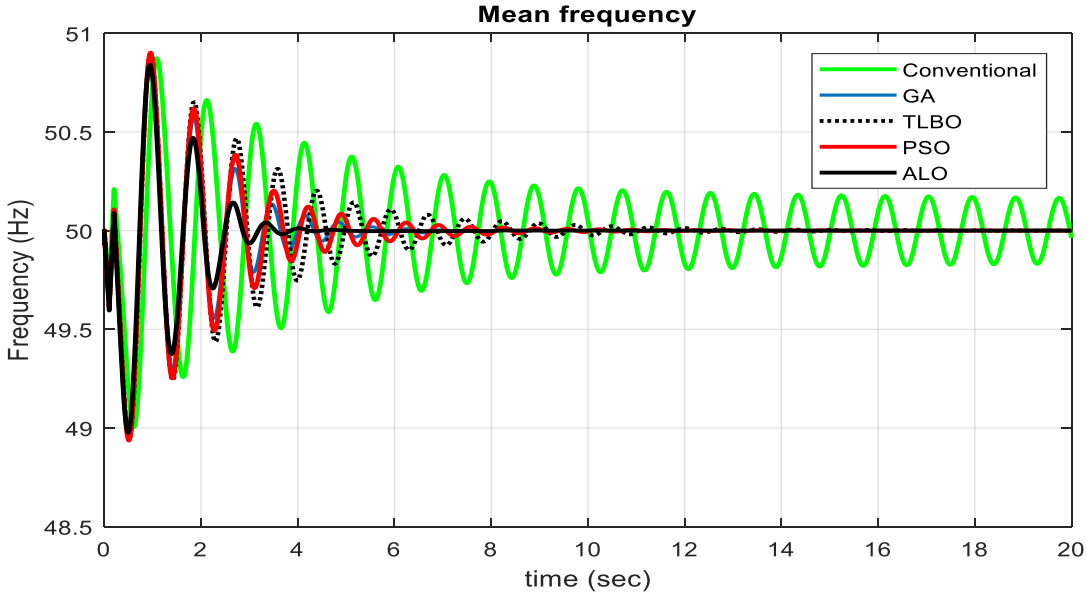

Figure 4.16: Frequency deviation of different algorithms with conventional fixed gain

From figure 4.16 above the frequency of different algorithms with conventional fixed gain in which the maximum overshoot and settling time of ALO is less than the remaining techniques and generally ALO technique gives more accurate results than the rest methods to damp out low frequency oscillation within shortest possible time.

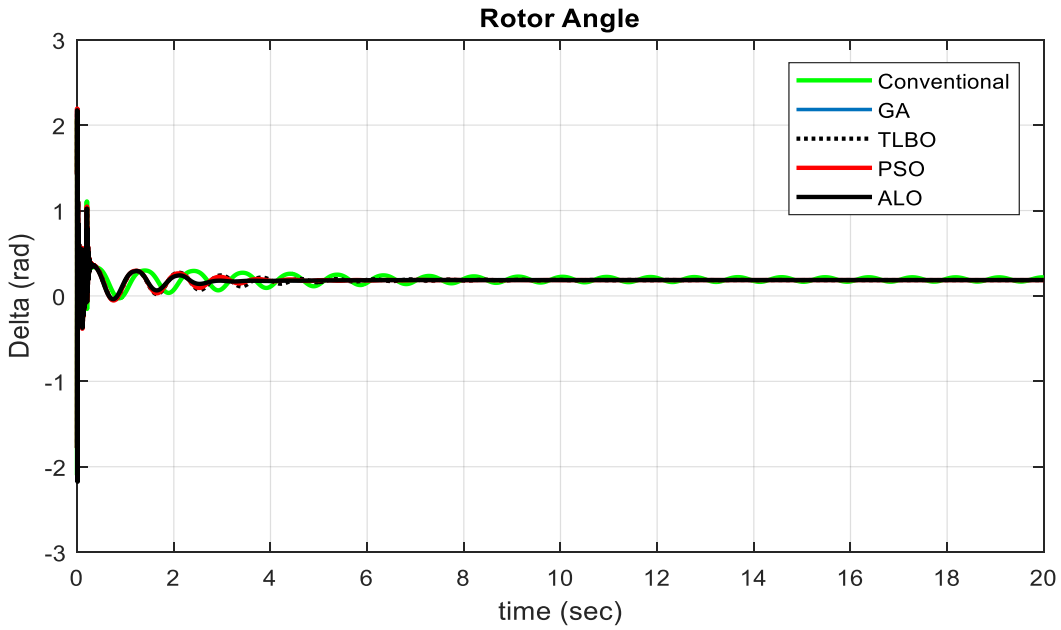

Figure 4.17: Rotor angle of different algorithms with conventional fixed gain model

From figure 4.17 above the rotor angle of different algorithms with conventional fixed gain model in which the maximum overshoot and settling time of ALO is less than the remaining techniques.

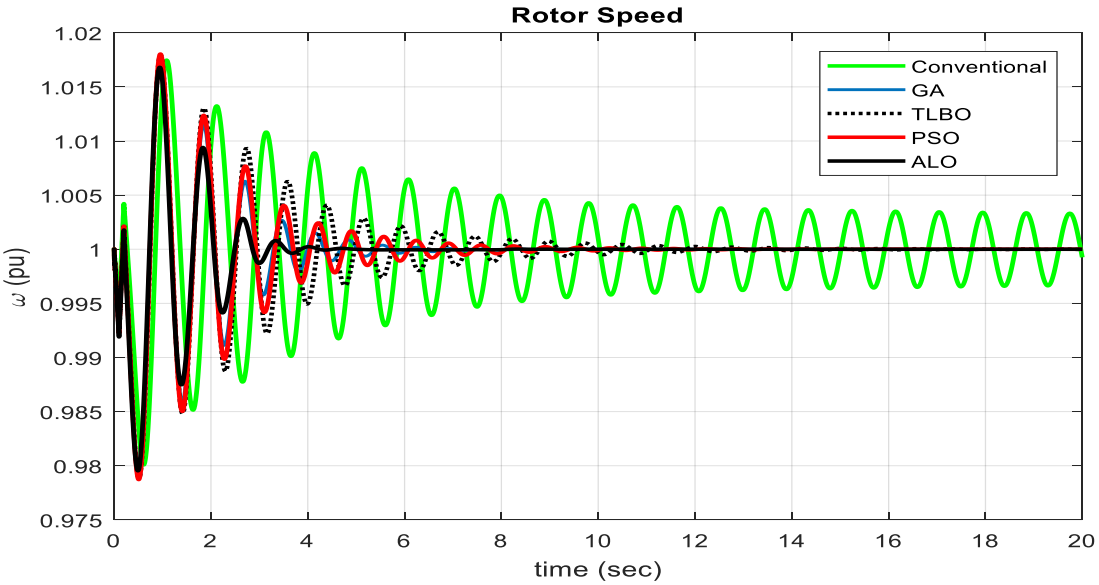

Figure 4.18: Rotor Speed of different algorithms with conventional fixed gain model

From the simulation result shown in figure 4.18 above the rotor speed of different algorithms in which the maximum overshoot and settling time of ALO is less than the remaining techniques and generally ALO gives more accurate results when compared to the other techniques to damp out low frequency oscillation within shortest possible time.

Although LFO are suppressed from the network using ALO based system, other applied techniques also damp out LFO but the only difference here is that the magnitude of maximum overshoot and settling time attain steady state system. Since the objective function and constrain equation incorporated in the mentioned algorithm is the same the result is nearly similar. Using damping ratio and damping factor as the objective function in the optimization process based ALO algorithm, the time of suppressing LFO is very small compared with the time given by other applied methods. The proposed ALO has good performances and gives better result in terms of minimizing fluctuations of low frequency oscillations and shows superiority compared with conventional fixed gain, GA, PSO and TLBO approaches. The comparative study shows that the ALO algorithm could rapidly converge to the correct optimal.

4.5 Comparison of Simulation Results with Different FACTs Device

Figure (4.19) and (4.20) shown below are the rotor angle deviation and speed deviation employed for PSS only, PSS equipped with SVC, TCSC, SSSC, STATCOM and UPFC with POD controller. Comparison analysis on the impact of all controllers to UPFC for controlling the effect of LFO to SMIB system had been illustrated from figure 4.19 to figure 4.23 below. So, the detailed explanation of maximum overshoot and settling time for different FACTS device combined with PSS has been presented on table 4.4 below.

Table 4.4: Maximum overshoot and settling time different FACTS device

Devices	Maximum overshoot					Settling time (sec)				
	$\Delta\omega$(pu)	$\Delta\delta$(rad)	δ (rad)	ω(pu)	F(Hz)	$\Delta\,\omega$	$\Delta\delta$	δ	ω	F
PSS	0.0192	-2.331	2.910	0.019	0.96	9.85	9.983	3.317	9.517	9.6
SVC	0.0179	-2.283	2.9118	0.018	0.90	8.12	7.7	3.6	7.45	7.82
TCSC	0.0171	-2.282	2.9078	0.0171	0.87	6.95	7.417	4.167	6.533	6.63
SSSC	0.0169	-2.241	3.1498	0.0178	0.81	7.73	8.283	6.517	7.767	8.07
STATCOM	0.0176	-2.282	3.1501	0.0170	0.88	7.08	7.317	3.167	7.067	6.82
UPFC	0.0162	-2.230	2.9058	0.016	0.80	4.52	6.196	2.717	4.602	4.35

The above table 4.4 clearly shows the tabular representation and comparison results of different FACTS device which are depicted from figure 4.19 to 4.23.

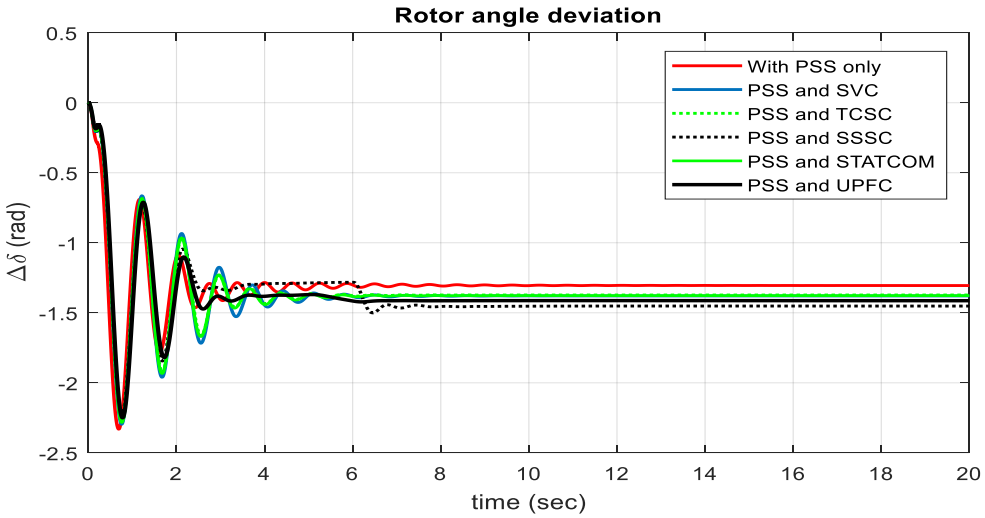

Figure 4.19: Rotor angle deviation of different FACTS device

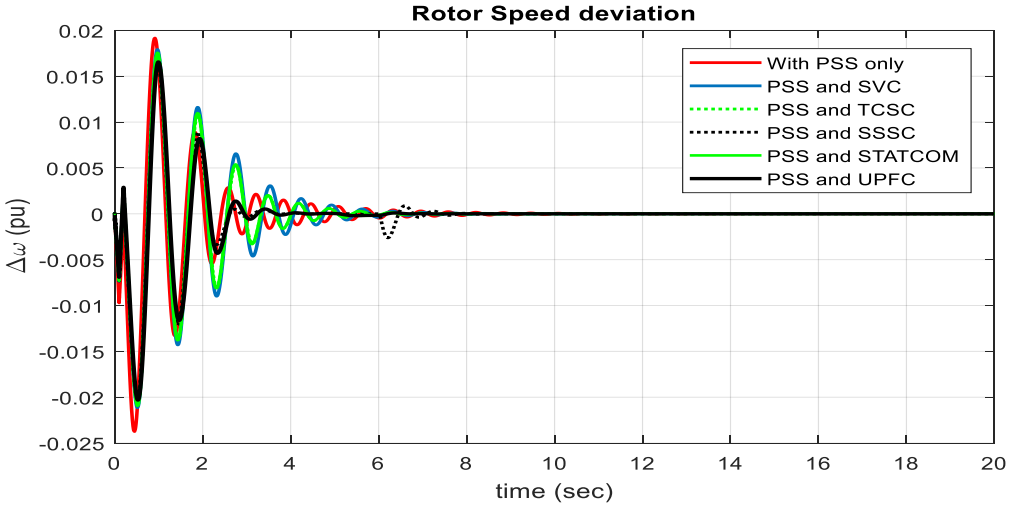

Figure 4.20: Rotor Speed deviation of different FACTS device

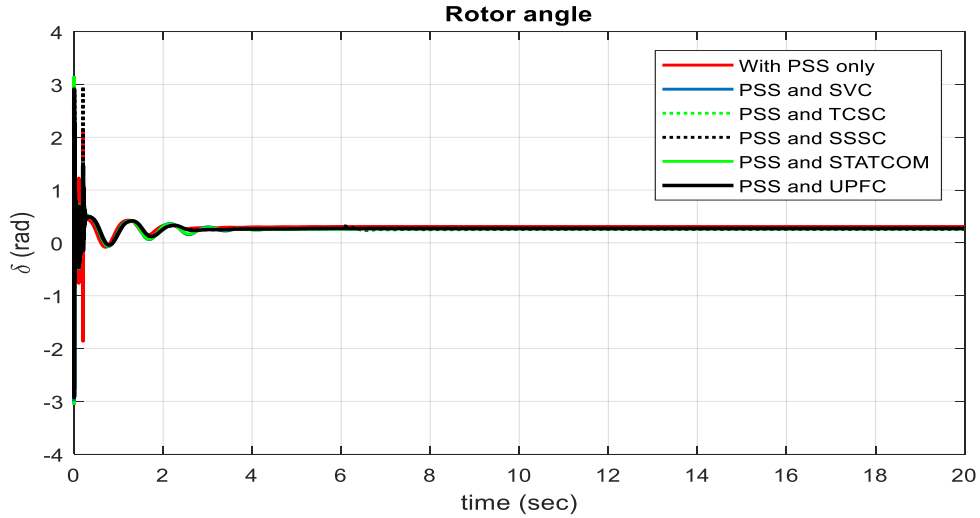

Figure 4.21: Rotor angle of different FACTS device

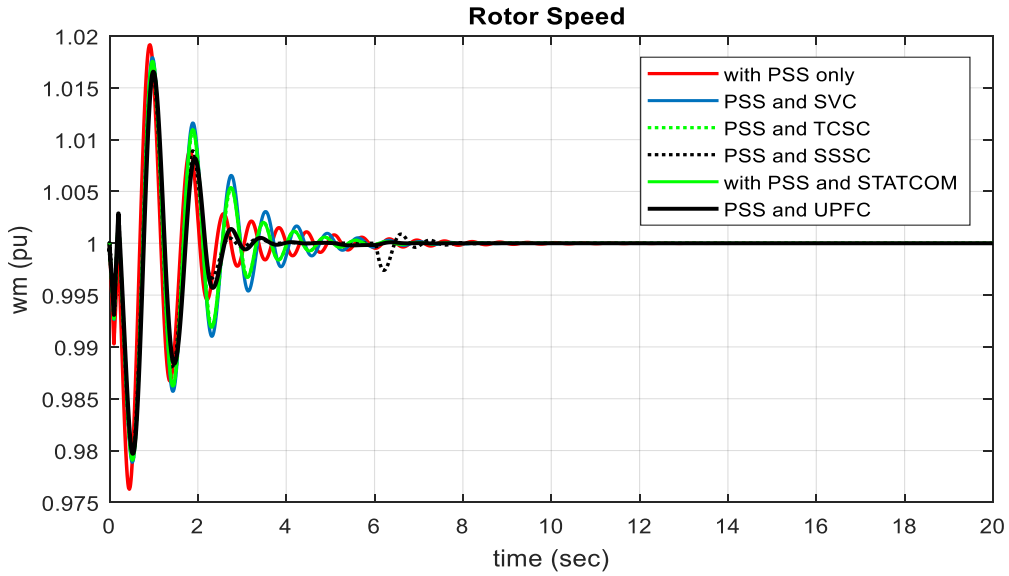

Figure 4.22: Rotor Speed of different FACTS device

Figure 4.21 and figure 4.22 shows that the rotor angle and rotor speed of incorporating different FACTs device. In this case the maximum overshoot and settling time of UPFC is smaller that shows the superiority of the proposed system.

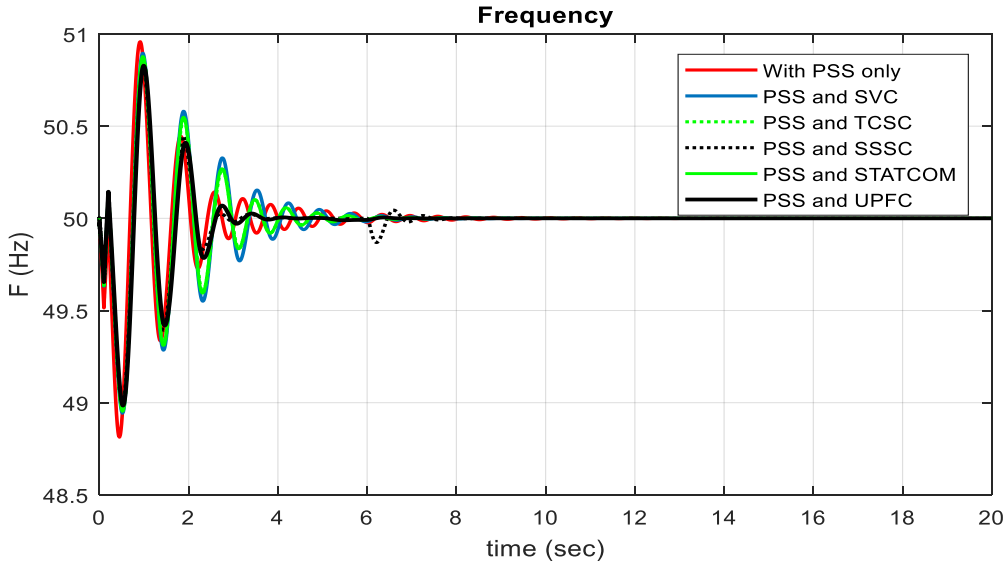

Figure 4.23: Frequency of different FACTS device

The above result shows that UPFC is the most comprehensive FACTs devices for Tana Beles 400kV high-voltage transmission networks to effectively damp out low-frequency oscillation. It is developed for damping out low frequency oscillation and improve the transmission capacity of power system and power system transient stability. Moreover, it can improve damping of system oscillation and power angle stability. In this thesis, UPFC is intended to damp out low frequency oscillation of 400kV line for northwest region of

Ethiopian electric network. When the NWR of Ethiopian power system is exposed to large power unbalance between generation and load variations, the UPFC adjusts power system quantitative values to balance the power by delivering voltage, active power and reactive power to or from the compensators. As compared to other devices the proposed UPFC has the most effective FACTS devices having short settling time and less maximum overshoot. For comparative analysis of different FACTs device the objective function and constraint equation provided is the same for those mentioned device to optimally size FACTS device controller. The parameters of the controllers are properly tuned for all FACTs but the result is different because of the different behavior of FACTs compatibility with the proposed system. Although LFO are suppressed from the network using UPFC devices, other applied FACTs also damp out LFO but the only difference here is that the magnitude of maximum overshoot and settling time to attain steady state system.

4.6 System Simulation Results at Various Operating Conditions

In a power system, the operating load varies over a wide range. It is extremely important to investigate the variation of operating conditions on the dynamic performance of the system. To evaluate the performance of the proposed simultaneous sizing approach the response with proposed controllers are compared with the response of PSS and UPFC individual controller sizing. The speed deviation, rotor angle deviation, rotor speed, rotor angle and other power system states are determined and discussed below at different operating conditions with conventional existing system, PSS only and UPFC equipped with PSS sizing of controllers. The real-time sizing of PSS and UPFC controller by the proposed approach can considerably damp out the unwanted LFO and enhances power system stability performance of Tana Beles 400kV transmission network. Three different cases as nominal, light and heavy loading conditions are considered over a wide range of loading conditions for comparison purpose.

4.6.1 Simulation result at normal loading condition

Time domain simulation for normal operating condition was carried out to compare the performance of ALO optimized PSS-UPFC with conventional existing system in damping out LFOs of an electric network. A 10% pulse input of mechanical torque was applied and the corresponding system responses are presented from figure (4.24) to (4.30) for 20sec. From these results the oscillations does not damped in case of conventional existing system

due to some disturbance while the coordinated controller of PSS equipped with UPFC shows better damping effect to low frequency oscillations.

Table 4.5: Maximum overshoot and settling time at normal loading conditions

Power system states	Maximum overshoot			Settling time (sec)		
	Existing system	PSS only	PSS and UPFC	Existing system	PSS only	PSS and UPFC
$\Delta\omega\ (pu)$	0.01738	0.01737	0.0165	Oscillatory	10.37	4.617
$\Delta\delta\ (rad)$	-2.048	-2.049	-1.908	Oscillatory	10.45	4.133
$\delta\ (rad)$	2.386	2.385	2.155	14	5.417	2.897
$\omega\ (pu)$	0.017	0.017	0.016	Oscillatory	10.73	4.483
F (Hz)	0.87	0.86	0.82	Oscillatory	10.72	4.583
$\Delta V\ (pu)$	1.5571	1.5281	1.5131	Oscillatory	10.32	4.15
$E_t\ (pu)$	7.393	7.509	7.67	Oscillatory	16.47	4.967

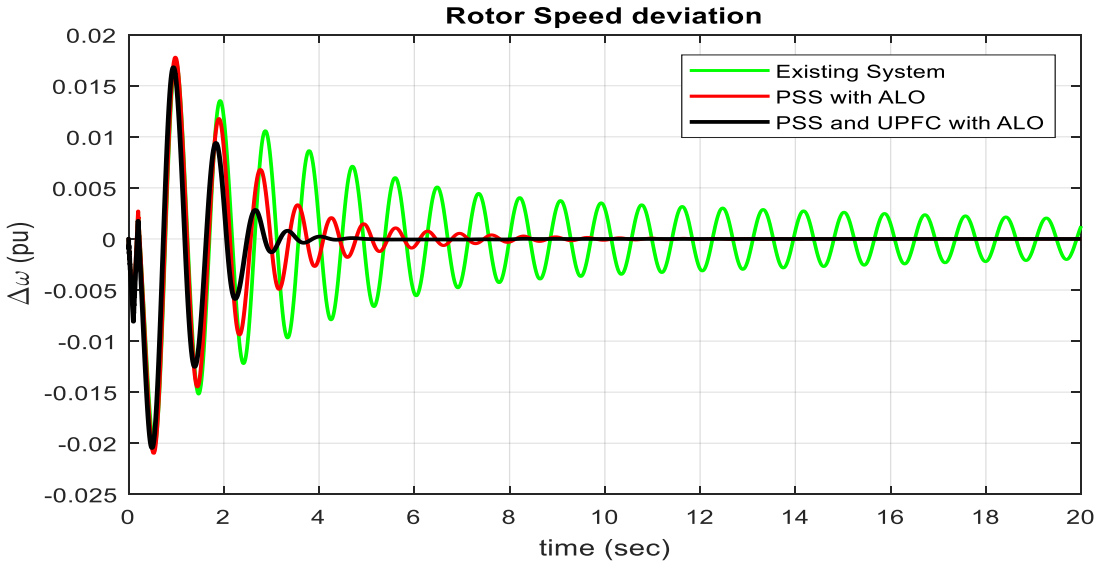

Figure 4.24: Rotor speed deviation of the system at normal loading condition

From figure 4.24 the rotor speed deviation ($\Delta\omega$) of the generator has been demonstrated with conventional existing system, with PSS and UPFC equipped with PSS at nominal loading conditions. Due to small disturbance of turbine the maximum overshoot varies from 0.06% to 5.06% with settling time from 48.15% to 76.92% for PSS only and PSS equipped with UPFC respectively which quickly damp out rotor speed oscillations and attains steady state system. Therefore the generator rotor speed oscillations with PSS and UPFC equipped with a POD controller shows increased damping as compared to conventional existing system

and only PSS controller. In general, with conventional existing system the result is oscillatory and becomes unstable while stability of the system is maintained and LFO are effectively damped out when PSS is equipped with UPFC.

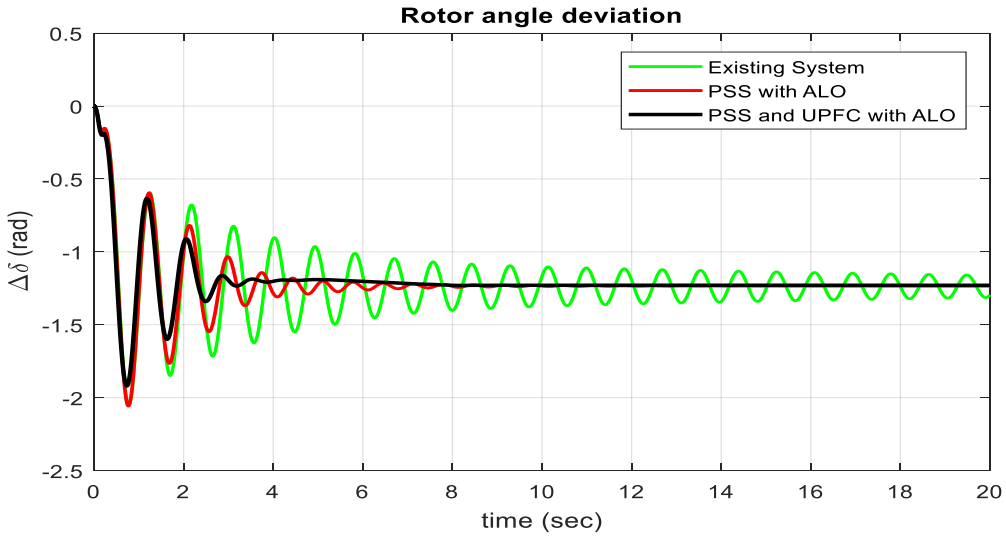

Figure 4.25: Rotor angle deviation of the system at normal loading condition

Rotor angle deviation with conventional existing system is an oscillatory system and takes a long time to damp out LFO while when UPFC is equipped with PSS and POD controller the system damps out and diminishes the oscillations with very short time. So, using ALO based UPFC controller can quickly damp out LFO. When rotor angle deviation is subjected to a positive change $\Delta\delta > 0$ then the power would be subjected to ΔP and the machine falls towards instability. While when $\Delta\delta < 0$ the machine had returned back to its initial state.

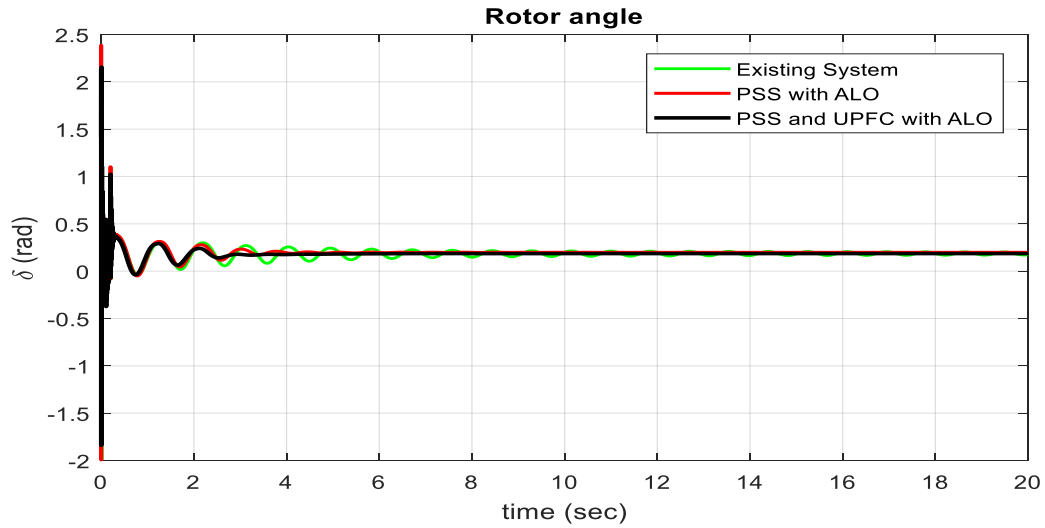

Figure 4.26: Rotor angle of the system at normal loading condition

The results of PSS and UPFC equipped with POD controller for series inverter has actually shown that POD controller is appropriate and provides improved damping to rotor angle oscillations. The time taken to damp out low frequency oscillation is 2.897 sec for PSS with UPFC, 5.417 sec for PSS only and 14 sec for conventional existing system. According to IEEE standards of rotor angle stability, the obtained result shows that the generator oscillates and attains steady state values. Therefore, the generator fulfills inter area mode of oscillation having 2.386 rad, 2.385 rad and 2.155 rad peak overshoot for conventional existing system, with PSS only and PSS equipped with UPFC respectively. Since δ starts to decrease after reaching a maximum value, the machine attains its steady state value. The settling time of PSS only and PSS equipped with UPFC has 61.3% and 79.3% with maximum overshoot of 0.05% and 9.7% respectively.

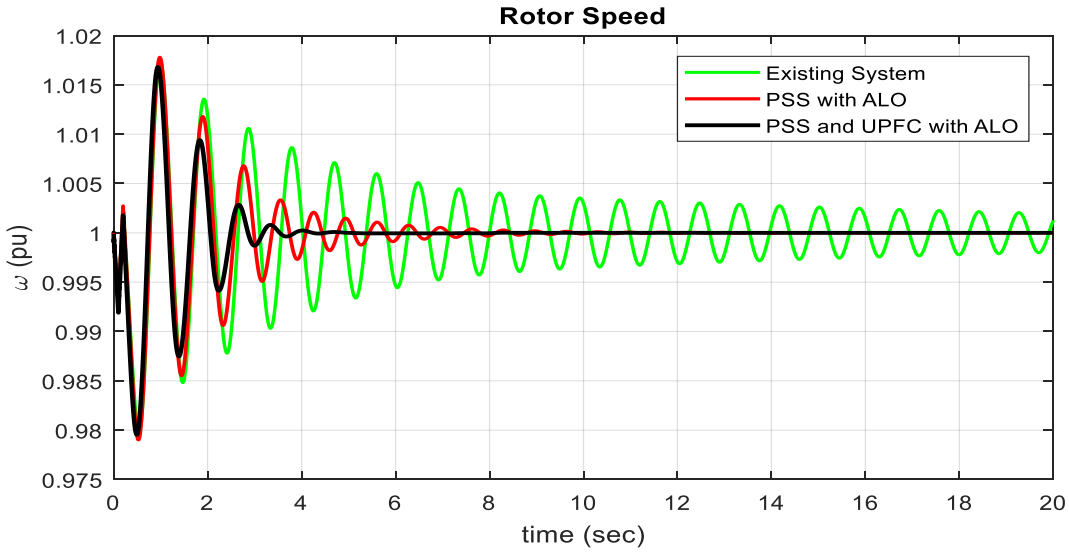

Figure 4.27: Rotor speed of the system at normal loading condition

Figure 4.27 shows generator rotor speed (ω) of existing system and PSS equipped with UPFC controller. A step increase in load is taken as a disturbance which shows that the per unit speed of Tana Beles generator. The speed of generator oscillates from 0.9798 to 1.016 with smallest settling time around 4.483 second which indicates that the addition of UPFC has improved damping of the generator rotor speed oscillations. The rotor speed oscillations of the generator with conventional existing system is oscillatory and when only PSS is added, it takes around 10.73 seconds while when PSS is equipped with UPFC, it takes around 4.483 seconds to damp out oscillations and attains steady state system. The rotor speed with UPFC

and PSS equipped with POD controller shows increased damping as compared to conventional existing system and PSS only.

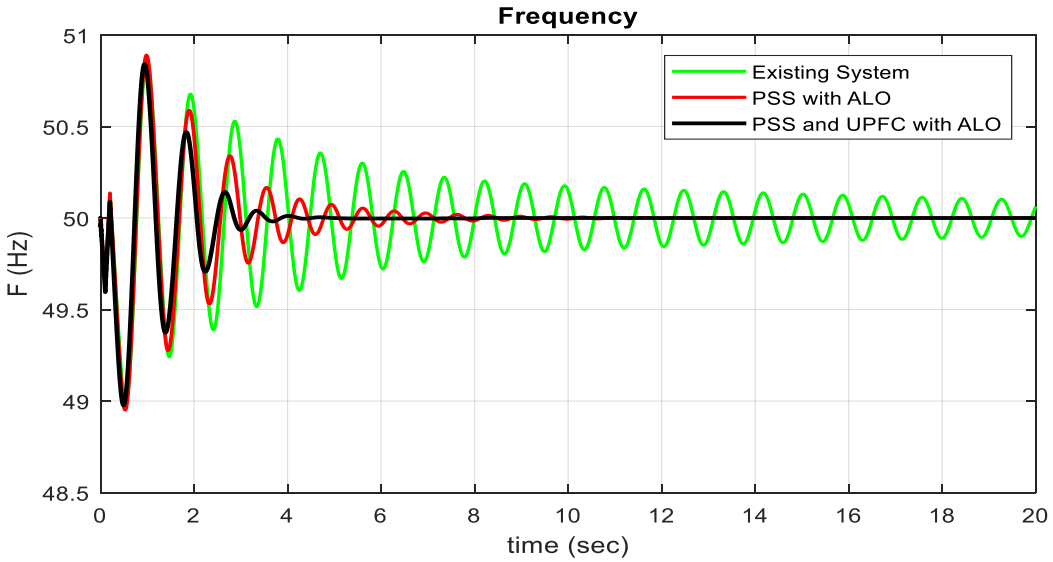

Figure 4.28: Frequency of the system at normal loading condition

Frequency with conventional existing system is oscillatory which varies between 48.94Hz and 50.87 Hz which takes a long time to damp out oscillations and attains steady state operation and with PSS only a frequency varies between 48.95Hz and 50.86Hz while when UPFC is equipped with PSS and POD controller the system can damp out LFO and attains steady state system with 4.583 seconds settling time and maximum overshoot varies between 49Hz and 50.82Hz.

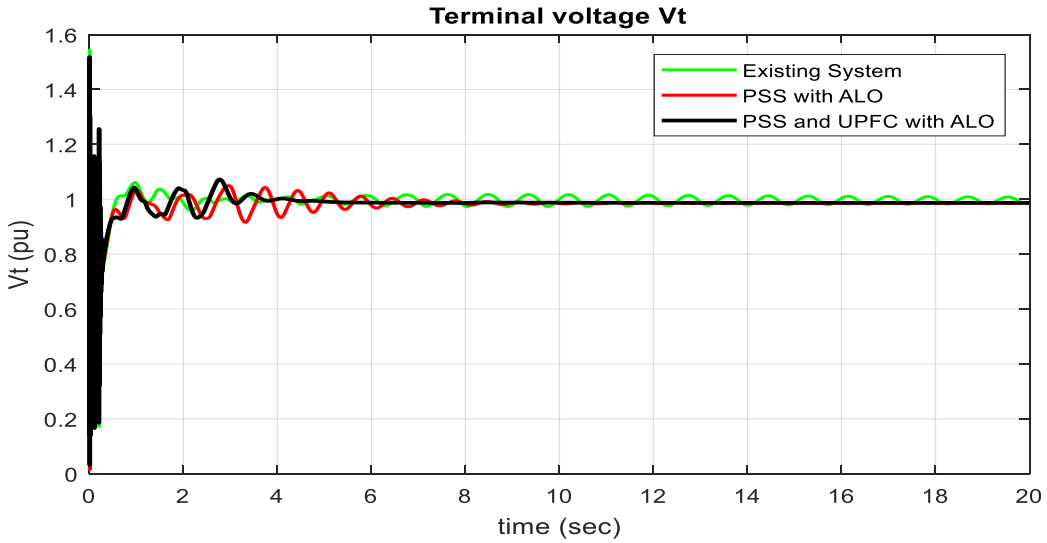

Figure 4.29: Terminal voltage of the system at normal loading condition

Figure 4.29 Shows that the terminal voltage V_t is 1 pu throughout the simulation. Voltage stability is the ability of power system to keep steady voltages at all buses after disturbance from a given initial loading conditions. The addition of UPFC equipped with PSS is to damp out low frequency oscillation of power system. But from the simulation result, there is a very small significant effect on terminal voltage of the system because the terminal voltage of synchronous generator is controlled by automatic voltage regulator. At normal operation the model runs in steady state.

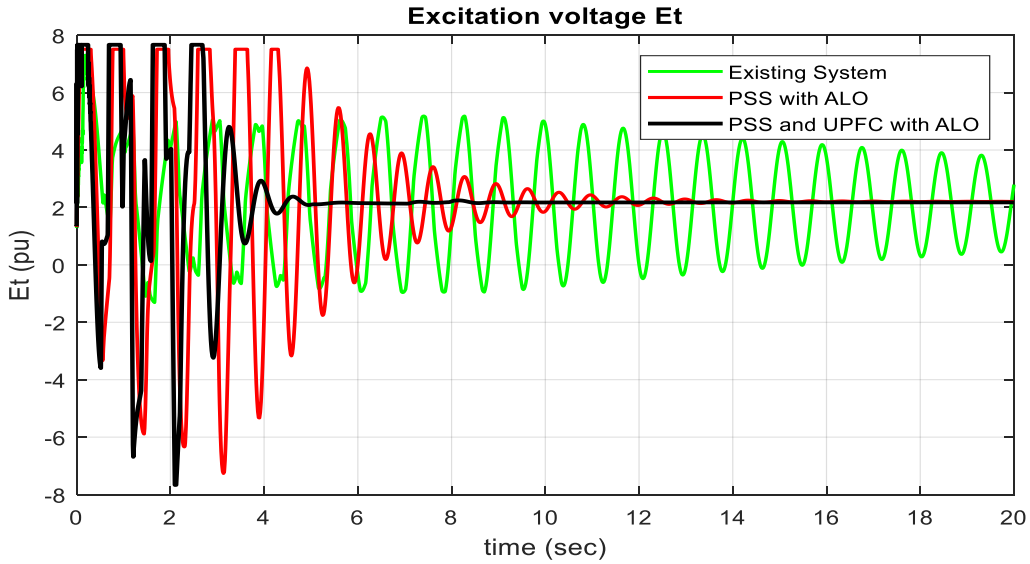

Figure 4.30: Excitation voltage of the system at normal loading condition

From the result shown in figure 4.30 it is observed that the excitation voltage can go as high as 7.393 pu with conventional existing system and it is oscillatory to attain steady state but for UPFC equipped with PSS the maximum overshoot has 7.67 pu and stabilizes quickly after 4.967 sec. Generally, at normal loading condition the simulation result shows that the system employed with PSS & UPFC controller provides good damping characteristics to low frequency oscillations. When compared with conventional existing system, PSS equipped with UPFC controller quickly stabilizes the system under a mechanical disturbance present in the system. Hence it can conclude that the system with proper and optimal tuning of damping controller can effectively damp out the low frequency oscillations and provides good damping characteristics to attain power system steady state stability. From the above results both PSS only and optimized UPFC-PSS damp out the LFOs of the electric network after being subjected to mechanical disturbance but optimized UPFC-PSS provides quick response compared to conventional existing system and PSS only. Therefore, the

conventional system took relatively long time over UPFC equipped with PSS to damp out the LFOs originated by the external mechanical disturbance to all system states.

4.6.2 Simulation result at heavy loading condition

To test the robustness of proposed PSS-UPFC controller a sudden increase in load is taken as a disturbance and the system is operated even in heavy loading condition. From the results obtained below the conventional existing system is oscillatory and generator loses their synchronism.

Table 4.6: Maximum overshoot and settling time of power system at heavy loading

Power system states	Maximum overshoot			Settling time (sec)		
	Existing system	PSS only	PSS and UPFC	Existing system	PSS only	PSS and UPFC
$\Delta\omega\ (pu)$	0.01748	0.01747	0.0167	Oscillatory	10.35	4.767
$\Delta\delta\ (rad)$	-2.075	-2.075	-1.942	Oscillatory	10.37	4.183
$\delta\ (rad)$	2.372	2.373	2.144	15	4.829	2.75
$\omega\ (pu)$	0.018	0.0175	0.016	Oscillatory	9.733	4.667
F (Hz)	0.885	0.88	0.84	Oscillatory	9.733	4.6
$\Delta V\ (pu)$	1.5553	1.5253	1.3533	Oscillatory	9.633	4.076
$E_t\ (pu)$	7.369	7.829	7.66	Oscillatory	15.28	4.981

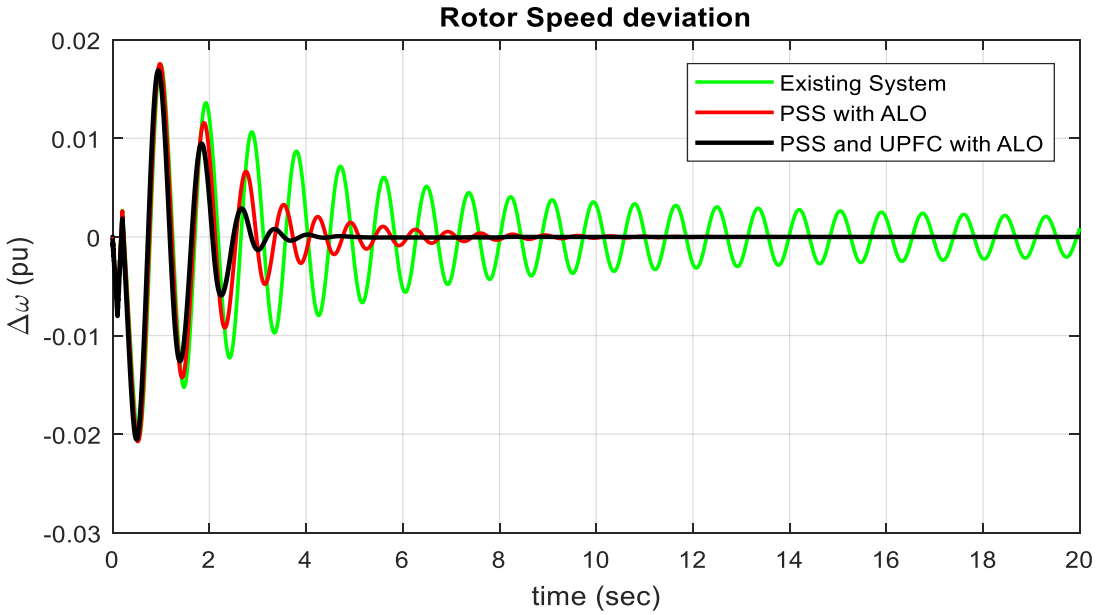

Figure 4.31: Rotor speed deviation of the system at heavy loading condition

Figure 4.31 describes the rotor speed deviation of the generator with and without PSS equipped with UPFC at heavy loading conditions. The addition of UPFC has improved damping of generator rotor speed oscillations. Due to small disturbance of turbine the maximum overshoot is 0.01748, 0.01747, 0.0167pu with settling time of oscillatory, 10.35 and 4.767 second for conventional existing system, PSS only and UPFC equipped with PSS respectively. Therefore the generator rotor speed oscillations of PSS and UPFC equipped with a POD controller which quickly damp out oscillations and attains steady state system as compared to conventional existing system and only PSS controller at heavy loading condition.

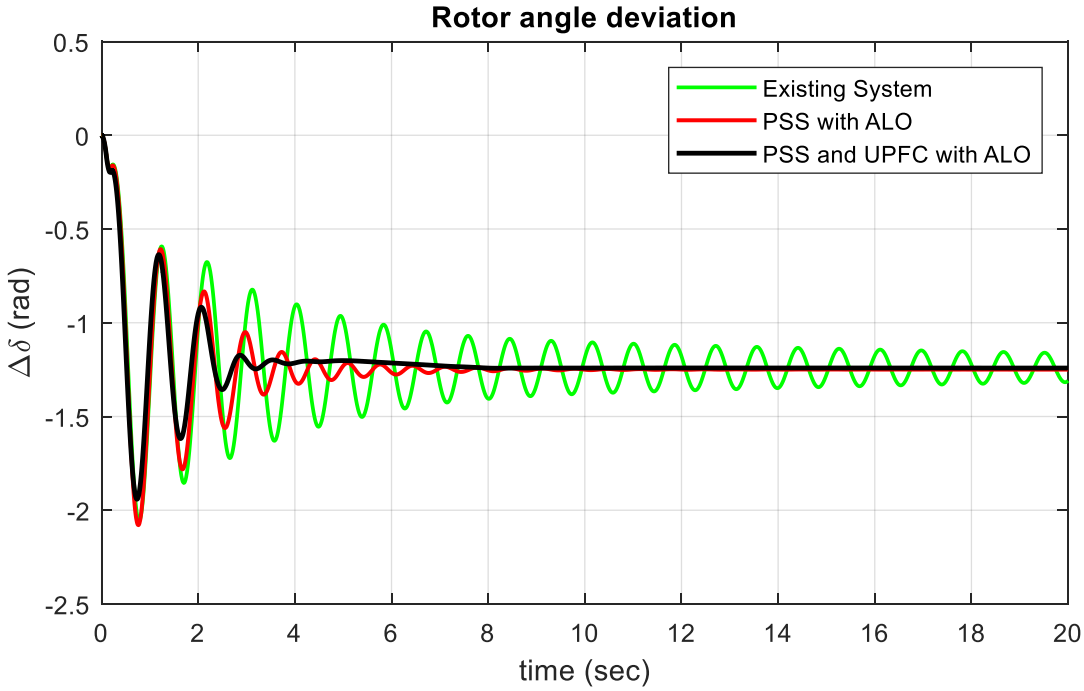

Figure 4.32: Rotor angle deviation of the system at heavy loading condition

Rotor angle deviation of conventional existing system is oscillatory and takes a long time to damp out low frequency oscillations and attains steady state operation. While when UPFC is equipped with PSS and POD controller the system damps out LFO and diminishes the oscillations with very short time. So, using ALO based UPFC damping controller can quickly damp out low frequency oscillations. When rotor angle deviation is subjected to a positive change $\Delta\delta > 0$ then the power would be subjected to ΔP and the machine falls towards instability. While when a deviation $\Delta\delta < 0$ the machine had been attained back to its initial steady state.

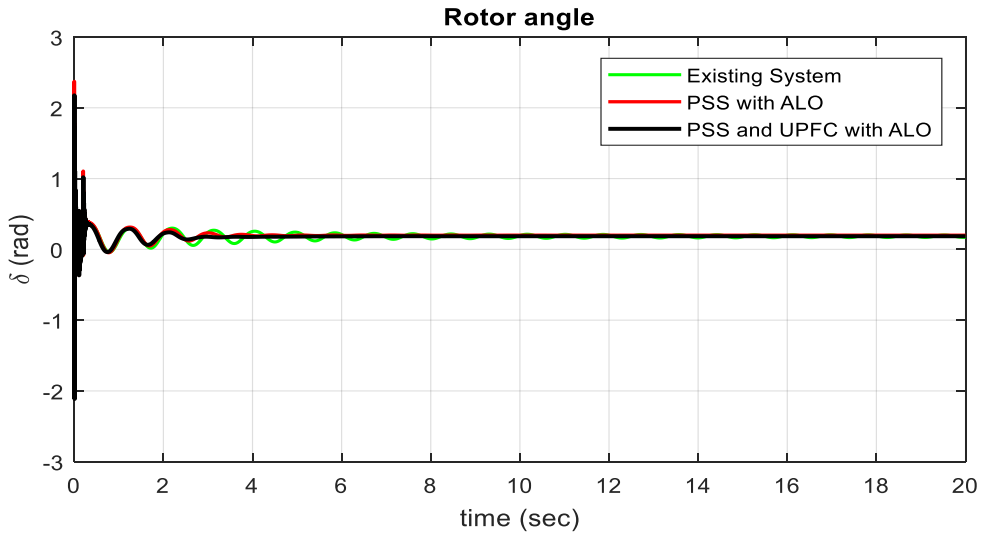

Figure 4.33: Rotor angle of the system at heavy loading condition

According to IEEE standards of rotor angle stability, the generator fulfill inter area mode of oscillation having a maximum overshoot of around 2.372, 2.373 and 2.144 rad for conventional existing system, with PSS only and PSS equipped with UPFC respectively. The settling time to damp out low frequency oscillations are 2.75 sec for PSS with UPFC, 4.829 sec for PSS only and 15 sec for conventional existing system. Since δ starts to decrease after reaching a maximum value, the machine attains to its steady state. Using only PSS has a settling time of 67.9% and when PSS is equipped with UPFC has the settling time of 81.7% which shows that the proposed system has a damping efficiency of 81.7% to attain steady state operation.

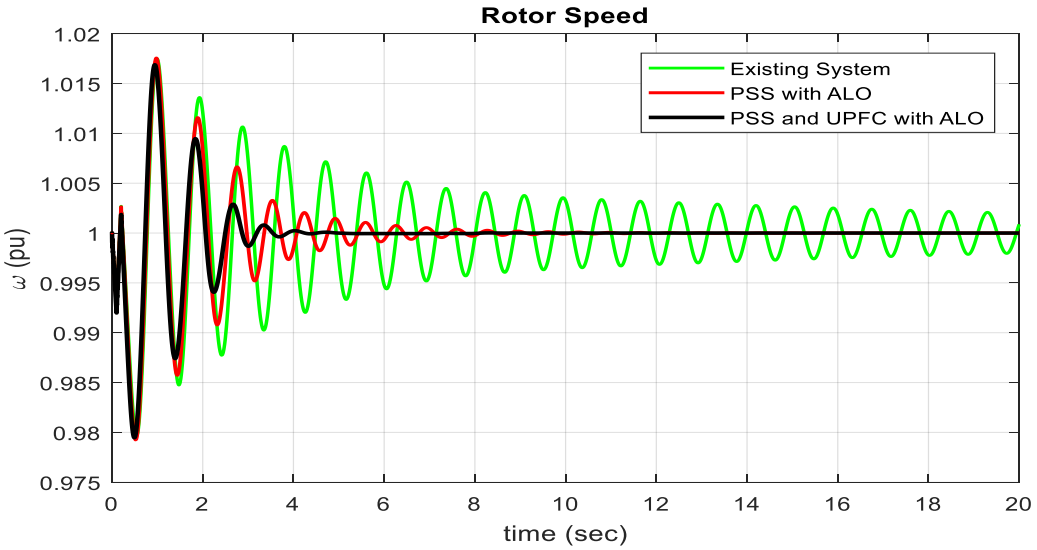

Figure 4.34: Rotor speed of the system at heavy loading condition

Figure 4.34 shows the per unit rotor speed of Tana Beles generator with and without PSS & UPFC controller. The rotor speed of the generator with conventional existing system is oscillatory and when only PSS is added, the settling time is around 9.733 seconds. The rotor speed oscillations with UPFC and PSS equipped with a POD controller shows improved damping as compared to conventional existing system and only PSS. The speed of the generator have maximum overshoot of 0.016pu with smallest settling time of 4.667 second which indicates that UPFC has improved damping of generator rotor speed oscillations and attains steady state system.

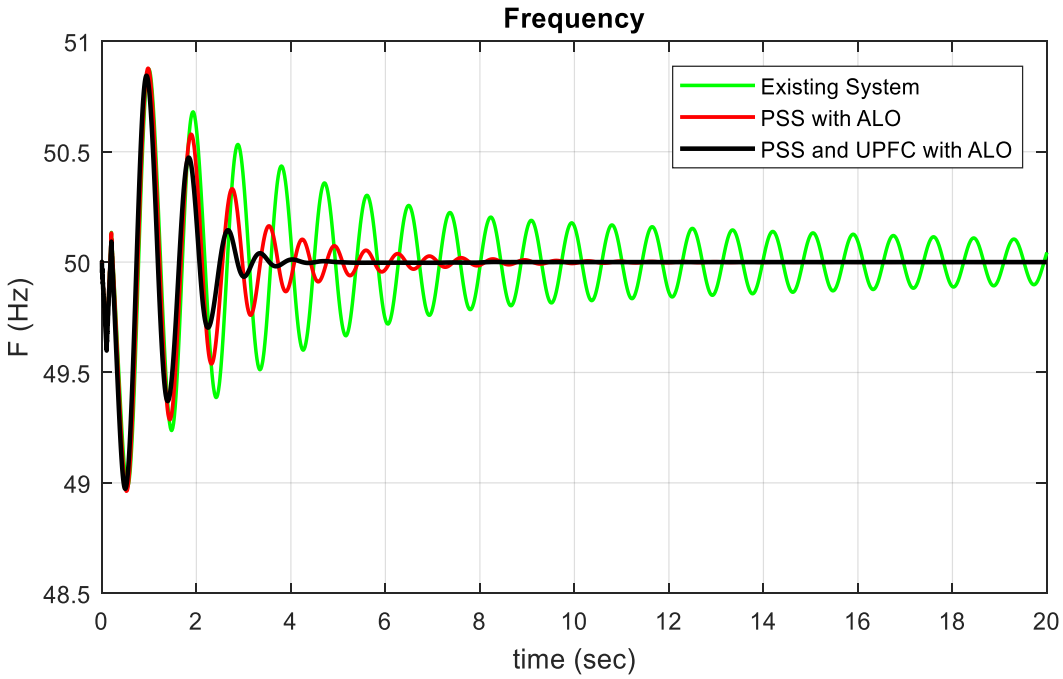

Figure 4.35: Frequency of the system at heavy loading condition

Mean frequency with conventional existing system is oscillatory which varies between a frequency of 49Hz and 50.885Hz which takes a long time to damp out those oscillations and attains steady state operation and with PSS only a frequency varies between 48.96Hz and 50.88Hz. While when UPFC is equipped with PSS and POD controller the system can damp out the oscillations and attains steady state system with shortest possible time and frequency varies between 49Hz and 50.84Hz and have settling time of 4.6 seconds.

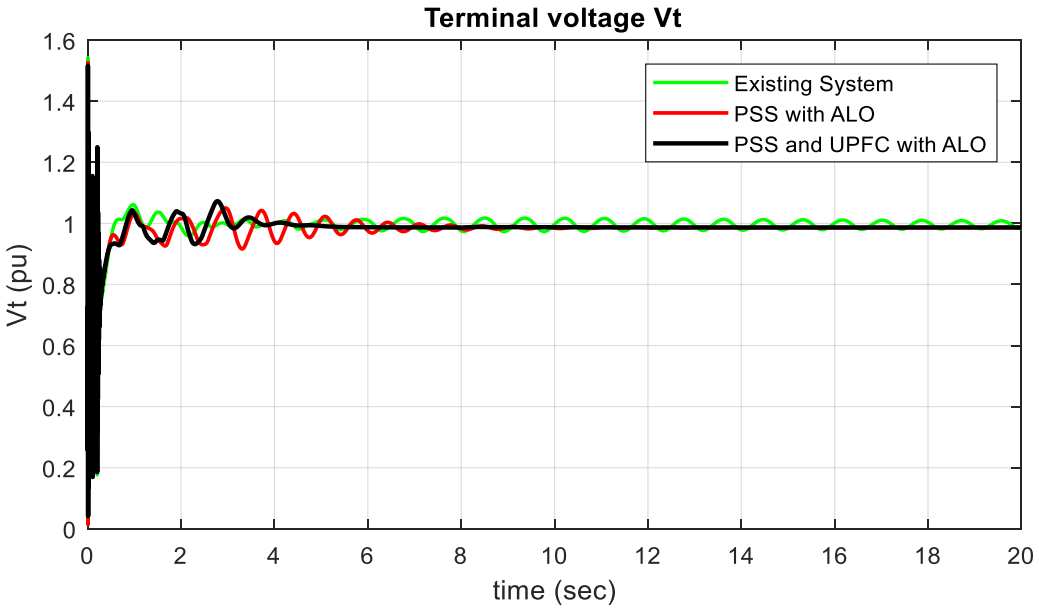

Figure 4.36: Terminal voltage of the system at heavy loading condition

Voltage stability is the ability of power system to keep steady voltage at all buses after subjected to disturbance from heavy loading conditions. The addition of UPFC equipped with PSS is used to damp out low frequency oscillation of power system. But from the result, there is a very small significant effect on terminal voltage of the system because terminal voltage of synchronous generator is controlled by automatic voltage regulator.

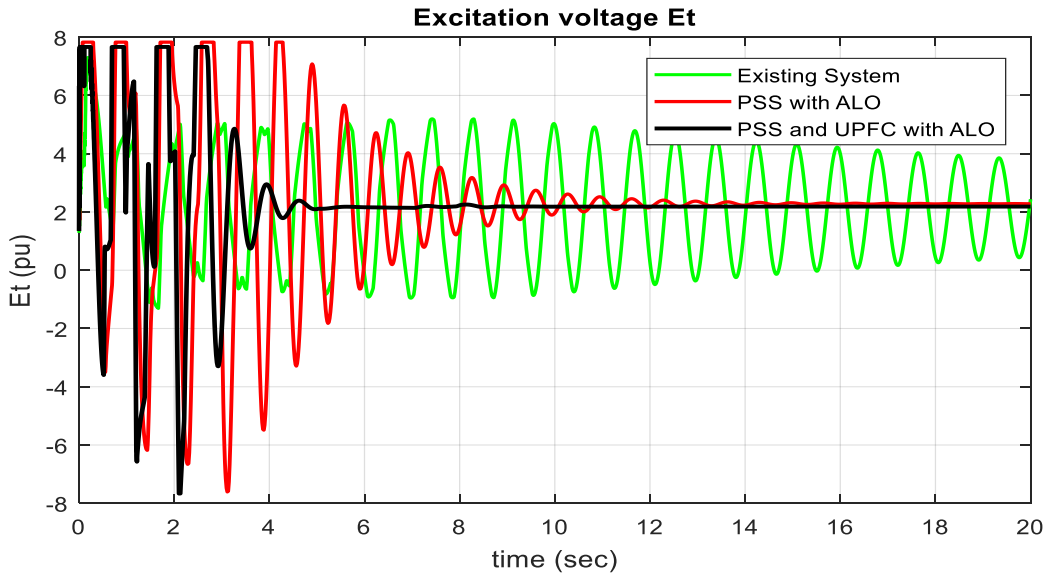

Figure 4.37: Excitation voltage of the system at heavy loading condition

From the results shown in figure 4.37 it is observed that the excitation voltage can go as high as 7.369 pu with conventional fixed gain model and attains its steady state after many

seconds but for UPFC equipped with PSS the maximum overshoot should be 7.66 pu and it stabilizes quickly after 4.981 sec.

Generally, the simulation result shows that the system employed with PSS & UPFC controllers provides good damping characteristics to low frequency oscillations and quickly stabilizes the system under a disturbance. Hence, it can conclude that the system with proper tuning of damping controller provides good damping characteristics and attains power system stability quickly. From the above study the system can effectively damp out the low frequency oscillations by using optimized PSS with UPFC and hence the stability of the system has been improved.

4.6.3 Simulation result at lightly loading condition

The figure shown below represents simulation results of the system at lightly loading condition. A sudden loss in load (large load is disconnected from the system) is take as a disturbance. The low frequency oscillations damp out quickly with the proposed system compared with other conventional system. However, conventional existing system is unable to damp out the oscillations. The proposed system gives acceptable damping effect and adequate settling time for power oscillations under severe disturbance.

Table 4.7: Maximum overshoot and settling time of power system at light loading

Power system states	Maximum overshoot			Settling time (sec)		
	Existing system	PSS only	PSS and UPFC	Existing system	PSS only	PSS and UPFC
$\Delta\omega\ (pu)$	0.01727	0.01725	0.01631	Oscillatory	9.967	4.467
$\Delta\delta\ (rad)$	-2.037	-2.037	-1.896	Oscillatory	8.183	4.033
$\delta\ (rad)$	2.353	2.353	2.126	13	4.8	2.833
$\omega\ (pu)$	0.0175	0.017	0.016	Oscillatory	10.32	4.45
F (Hz)	0.88	0.87	0.81	Oscillatory	9.667	4.55
$\Delta V\ (pu)$	1.548	1.5339	1.3169	Oscillatory	10.23	4.252
$E_t\ (pu)$	7.3	7.512	7.707	Oscillatory	15.05	5.617

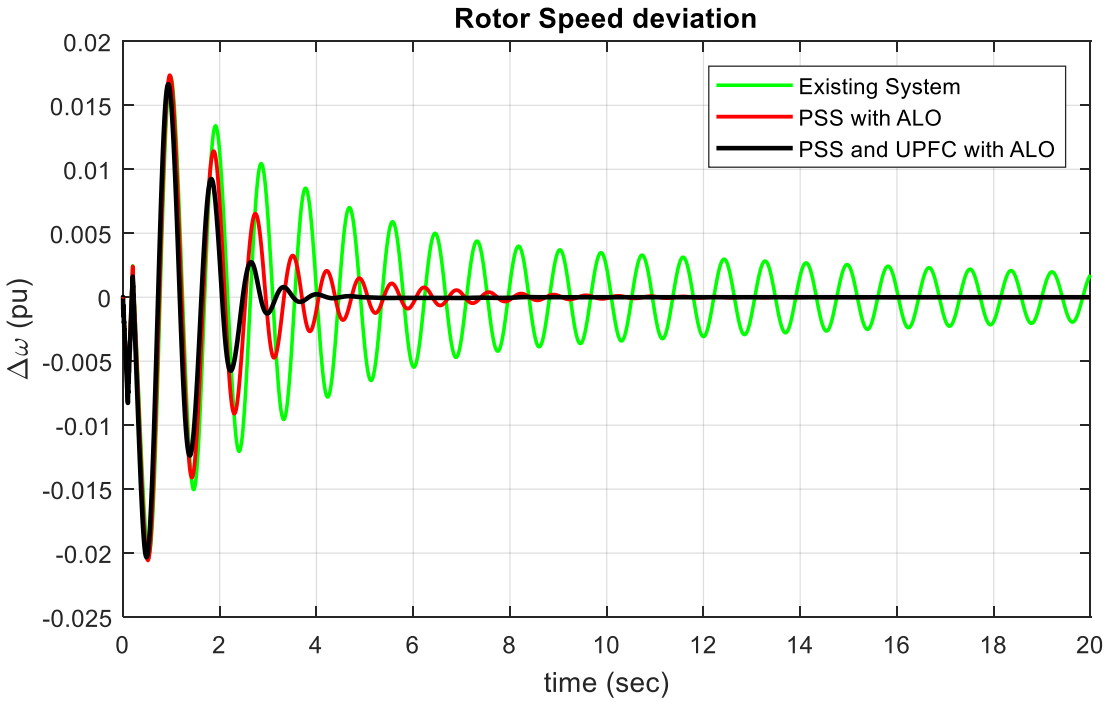

Figure 4.38: Rotor speed deviation of the system at light loading condition

From figure 4.38 rotor speed deviation of the generator has been demonstrated with conventional existing system and PSS equipped with UPFC at lightly loading conditions. The addition of UPFC has improved damping of generator rotor speed oscillations. Due to disturbance of turbine the maximum overshoot of rotor speed deviation varies from 0.01727, 0.01725, 0.01631pu with settling time of oscillatory, 9.967 and 4.467 second for existing system, PSS only and PSS equipped with UPFC respectively. Therefore the generator rotor speed oscillations with PSS and UPFC equipped with a POD controller shows improved damping as compared to conventional existing system and only PSS controller. Therefore, with conventional existing system the result is oscillatory and becomes unstable while stability of the system is maintained and low frequency oscillations are effectively damped out when PSS is equipped with UPFC.

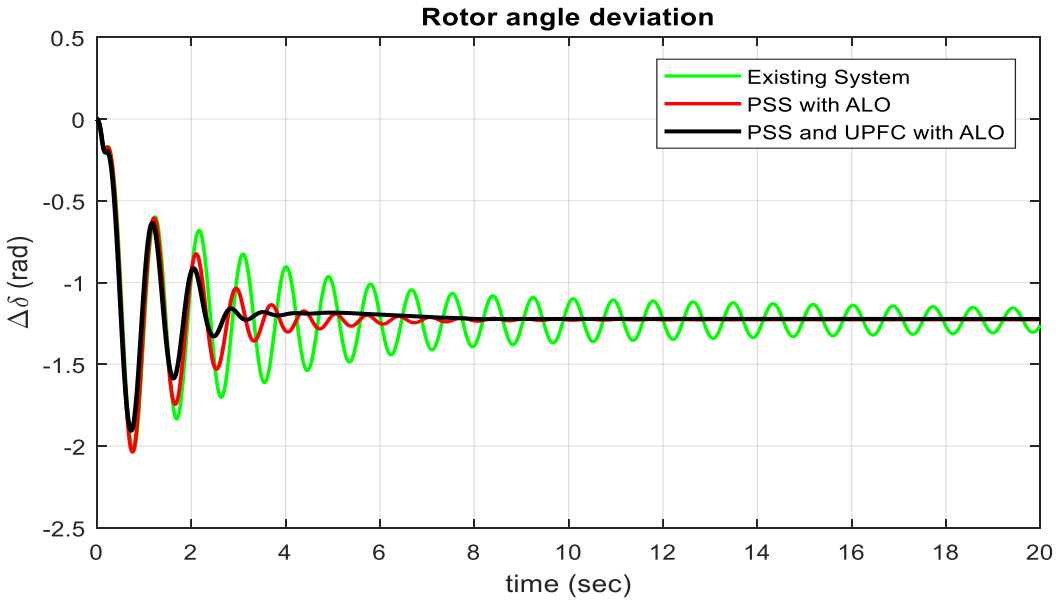

Figure 4.39: Rotor angle deviation of the system at light loading condition

In this case the rotor angle deviation of existing system is oscillatory while when UPFC is equipped with PSS and POD controller the system damps out and diminishes the oscillations with short time. So, ALO based UPFC damping controller can quickly damp out LFO. When rotor angle deviation is subjected to a positive change $\Delta\delta > 0$ then the power would be subjected to ΔP and the machine falls towards the instability but $\Delta\delta < 0$ the machine attains to its initial steady state system.

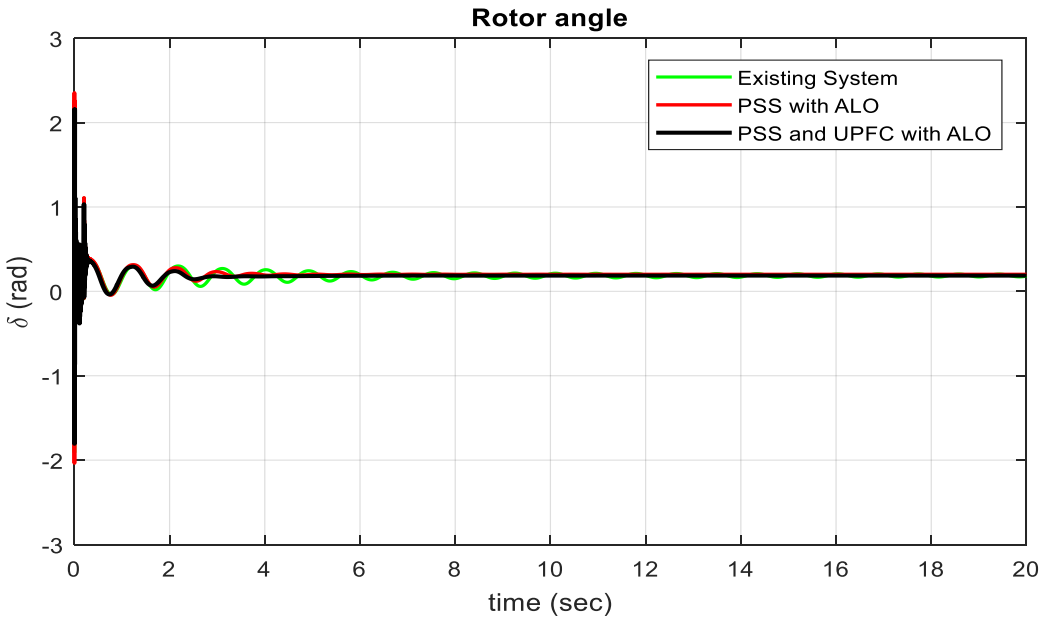

Figure 4.40: Rotor angle of the system at light loading condition

The initial generator rotor angle (δ) is around 2.353, 2.353 and 2.126 rad with conventional existing system, with PSS only and PSS equipped with UPFC respectively. According to IEEE standards of rotor angle stability, the obtained result shows that the generator oscillates and attains steady state values. Therefore, the generator fulfill inter area mode of oscillation having 2.833 sec settling time. The time taken to damp out low frequency oscillation is 2.833 sec for PSS with UPFC, 4.8 sec for PSS only and 13 sec for conventional existing system. Since δ starts to decrease after reaching a maximum value, the machine attains to its steady state system.

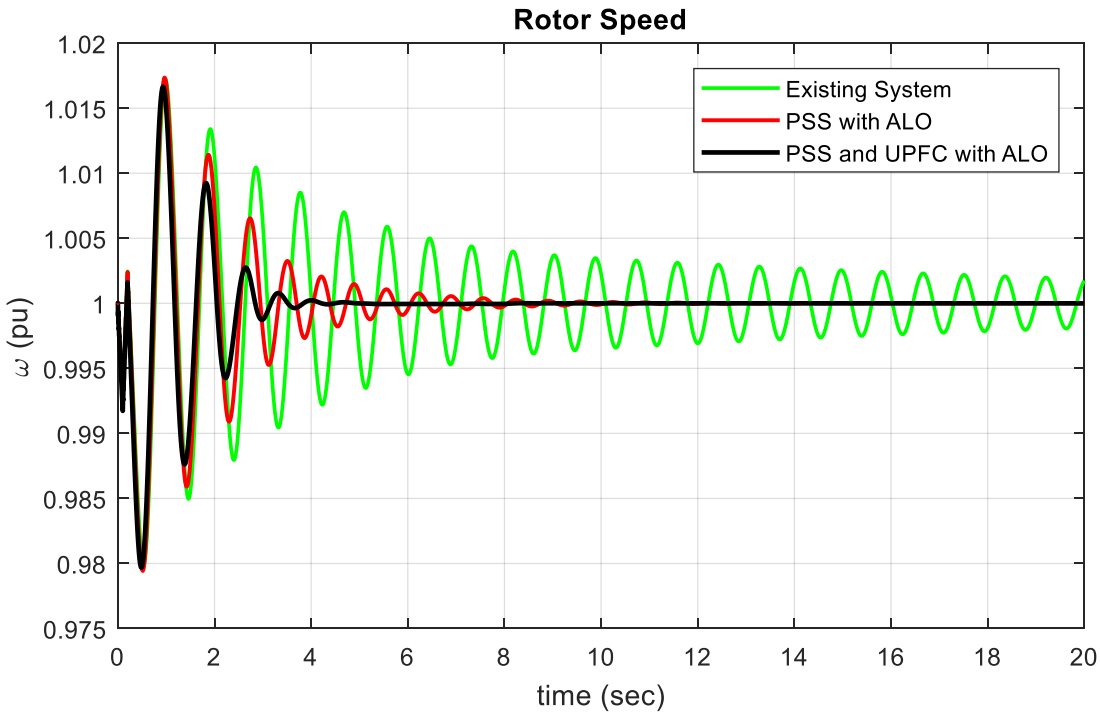

Figure 4.41: Rotor speed of the system at light loading condition

Figure 4.41 shows generator rotor speed with conventional existing system and with PSS & UPFC controller at lightly loaded condition. The speed of generator oscillates from 0.98 to 1.016 with smallest settling time of around 4.45 second which indicates that the addition of UPFC has improved damping of generator rotor speed oscillations. The rotor speed oscillations of the generator with conventional existing system is oscillatory and when only PSS is added, it takes around 10.32 seconds while when PSS is equipped with UPFC, it takes around 4.45 seconds to quickly damp out oscillations and attains steady state system. The rotor speed oscillations with PSS and UPFC equipped with a POD controller shows increased damping as compared to conventional existing system and only PSS.

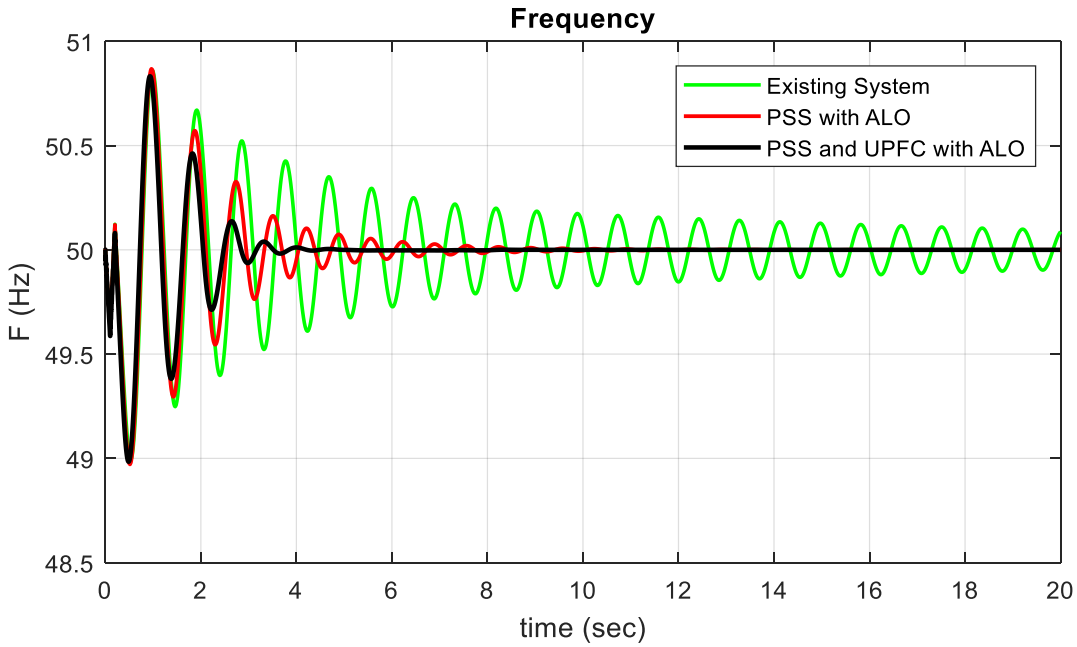

Figure 4.42: Frequency of the system at light loading condition

In this case the frequency with existing system is an oscillatory which varies with a maximum overshoot of 0.88Hz and with PSS only its overshoot is 0.87Hz while when UPFC is equipped with PSS and UPFC-POD controller the system has an overshoot of 0.81Hz that can damp out LFO and attains steady state system at 4.55 seconds.

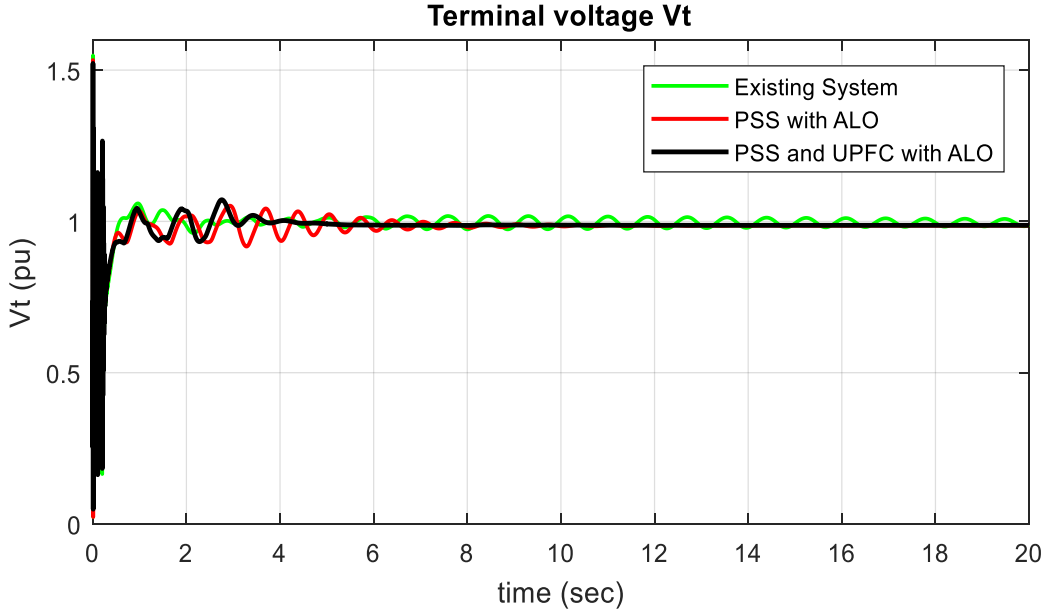

Figure 4.43: Terminal voltage of the system at lightly loading condition

The addition of UPFC equipped with PSS is to damp out low frequency oscillation of power system to maintain terminal voltage at nominal value. But from the simulation result, there

is a very small significant effect on terminal voltage of the system because the terminal voltage of the synchronous generator is controlled by automatic voltage regulator.

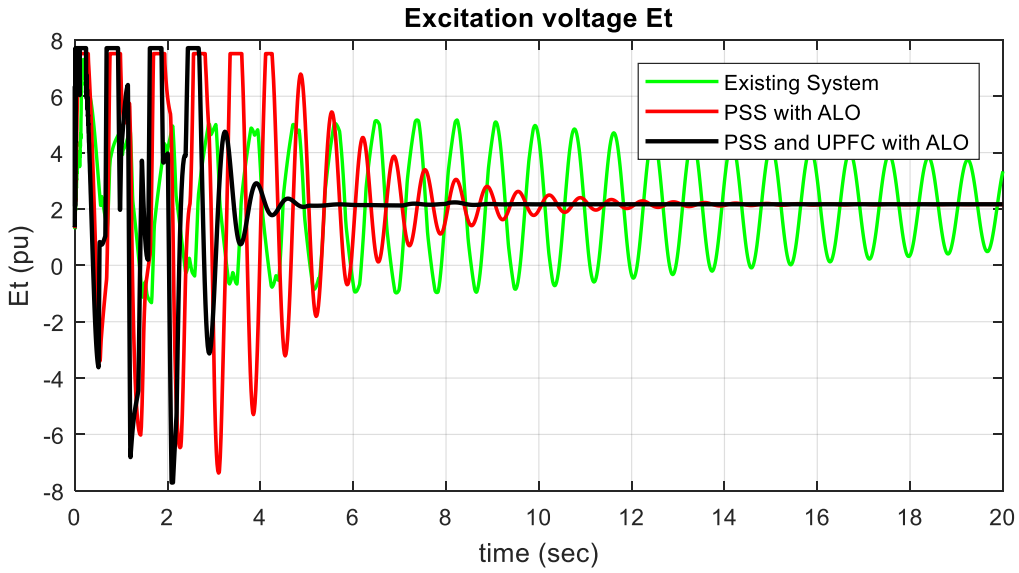

Figure 4.44: Excitation voltage of the system at light loading condition

From the simulation result shown in figure 4.44 it is observed that the excitation voltage can go as high as around 7.3pu with conventional fixed gain model and oscillatory but for UPFC equipped with PSS the maximum overshoot is 7.707pu and stabilizes quickly after 5.617 second. Generally when the equilibrium is upset because of any perturbation, the speed of the rotor changes or accelerates from its synchronous speed in response. The change in rotor speed leads to a change in relative rotor angle. The change in rotor angular position leads to a change in generated output power according to the power angle characteristics. When the output power changes, the rotor changes its speed; consequently, the rotor angle also changes again. Generally, during lightly loading condition the simulation result shows that the system employed with PSS & UPFC controllers provides good damping characteristics to low frequency oscillations and quickly stabilizes the system under a disturbance when compared with conventional existing system and only PSS controllers. Hence it can conclude that the system with proper sizing of damping controllers provides good damping characteristics and attains power system stability quickly. It can also conclude that if the settling time is less, stability had improved quickly and less power system stability improvement occurs if settling time is more. The system can effectively damp out the low frequency oscillations by using ALO based PSS with UPFC and hence, the stability of the system is maintained.

4.7 Comparison of Maximum Overshoot and Settling Time

Figure 4.45 to 4.47 shows the maximum overshoot and settling time at various loading conditions.

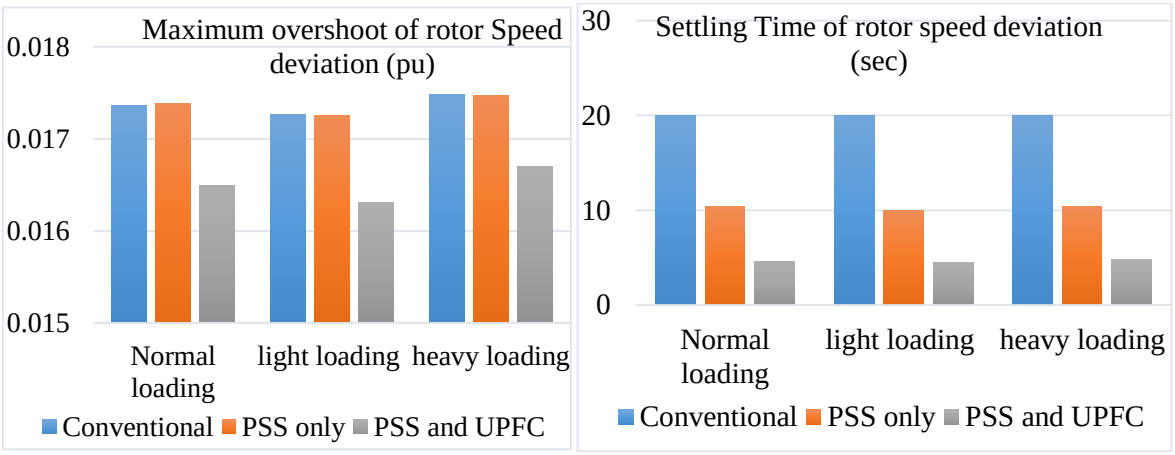

Figure 4.45: Maximum overshoot and settling time of rotor speed deviation

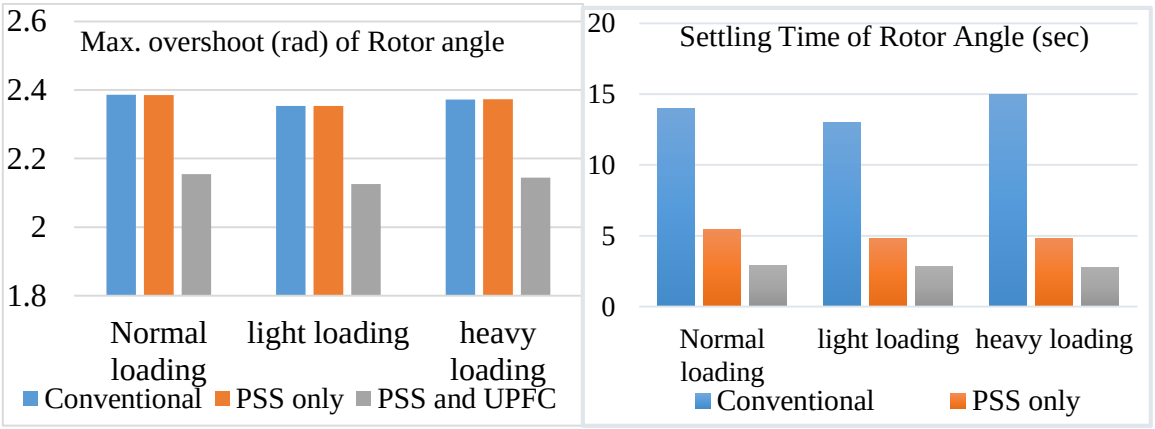

Figure 4.46: Maximum overshoot and settling time of rotor angle

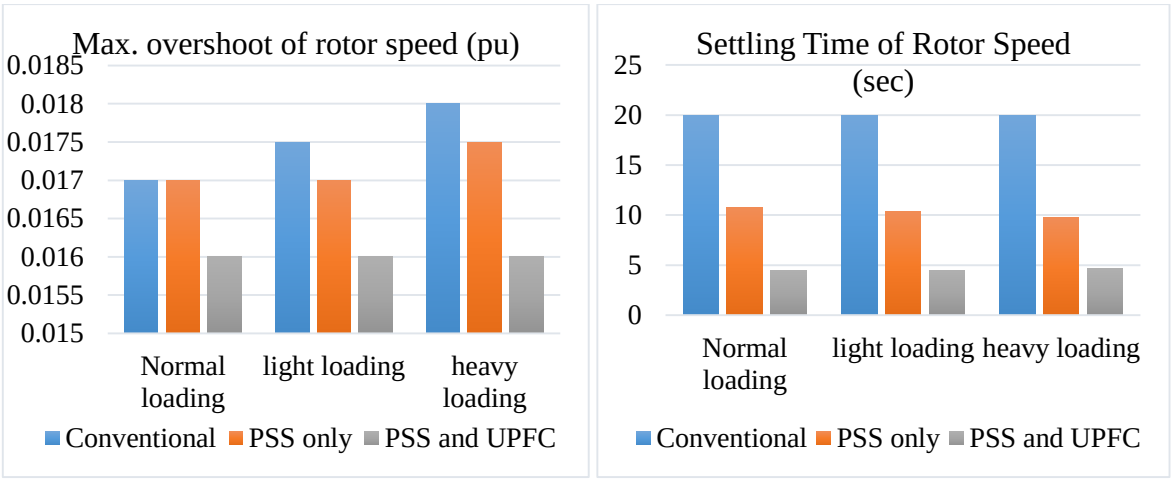

Figure 4.47: Maximum overshoot and settling time of rotor speed

4.8 Detailed Cost Analysis

In this thesis three types of losses are considered for cost analysis purpose, these are disturbance losses due to low frequency oscillation, transmission line loss and other types of losses. Along with optimal power flow, the installation cost of UPFC devices are obtained from the Siemens company database. The location which gives the minimum installation cost, reduced low frequency oscillations, better voltage profile and power flow is considered as the optimal location for the UPFC devices in the system. The cost of installation of UPFC devices has been mathematically given by:

$$IC = CUPFC \times S \times 1000 \quad (4.1)$$

Where, IC is the installation cost of UPFC devices in US$ and CUPFC is the cost of UPFC devices in US$/kVAr. The cost of installation of UPFC is taken from Siemens database. Cost function for UPFC is developed as follows:

$$C_{UPFC} = 0.0003S^2 - 0.2691S + 188.22US\$/kVAR \quad (4.2)$$

Where, C_{UPFC} is the cost of UPFC in US$/kVA and S is operating range of UPFC in MVAR

$$S = Q_2 - Q_1 \quad (4.3)$$

Q_1- MVAR flow through the branch before placing UPFC device

Q_2 - MVAR flow through the branch after placing UPFC device

4.9 Cost Comparative Analysis of Different Algorithms

The following table shows cost comparison analysis of different algorithms with various operating conditions and the one which have less cost have been selected and further analyzed below.

4.9.1 Cost comparison pre-UPFC

Table 4.8: Comparison of pre UPFC cost analysis at heavy loading

Algorithm	Total loss (MW) LFO	Cost due to loss ($)	UPFC Size (MVAR)	Total annual cost without UPFC($)
ALO	4.921	1864628.62	0	1864628.62
GA	4.948	1874695.3	0	1874695.3
PSO	4.974	1884796.8	0	1884796.8
TLBO	5.001	1894933.11	0	1894933.11

Table 4.9: Comparison of pre UPFC cost analysis at light loading

Algorithm	Total loss (MW) LFO	Cost due to loss ($)	UPFC Size (MVAR)	Total annual cost without UPFC($)
ALO	4.486	1699605.77	0	1699605.77
GA	4.618	1749618.96	0	1749618.96
PSO	4.789	1814232.36	0	1814232.36
TLBO	4.898	1855866.27	0	1855866.27

4.9.2 Cost comparison post-UPFC

Table 4.10: Comparison of post UPFC cost analysis at Normal loading

Algorithm	Total loss (MW)	Cost due to loss ($)	UPFC Bus	UPFC Size (MVAR)	UPFC cost $/kVAr	UPFC cost ($)
ALO	1.096	415320.85	3	26	50	1300000
GA	1.103	417783.19	3	26.3	50	1315000
PSO	1.109	420255.79	3	26.5	50	1325000
TLBO	1.116	422738.66	3	26.8	50	1340000

Table 4.11: Comparison of post UPFC cost analysis at light loading

Algorithm	Total loss (MW)	Cost due to loss ($)	UPFC Bus	UPFC Size (MVAR)	UPFC cost $/kVAr	UPFC cost ($)
ALO	1.096	415320.85	3	24.00	50	1200000
GA	1.103	417783.19	3	24.60	50	1230000
PSO	1.109	420255.79	3	24.80	50	1240000
TLBO	1.116	422738.66	3	24.94	50	1247000

Table 4.12: Comparison of post UPFC cost analysis at heavy loading

Algorithm	Total loss (MW)	Cost due to loss ($)	UPFC Bus	UPFC Size (MVAR)	UPFC cost $/kVAr	UPFC cost ($)
ALO	1.883	713332.17	3	28.0	50	1400000
GA	1.938	734275.27	3	28.4	50	1,420,000
PSO	2.0006	757977.6	3	28.7	50	1435000
TLBO	2.032	769982.1	3	28.82	50	1441000

Generally from the above cost analysis result shows light loading and heavy loading condition are compared with each other without adding the cost of energy not supplied and

ALO based optimization technique have least annual cost compared with the rest of the optimization techniques, which shows that ALO technique is more preferable than the other techniques. The annual cost analysis for various loading condition of ALO technique can be calculated as follows:

Case 1: **Financial losses of the system pre installation of UPFC**

Scenario 1: At heavy loading condition

Disturbance loss are 4.921 MW

Annual MWh= (peak loss in MW) * t= 4.921MW*8760h =43,107.96MWh=43.108GWh

Scenario 2: At light loading condition

Disturbance loss are 4.486 MW

Annual MWh = (peak loss in MW) * t= 4.486MW*8760h = 39,297.36MWh=39.297GWh

Case 2: Financial losses of the system post installation of UPFC with proposed ALO

Scenario 1: At heavy loading post UPFC

System loss are 1.883MW

Annual MWh loss = (peak loss in MW) * 8760h=1.883*8760=16,495.08MWh=16.495GWh

Scenario 2: At light loading post UPFC

System loss are 1.096MW

Annual MWh loss = (peak loss in MW) * 8760h=1.096*8760=9,600.96MWh=9.601GWh

4.10 Energy Not Supplied

When load demand exceeds available supply and no corrective action is taken, the system becomes unstable. A dynamic process is triggered, which starts with frequency fluctuations and power surges, followed by unpredictable tripping and damage to generators and lines, finally culminating in widespread blackouts or load shedding. ENS gives the total amount of energy that would have been supplied to the interrupted customers in case of low frequency oscillation if there would not have been any interruption. It is usually expressed in MWh.

$$ENS = \sum_i P_i \times r_i = \sum_i E_i \quad (4.4)$$

Where, Pi is the average load interrupted by each interruption i and Ei is the energy not supplied because of each interruption i.

From appendix E there are 16 interruptions per year out of this 11 interruptions are during loading problem when the system is overloaded the frequency is reduced. So, interruption

number 3, 5, 9, 11 and 12 are not included in the energy not supplied cost calculation because it is beyond scope of this thesis. Therefore there are 11 interruption due to low frequency oscillation problems which are considered in this study.

$$ENS = 51.6 + 63.7 + 49.6 + 53.67 + 48.95 + 48.53 + 58.1 + 44.95 + 54.47 + 60.6 + 52.5$$

ENS =586.72 MWh

The cost of energy not supplied (CENS) can be calculated as:

CENS=ENS* cost of electricity tariff (4.5)

4.11 Cost of UPFC Rating

Although UPFC controllers can offer high-speed control for enhancing electric power system damping oscillation, one significant disadvantage of power electronic based controllers is more expense per unit of rating than that of similar conventional equipment [44].

Table 4.13: Costs of various FACTS controllers

FACTs Controller	Cost(US$)
DSTATCOM	$36 per kVAr
SVC	$40 per kVAr
STATCOM	$50 per kVAr
TCSC	$40 per kVAr
UPFC	$50 per kVAr

Based on table 4.13 and the exchange rate of Commercial Bank of Ethiopia on October 19, 2021 G.C is one US Dollar =47.04 Ethiopian Birr (ETB).

Table 4.14: Cost of UPFC

Scenario	Rating(MVAr)	Cost/kVAr	UPFC cost ($)
1	28	$50	1,400,000
2	24	$50	1,200,000

4.11.1 Total cost implication

The cost evaluation is based on ETB/kWh energy rates for Ethiopian Electric Utility, under the new power tariff. The cost of energy till December 2021 is rated at 1.385 ETB/kWh when the total energy consumed is greater than 500kWh (0.02944$/kWh) or 29.44 $/MWh, by taking the average of all the tariff class energy unit costs ($/kWh). Using 29.44 $/MWh, the total amount of annual financial loss due to disturbance is estimated as follows:

Case 1: Cost implication of the system pre installation of UPFC

Scenario 1: For heavy loading condition

The annual financial loss for a year is 43,107.96MWh *29.44 $/MWh=1,269,228.84$

Scenario 2: For light loading condition

The annual financial loss for a year is 39,297.36MWh *29.44 $/MWh=1,156,914.27$

Case 2: Cost implication of the system post installation of UPFC

Scenario 1: For heavy loading condition

The annual financial loss for a year is 16495.08MWh *29.44 $/MWh=485,615.16$

Scenario 2: For light loading condition

The annual financial loss for a year is 9,600.96MWh*29.44 $/MWh=282,652.26$

The cost of energy not supplied (CENS) can be calculated as:

$CENS = ENS * \text{ Cost of electricity tariff} = 586.72\text{MWh/year} * 29.44\ \$/\text{MWh} = 17{,}273.04\$$

Therefore, the total cost due LFO problem before installation of UPFC can be calculated as:

Scenario 1: For heavy loading condition

The total cost before installation of UPFC = $1,269,228.84+$17273.04=$1,286,501.88

Scenario 2: For light loading condition

The total cost before installation of UPFC = 1156914.27$ +$17273.04=$1,174,187.31

Table 4.15: Cost comparison pre and post UPFC

Scenario	Cost pre-UPFC ($/year) A	Cost Post UPFC ($/year) B	Saving ($/year) A-B	Cost of UPFC ($/year)
1	1,286,501.88	485,615.16	800,886.72	1,400,000
2	1,174,187.31	282,652.26	891,535.05	1,200,000

4.11.2 Methods of financial losses analysis

The economic analysis in this study uses standard financial measures, such as Payback Period and Net Present Value (NPV) [44].

4.11.3 Payback period

The Payback Period is the number of months/years of benefits required for the project to breakeven point. The payback time can be estimated by the following equation.

$$\text{Payback Period} = \frac{\text{Net investment Cost for UPFC}}{\text{Net Annual return}} \quad (4.6)$$

This method determines the period after which the initial investment is recovered. A project is only carried out if the payback period is lower than a certain threshold defined by the company. Typically used thresholds for the payback time vary between 2 to 4 years. However it is inferior to the NPV method, as it takes into account any cash flows after the payback time. The shorter the payback, the more desirable the investment. Conversely, the longer the payback, the less desirable it is. The total investment cost is the sum of installation cost (10%) and maintenance cost (2%).

Scenario 1: For heavy loading condition, the investment cost can be calculated as:

Installation cost (10%) =0.1* 1,400,000=140000$

Operation and maintenance cost (2%) =0.02*1,400,000=28000$

Total investment cost=UPFC cost + installation cost + maintenance cost

Total investment cost=1400000$+140000$+28000=1,568,000$

$$\text{Payback Period } = \frac{\text{Total investment cost}}{\text{Saving}} = \frac{1{,}568{,}000}{800{,}886.72} = \text{ 2 years}$$

Scenario 2: For light loading condition the investment cost can be calculated as:

Installation cost (10%) =0.1* 1,200,000=120000$

Operation and maintenance cost (2%) =0.02*1,200,000=24000$

Total investment cost=UPFC cost + installation cost + maintenance cost

Total investment cost=1200000$+120000$+24000=1,344,000$

$$\text{Payback Period } = \frac{\text{Total investment cost}}{\text{Saving}} = \frac{1{,}344{,}000}{891{,}535.05} = \text{ 1.51 years}$$

4.11.4 Net Present Value method

Net present value (NPV) is the value of all future positive and negative cash flows over the whole life of the project discounted to the present value. In the NPV method, all marginal cash flows of a project are taken into account during its entire lifetime. Cash flows in upcoming years are discounted to t = 0 by using an appropriate rate called the Opportunity Cost of Capital (OCC), hurdle rate, discount rate or required rate of return, which results in the present value of these cash flows. The NPV method is typically used for large capital projects. The Net Present Value of these cash flows (if the salvage value of the equipment is assumed to be negligible) is calculated by:

$$PV = \sum_{t=0}^{n} \frac{CF_t}{(1+r)^t} \quad (4.7)$$

$$NPV = PV - C_0 \quad (4.8)$$

Where, CFt =the net cash flow at time t

C0 = the initial investment, r = the cost of capital (discount rate) = 12%, t = the number of years = 0, 1, 2….n, n = life time of the project = 20 years. Data from the electric power research institute and American electric power suggests that the life time of UPFC device averages to twenty years.

Table 4.16: Cost benefit analysis of NPV of UPFC installation for scenario 1 [44]

Years	Financial loss without UPFC($) A	Financial loss with UPFC ($) B	CFt ($) A - B (Saving)	PV ($)	NPV ($)
0	1,286,501.88	485,615.16	800,886.72	-1,568,000	-1,568,000
1	1,286,501.88	485,615.16	800,886.72	715,077.43	-852,922.57
2	1,286,501.88	485,615.16	800,886.72	638,461.98	-214,460.59
3	1,286,501.88	485,615.16	800,886.72	570,055.35	355,594.76
4	1,286,501.88	485,615.16	800,886.72	508,977.99	864,572.75
5	1,286,501.88	485,615.16	800,886.72	454,444.63	1,319,017.38
6	1,286,501.88	485,615.16	800,886.72	405,754.14	1,724,771.52
7	1,286,501.88	485,615.16	800,886.72	362,280.48	2,087,052
8	1,286,501.88	485,615.16	800,886.72	323,464.71	2,410,516.71
9	1,286,501.88	485,615.16	800,886.72	288,807.78	2,699,324.49
10	1,286,501.88	485,615.16	800,886.72	257,864.09	2,957,188.58
11	1,286,501.88	485,615.16	800,886.72	230,235.79	3,187,424.37
12	1,286,501.88	485,615.16	800,886.72	205,567.67	3,392,992.04
13	1,286,501.88	485,615.16	800,886.72	183,542.56	3,576,534.6
14	1,286,501.88	485,615.16	800,886.72	163,877.29	3,740,411.89
15	1,286,501.88	485,615.16	800,886.72	146,319.01	3,886,730.9
16	1,286,501.88	485,615.16	800,886.72	130,641.97	4,017,372.87
17	1,286,501.88	485,615.16	800,886.72	116,644.6	4,134,017.47
18	1,286,501.88	485,615.16	800,886.72	104,146.98	4,238,164.45
19	1,286,501.88	485,615.16	800,886.72	92,988.37	4,331,152.82
20	1,286,501.88	485,615.16	800,886.72	83,025.33	4,414,178.15

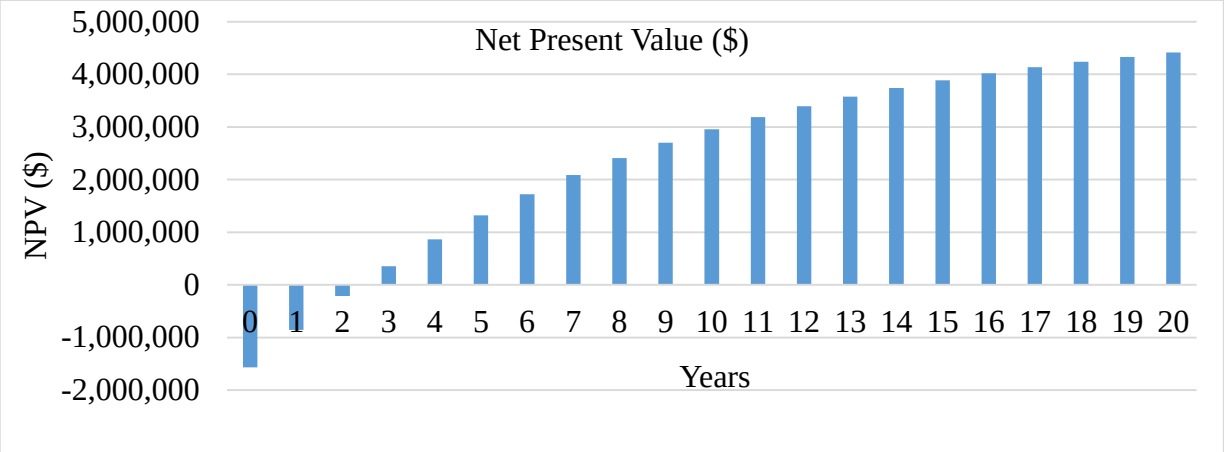

Figure 4.48: NPV analysis of installation UPFC at heavy loading condition

From the above figure 4.48, the UPFC rating is capable of providing positive cash flows after two year of service but funds accumulated after the end of years of service, is $4,414,178.15.

Table 4.17: Cost benefit analysis of NPV of UPFC installation for scenario 2 [44]

Years	Financial loss without UPFC($) A	Financial loss with UPFC ($) B	CFt ($) A-B (Saving)	PV ($)	NPV ($)
0	1,174,187.31	282,652.26	891,535.05	-1,344,000	-1,344,000
1	1,174,187.31	282,652.26	891,535.05	796,013.44	-547,986.56
2	1,174,187.31	282,652.26	891,535.05	710,726.28	162,739.72
3	1,174,187.31	282,652.26	891,535.05	634,577.04	797,316.76
4	1,174,187.31	282,652.26	891,535.05	566,586.64	1,363,903.4
5	1,174,187.31	282,652.26	891,535.05	505,880.93	1,869,784.33
6	1,174,187.31	282,652.26	891,535.05	451,679.40	2,321,463.73
7	1,174,187.31	282,652.26	891,535.05	403,285.18	2,724,748.91
8	1,174,187.31	282,652.26	891,535.05	360,076.05	3,084,824.96
9	1,174,187.31	282,652.26	891,535.05	321,496.47	3,406,321.43
10	1,174,187.31	282,652.26	891,535.05	287,050.42	3,693,371.85
11	1,174,187.31	282,652.26	891,535.05	256,295.02	3,949,666.87
12	1,174,187.31	282,652.26	891,535.05	228,834.84	4,178,501.71
13	1,174,187.31	282,652.26	891,535.05	204,316.82	4,382,818.53
14	1,174,187.31	282,652.26	891,535.05	182,425.73	4,565,244.26
15	1,174,187.31	282,652.26	891,535.05	162,880.12	4,728,124.38

16	1,174,187.31	282,652.26	891,535.05	145,428.67	4,873,553.05
17	1,174,187.31	282,652.26	891,535.05	129,847.034	5,003,400.08
18	1,174,187.31	282,652.26	891,535.05	115,934.85	5,119,334.93
19	1,174,187.31	282,652.26	891,535.05	103,513.26	5,222,848.19
20	1,174,187.31	282,652.26	891,535.05	92,422.55	5,315,270.74

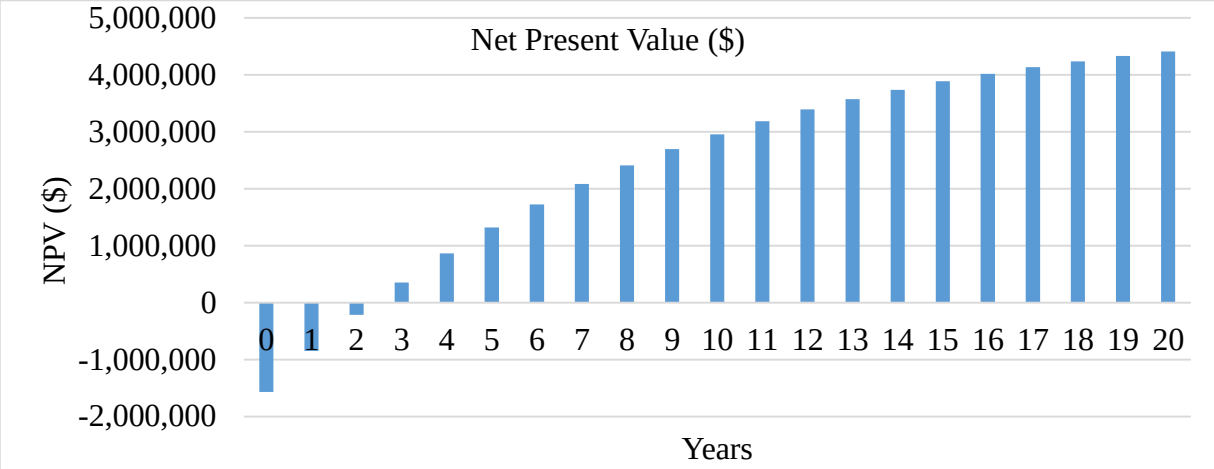

Figure 4.49: NPV analysis of installation UPFC at light loading condition

From the above Figure 4.49, the UPFC rating is capable of providing positive cash flows after one year of service but funds accumulated after the end of years of service, is $5,315,270.74.

Table 4.18: Economic Analysis of UPFC based on Payback period and NPV

Scenarios	Payback period (in years)	NPV ($)
1	2	7,090,485.19
2	1.5	5,315,270.74

From table 4.19 above the payback periods are 2 years for heavy load conditions and 1.5 years for light load conditions. Therefore, the installed UPFC provides good and very short time recovery of installation cost and implies the UPFC installation is most efficient since large amount of energy is lost due to instability of power system caused by low frequency oscillation [44].

Chapter Five

Conclusions and Recommendations

5.1 Conclusion

In this thesis, low-frequency oscillation damping using PSS and UPFC controller was investigated. This thesis examined the performance of ALO to damp out LFO in the electric network by optimally tuning UPFC and PSS parameters. ALO have been chosen by comparing with conventional fixed gain model, PSO, GA and TLBO. The superiority of the proposed ALO approach over GA, PSO and TLBO approach was confirmed through presented simulation result of rotor angle deviation, rotor speed deviation, rotor angle, rotor speed and terminal voltage. The improvement of maximum overshoot for TLBO, PSO, GA, and ALO is 6.03%, 5.97%, 6.055% and 8.3%. In addition, a 38.9%, 52.54%, 70.7% and 80.5% settling time improvement was achieved for TLBO, PSO, GA and ALO algorithms respectively. Furthermore, the time constant and controller gain of ALO is small as compared with GA, PSO and TLBO which indicates that real time implementation of the developed model in power system requires less time to attain steady state system and avoid adverse interaction with active power generation and amplification of high frequency noise. Consequently, the robustness, efficacy and convergence criterion of the proposed approach has confirmed that the approach can be applied in real time to enhance power system stability by damping out the unwanted LFOs. Also, robustness analysis was performed by varying the loading conditions and system parameters. From the obtained results, ALO is the most effective and robust as the rotor speed deviations and rotor angle deviation are relatively small compared to other techniques. The effectiveness of the proposed PSS-UPFC controller for damping low-frequency oscillation of a power system were demonstrated by Tana Beles 400kV line power system subjected to a disturbance. The eigenvalue analysis and time-domain simulation result also shows that the effectiveness of PSS-UPFC system performance analysis under different operating conditions and the properly sized controller in damping low-frequency oscillations. Generally for PSS only the percentage overshoot is 42.2% and settling time is 63.7% but the proposed PSS equipped with UPFC for damping of LFO had a percentage overshoot of 56.06% and settling time of 78.7% which shows that the proposed ALO based PSS equipped with UPFC technique is the most effective for damping LFO problem for Tana Beles 400kV electric network.

5.2 Recommendation

There are some recommendation which are given for different companies to implement this thesis work. It is strongly recommended that the northwest region of Ethiopian power system should use UPFC to reduce low frequency oscillations and related problems to minimize system instability. Using UPFC at Bahir Dar substation is important for damping out LFO caused by the number of overloaded lines. Therefore, it is highly recommended that the northwest region of EEP should use UPFC on Bahir Dar substation to make the system stable and reliable. Additionally very little research has been done in the area of designing a control system and operation of UPFC. The main difficulties in using UPFC is the complexity of its controller. Therefore, researchers should do a lot for reducing the complexity of its controller and recommend power companies to use.

5.3 Future Work

Suggestions for future work based on this thesis that would be included and given for future researchers in the area are listed as follow:

- In this thesis, low frequency oscillation damping for single machine infinite bus system were done, but future researcher should do for multi-machine infinite bus system network.
- For power system low frequency oscillation minimization controller like power system stabilizer, ALO and UPFC based controller are done, but a future researcher should do another techniques like ANN and FLC.

List of Publications

Published Papers

[1] Endeshaw Solomon, Baseem Khan, “DC Smart Micro Grid Protection System”, Morgan Kaufmann (an imprint of **Elsevier** Inc.): "Smart Cities Policies and Financing Handbook".

[2] Bayu, E.S.; Khan, B.; Hagos, I.G.; Mahela, O.P.; Guerrero, J.M. Feasibility Analysis and Development of Stand-Alone Hybrid Power Generation System for Remote Areas: A Case Study of Ethiopian Rural Area. Wind 2022, 2, 68–86.

https://doi.org/10.3390/wind2010005

Accepted Papers/Book chapters

[1] Endeshaw Solomon, *Issaias Gidey Hagos, “Smart Distribution System State estimation”, accepted in the book Active Electrical Distribution Network: Issues, Solution Techniques and Applications, Published by **Elsevier**.

[2] Endeshaw Solomon, Issaias Gidey Hagos, *Baseem Khan, “Outage Management in a Smart Distribution Grid PEV with V2B Applications”, accepted in the book Active Electrical Distribution Network: Issues, Solution Techniques and Applications, Published by **Elsevier**.

[3] Endeshaw Solomon, Baseem Khan, Issaias Gidey Hagos, Om Prakash Mahela *, Josep M. Guerrero, “Feasibility Analysis and Development of Stand-Alone Hybrid Power Generation System for Remote Areas”, communicated in **Wind Journal (MDPI).**

Communicated Papers

[1] Endeshaw Solomon, Baseem Khan, Zaid M. Ali, Mitigating low frequency oscillations in power system through optimal design of Power system Stabilizer, “Communicated in **Energies Journal MPDI (SCI Journal).**

[3] Endeshaw Solomon, Baseem Khan, Zaid M. Ali, “Low frequency oscillations damping through optimal design of Unified power flow controller employing Ant-lion optimization”, communicated in **Sustainability Journal, MDPI. (SCI Indexed)**

References

[1] P. Kundur, “Power System stability and control,” Electric power research institute.

[2] M. A. Abido, A. T. Al-Awami, and Y. L. Abdel-Magid, “Simultaneous design of damping controllers and internal controllers of a unified power flow controller,” *2006 IEEE Power Eng. Soc. Gen. Meet. PES*, p. 2006, 2006, doi: 10.1109/pes.2006.1709297.

[3] K. Prasertwong, N. Mithulananthan, and D. Thakur, “Understanding low frequency oscillation in power systems,” pp. 1–12.

[4] A. S. Al-Hinai and S. M. Al-Hinai, “Dynamic stability enhancement using particle swarm optimization power system stabilizer,” *ICAST 2009 - 2nd Int. Conf. Adapt. Sci. Technol.*, pp. 117–119, 2009, doi: 10.1109/ICASTECH.2009.5409738.

[5] S. Datta and A. K. Roy, “Fuzzy logic based STATCOM controller for enhancement of power system dynamic stability,” *ICECE 2010 - 6th Int. Conf. Electr. Comput. Eng.*, no. December, pp. 294–297, 2010, doi: 10.1109/ICELCE.2010.5700686.

[6] K. C. Rout and P. C. Panda, “An adaptive fuzzy logic based power system stabilizer for enhancement of power system stability,” *2010 Int. Conf. Ind. Electron. Control Robot. IECR 2010*, pp. 175–179, 2010, doi: 10.1109/IECR.2010.5719844.

[7] M. M. Linda and N. K. Nair, “Dynamic stability enhancement with fuzzy based power system stabilizer tuned by hottest non-traditional optimization technique,” *2010 2nd Int. Conf. Comput. Commun. Netw. Technol. ICCCNT 2010*, 2010.

[8] S. Paliwal, P. Sharma, and A. K. Sharma, “Dynamic stability enhancement of power system using intelligent power system stabilizer,” *Adv. Intell. Syst. Comput.*, vol. 335, pp. 571–583, 2015, doi: 10.1007/978-81-322-2217-0_46.

[9] Yao-nan Yu, “Electric power system dynamics,’’ *Academic press inc*.

[10] M. Rani and A. Gupta, “Steady state voltage stability enhancement of power system using facts devices,” *Proc. 6th IEEE Power India Int. Conf. PIICON 2014*, 2014.

[11] M. Haghshenas, M. Hajibabaee, and M. Ebadian, “Controller Design of STATCOM Using Modified Shuffled Frog Leaping Algorithm for Damping of Power System Low Frequency Oscillations,” *Int. J. Mechatronics, Electr. Comput. Technol.*, vol. 6, no. 19, pp. 2786–2799, 2016.

[12] A. Jalali and M. Aldeen, “Placement and operation of STATCOM-storage for voltage

stability enhancement of power systems with embedded wind farms," *IEEE PES Innov. Smart Grid Technol. Conf. Eur.*, pp. 948–953, 2016.

[13] T. Vigneysh and N. Kumarappan, "Stability analysis and dynamic performance enhancement of autonomous microgrid using adaptive fuzzy PI controller," *2017 IEEE Congr. Evol. Comput. CEC 2017 - Proc.*, pp. 1199–1206, 2017.

[14] V. Vantsevitch, "Enhancement of Dynamical Characteristics of a Fuzzy Control," *2018 IEEE Int. Conf. Fuzzy Syst.*, pp. 1–8, 2018.

[15] C. Andersson, J. E. Solem, and B. Eliasson, "Classification of power system stability using support vector machines," *2005 IEEE Power Eng. Soc. Gen. Meet.*, vol. 1, no. 2, pp. 650–655, 2005, doi: 10.1109/pes.2005.1489266.

[16] D. Lin and B. Eng, "Methods for Analyzing Power System Small Signal Stability By A thesis submitted to the school of Graduate Studies in partial fulfillment of the requirements for the degree of Master of Engineering Faculty of Engineering and Applied Science Memorial Univer," no. May, p. 7, 2015.

[17] G. Gajjar and S. A. Soman, "Power system oscillation modes identifications from wide area frequency measurement system," *2012 IEEE Int. Conf. Power Syst. Technol. POWERCON 2012*, no. October, 2012, doi: 10.1109/PowerCon.2012.6401400.

[18] S. K. R., I. M. Jomoah, and A. O. Bafail, "Optimal Placement of Unified Power Flow Controller for Minimization of Power Transmission Line Losses," *Int. J. Comput. Theory Eng.*, vol. 6, no. 5, pp. 377–381, 2014, doi: 10.7763/ijcte.2014.v6.893.

[19] O. Malyszko and M. Zenczak, "Low frequency oscillations in power system," *2018 Innov. Mater. Technol. Electr. Eng. i-MITEL 2018*, pp. 1–4, 2018.

[20] J. Berared, "IEEE 9 Bus System Example," *OPAL.RT Technol. Inc*, no. https://www.kios.ucy.ac.cy/testsystems/index.php/dynamic-ieee-test-systems/ieee-9bus-modified-test-system, pp. 1–13, 2017.

[21] P. S. Engineering, "Enhancement of A Power System Dynamic Stability Using Statcom And Flc Based Stabilizer," 2019.

[22] PES, *IEEE Recommended Practice for Excitation System Models for Power System Stability Studies*, vol. 2005, no. April. 2006.

[23] S. Kamble *et al.*, "Transient Stability Analysis of IEEE-9 Bus Electrical Power System," *Int. J. Eng. Comput. Sci.*, vol. 6, no. 4, pp. 20847–20850, 2017.

[24] S. N. Ahmed, "Damping of Low-Frequency Oscillations in Inter Connected Power Systems", October, 2017.

[25] A. Khodabakhshian, R. Hooshmand, and R. Sharifian, “Power system stability enhancement by designing PSS and SVC parameters coordinately using RCGA,” *Can. Conf. Electr. Comput. Eng.*, pp. 579–582, 2009.

[26] W. M. Thu and K. M. Lin, “Mitigation of Low Frequency Oscillations by Optimal Allocation of Power System Stabilizers: Case Study on MEPE Test System,” *Energy Power Eng.*, vol. 10, no. 08, pp. 333–350, 2018, doi: 10.4236/epe.2018.108021.

[27] P. Control, “Co-ordinated Design of PSS and TCSC Damping Controllers in Multi-machine Power System using PSO Co-ordinated Design of PSS and TCSC Damping Controllers in Multi-machine Power System using PSO Prof . Prafulla Chandra Panda Department of Electrical Engineer,” 2013.

[28] A. Hailemariam, “Power Flow Control and Bus Voltage Enhancement of Power Transmission System Using Unified Power Flow Controller (Upfc),” 2020.

[29] N. Parhizgar, M. Roopaei, P. Esfandiar, and Z. Dehghani, “Analysis of unified power flow controller (UPFC) parameters on power flow in power system,” *Aust. J. Basic Appl. Sci.*, vol. 5, no. 7, pp. 703–710, 2011.

[30] S. V Patil and P. K. Mahajan, “A Review on Implementation of UPFC for improvement of active power flow capability in power system using IEEE 14 bus system,” *Int. Res. J. Eng. Technol.*, vol. 4, no. 4, pp. 542–547, 2017.

[31] MENNITI D, ANDREOTTI A, DE MARTINIS U, and PINNARELLI A, “Modelling of Unified Power Flow Controller into Power System using P-Spice,” 2001.

[32] A. N. Hussain, F. Malek, M. A. Rashid, and M. F. Haji Abd Malek, “Performance improvement of power system stability by using multiple damping controllers based on PSS and the UPFC,” *Int. J. Eng. Technol.*, vol. 5, no. 4, pp. 3257–3269, 2013.

[33] M. S. Alam, M. Shafiullah, M. I. Hossain, and M. N. Hasan, “Enhancement of power system damping employing TCSC with genetic algorithm based controller design,” *2nd Int. Conf. Electr. Eng. Inf. Commun. Technol. iCEEiCT 2015*, no. May, pp. 21–23, 2015,

[34] H. F. Wang, “Damping function of unified power flow controller,” *IEE Proc. Gener. Transm. Distrib.*, vol. 146, no. 1, pp. 81–87, 1999, doi: 10.1049/ip-gtd:19990064.

[35] L. H. Hassan, M. Moghavvemi, and H. A. F. Mohamed, “Impact of UPFC-based

damping controller on dynamic stability of Iraqi power network," *Sci. Res. Essays*, vol. 6, no. 1, 2011.

[36] R. S. Utami, A. Abu-Siada, Suwarno, N. Hariyanto, M. R. Djalal, and J. Hartono, "Optimal tuning of unified power flow controller using firefly algorithm to improve damping of inter-area oscillations in multi-machine system," *2020 2nd Int. Conf. Smart Power Internet Energy Syst. SPIES 2020*, pp. 436–441, 2020.

[37] A. Ajami and M. Armaghan, "Application of multi-objective gravitational search algorithm (GSA) for power system stability enhancement by means of STATCOM," *Int. Rev. Electr. Eng.*, vol. 7, no. 4, pp. 4954–4962, 2012.

[38] P. K. Dhal, "Dynamic stability analysis by selection of optimal location of STATCOM through power system stabilizer tuned by particle swarm optimization technique," *2017 Int. Conf. Energy, Commun. Data Anal. Soft Comput. ICECDS 2017*, pp. 3074–3079, 2018.

[39] K. H. Prasad and S. Tirumalaiah, "Dynamic Performance of the Interline Unified Power Flow Controller (IUPFC) System Using 48-Pulse GTOThyristor," *Citeseer*, vol. 1, no. 1, pp. 13–22, 2014.

[40] M. R. Banaei and A. Hashemi, "An adaptive UPFC based stabilizer for damping of low frequency oscillation," *J. Electr. Eng. Technol.*, vol. 5, no. 2, pp. 197–208, 2010.

[41] M. S. Shahriar, M. Shafiullah, and M. J. Rana, "Stability enhancement of PSS-UPFC installed power system by support vector regression," *Electr. Eng.*, vol. 100, no. 3, pp. 1601–1612, 2018, doi: 10.1007/s00202-017-0638-8.

[42] H. Shayeghi, H. A. Shayanfar, S. Jalilzadeh, and A. Safari, "Design of output feedback UPFC controller for damping of electromechanical oscillations using PSO," *Energy Convers. Manag.*, vol. 50, no. 10, pp. 2554–2561, 2009.

[43] M. Shafiullah et al, "Low-frequency oscillation damping in the electric network through the optimal design of UPFC coordinated PSS employing MGGP," Int. J.Tech. pp.118-131 2019.

[44] M. Akhtar and L. Mathew, "Cost Comparison of FACTS Devices for Industrial Application – A study," *Int. J. Tech. Res. Sci.*, vol. 1, no. 4, pp. 39–46, 2016.

[45] Y. L. Abdel-Magid and M. A. Abido, "Optimal Multiobjective Design of Robust Power System Stabilizers Using Genetic Algorithms" IEEE transactions on power systems, vol. 18, no. 3, 2003.

Appendix

Appendix A: Network currents

$$i_{TLd} = \frac{1}{x_{t1}}\left(x_E i_{Ed} + \frac{m_E v_{dc}}{2} sin\delta_E - V_b cos\delta\right)$$

$$i_{TLq} = \frac{1}{xt1}(x_E i_{Eq} - \frac{m_E v_{dc}}{2} cos\delta_E - V_b sin\delta)$$

$$i_{Ed} = \frac{x_{BB}}{x_{d2}} E'_q + \frac{x_{d7}\, m_B v_{dc}}{2} sin\delta_B + x_{d5} V_b cos\delta + x_{d6} \frac{m_E v_{dc}}{2} sin\delta_E$$

$$i_{Eq} = \frac{x_{q7}\, m_B v_{dc}}{2} cos\delta_B + x_{q5} V_b sin\delta + x_{q6} \frac{m_E v_{dc}}{2} cos\delta_E$$

$$i_{Bd} = \frac{x_E}{x_{d2}} E'_q - \frac{x_{d1}}{x_{d2}} \frac{m_B v_{dc}}{2} sin\delta_B + x_{d3} V_b cos\delta + x_{q4} \frac{m_E v_{dc}}{2} sin\delta_E$$

$$i_{Bd} = \frac{x_{q1}}{x_{q2}} \frac{m_B v_{dc}}{2} cos\delta_B + x_{q3} V_b sin\delta + x_{q4} \frac{m_E v_{dc}}{2} cos\delta_E$$

Appendix B: Constant K parameters

$$K_1 = \frac{E'_{q0} V_{b0}}{X'_{d\Sigma}} * \cos(\delta_0) - \frac{V_{b0}^2 (X_q - X'_d)}{X'_{d\Sigma} * X_{d\Sigma}} * \cos(2\delta_0), \quad K_2 = \frac{V_{b0}}{X'_{d\Sigma}} \sin\delta_0, \quad K_3 = \frac{X_{d\Sigma}}{X'_{d\Sigma}}, \quad K_4 = \frac{(X_d - X'_d) V_b \sin\delta_0}{X'_{d\Sigma}}$$

$$K_5 = \frac{V_{td0}}{V_{t0}} \frac{X_q V_{b0}}{X_{d\Sigma}} * \cos\delta_0 - \frac{V_{tq0}}{V_{t0}} \frac{X'_d V_{b0}}{X'_{d\Sigma}} * \sin\delta_0, \; K_6 = \frac{V_{tq0}}{V_{t0}} * \frac{X_t}{X'_{d\Sigma}}$$

$$K_7 = \frac{3(X_{2d} m_E \cos(\delta_E) + X_{4d} m_B \cos(\delta_B))}{4 C_{dc} X_{q\Sigma}} V_b \sin(\delta) - \frac{3(X_{1q} m_E \sin(\delta_E) + X_{2q} m_B \sin(\delta_B))}{4 C_{dc} X_{q\Sigma}} V_b \cos(\delta)$$

$$K_8 = \frac{3}{4 C_{dc} X_{d\Sigma}} (m_E \cos(\delta_E) X_{1d} + m_B \sin(\delta_B) X_{Bd})$$

$$K_9 = -0.25 * C_{DC} * (m_B * \sin(\delta_B) * \frac{m_B * \cos(\delta_B) * x_{dt} - m_E * \cos(\delta_E) * x_{dE}}{2 * xdE} - m_E * \sin(\delta_E) * \frac{m_E * \cos(\delta_E) * x_{Bd} - m_B * \cos(\delta_B) * x_{dt}}{2 * xdE} + m_B * \cos(\delta_B) * \frac{m_B * \sin(\delta_B) * x_{qt} - m_E * \sin(\delta_E) * x_{qE}}{2 * xqE} - m_E * \cos(\delta_E) * \frac{-m_B * \sin(\delta_B) * x_{qE} + m_E * \sin(\delta_E) * x_{Bq}}{2 * x_{qE}})$$

$$K_{pe} = \frac{(u_{td} - i_{tq} * x_{d1}) * (x_{Bd} - x_{dE}) * V_{DC} * \sin(\delta_E)}{2 * x_{dE}} + \frac{(x_q * i_{td} + u_{tq}) * (x_{Bq} - x_{qE}) * V_{DC} * \cos(\delta_E)}{2 * xqE}$$

$$K_{pdE} = (u_{td} - i_{tq} * x_{d1}) \frac{*(x_{Bd} - x_{dE}) * V_{DC} * m_E * \cos(\delta_E)}{2 * x_{dE}} + (x_q * i_{td} + u_{tq}) * (-x_{Bq} + x_{qE}) * V_{DC} * m_E * \sin(\delta_E)/(2 * x_{qE}); \quad K_{pb} = (u_{td} - i_{tq} * x_{d1}) * (x_{dt} - x_{qE}) * V_{DC} * \frac{\sin(\delta_B)}{2 * x_{dE}} + (x_q * i_{td} + u_{tq}) * (x_{qt} - x_{qE}) * V_{DC} * \frac{\cos(\delta_B)}{2 * x_{qE}}; \quad K_{pdB} = (u_{td} - i_{tq} * x_{d1}) * (x_{dE} + x_{dt}) * V_{DC} * m_B * \frac{\cos(\delta_B)}{2 * x_{dE}} + (x_q * i_{td} + u_{tq}) * (-x_{qt} + x_{qE}) * \frac{V_{DC} * m_B * \sin(\delta_B)}{2 * xqE}; \quad K_{pd} = (u_{td} - i_{tq} *$$

$$x_{d1}) * (x_{dt} - x_{dE}) * \frac{m_B * \sin(\delta_B)}{2 * xdE} + \frac{(x_{Bd} - x_{dE}) * m_E * \sin(\delta_E)}{2 * x_{dE}} + (x_q * i_{td} + u_{tq}) * \left((x_{qt} - x_{qE}) * m_B * \frac{\cos(\delta_B)}{2 * x_{qE}} + (x_{Bq} - x_{qE}) * m_E * \frac{\cos(\delta_E)}{2 * x_{qE}} \right) \quad ; \quad K_{qd} = -(x_{d1} - x_d) * (x_{Bd} - x_{dE}) * V_{DC} * \frac{\sin(\delta_E)}{2 * xqE}$$

$$Kqde = -(x_{d1} - x_d) * (x_{Bd} - x_{dE}) * m_E * V_{DC} * \frac{\cos(\delta_E)}{2 * x_{dE}}; \quad K_{qb} = -(x_{d1} - x_d) * (x_{dt} - x_{dE}) * \frac{V_{DC} * \sin(\delta_B)}{2 * xdE}; \quad K_{qdB} = -(x_{d1} - x_d) * (x_{dE} - x_{dt}) * m_B * \frac{V_{DC} * \cos(\delta_B)}{2 * xdE}; \quad K_{qe} = -(x_{d1} - x_d) * ((x_{Bd} - x_{dE}) * \frac{m_E * \sin(\delta_E)}{2 * x_{dE}} + (x_{dt} - x_{dE}) * \frac{m_B * \sin(\delta_B)}{2 * xdE} \quad ; \quad K_{vqe} = u_{td} * (x_{Bq} - x_{qE}) * \frac{V_{DC} * \cos(\delta_E)}{2 * U_t * x_{qE}} - u_{tq} * (x_{Bd} - x_{dE}) * V_{DC} * \frac{\sin(\delta_E)}{2 * U_t * x_{dE}} \quad ; \quad K_{vde} = u_{td} * x_q * (x_{qE} - x_{Bq}) * m_E * V_{DC} * \frac{\sin(\delta_E)}{2 * U_t * x_{qE}} - u_{tq} * x_{d1} * (x_{Bd} - x_{dE}) * m_E * \frac{V_{DC} * \cos(\delta_E)}{2 * U_t * x_{qE}} \quad ; \quad K_{vb} = u_{td} * x_q * (x_{qt} - x_{qE}) * V_{DC} * \frac{\cos(\delta_E)}{2 * Ut * xqE} - u_{tq} * x_{d1} * (x_{dt} - x_{dE}) * V_{DC} * \frac{\sin(\delta_E)}{2 * U_t * x_{dE}}; \quad K_{vdB} = u_{td} * x_q * (x_{qE} - x_{qt}) * m_B * V_{DC} * \frac{\sin(\delta_E)}{2 * U_t * x_{qE}} + u_{tq} * m_B * x_{d1} * (x_{dE} + x_{dt}) * V_{DC} * \frac{\cos(\delta_E)}{2 * U_t * x_{dE}}$$

$$K_{vd} = u_{td} * x_q * (x_{Bq} - x_{qE}) * m_E * \frac{\cos(\delta_E)}{2 * U_t * x_{qE}} + (x_{qt} - x_{qE}) * m_B * \frac{\cos(\delta_B)}{2 * x_{qE}} - u_{tq} * m_E * x_{d1} * (x_{Bd} - x_{dE}) * \frac{\sin(\delta_E)}{2 * U_t * x_{dE}} + m_B * (x_{dt} - x_{qE}) * \frac{\sin(\delta_E)}{2 * xdE}; \quad Kce = 0.25 * C_{DC} * V_{DC} * \sin(\delta_E) * \frac{m_E * \cos(\delta_E) * x_{Bd} - m_B * \cos(\delta_B) * x_{dE}}{2 * xdE} + VDC * \cos(\delta_E) * \frac{m_E * \sin(\delta_E) * x_{Bq} - m_B * \sin(\delta_B) * x_{qE}}{2 * xqE}$$

$$Kcde = 0.25 * m_E * \frac{\cos(\delta_E) * I_{Eq} - \sin(\delta_E) * I_{Ed}}{C_{DC}} + 0.25 * (m_E * V_{DC} * \cos(\delta_E) * \frac{m_E * \cos(\delta_E) * x_{Bd} - m_B * \cos(\delta_B) * x_{dE}}{2 * C_{DC} * x_{dE}} + m_E * V_{DC} * \sin(\delta_E) * \frac{m_B * \sin(\delta_B) * x_{qE} + m_E * \sin(\delta_E) * x_{Bq}}{2 * CDC * xqE}$$

$$K_{cb} = -0.25 * C_{DC} * V_{DC} * \sin(\delta_B) * (m_E * \cos(\delta_E) * x_{dE} + m_B * \cos(\delta_B) * x_{dt})/(2 * x_{dE}) + V_{DC} * \cos(\delta_B) * \frac{m_B * \sin(\delta_E) * x_{qt} - m_E * \sin(\delta_E) * x_{qE}}{2 * x_{qE}}$$

$$K_{cdB} = 0.25 * m_B * \frac{\cos(\delta_B) * I_{Bq} - \sin(\delta_B) * I_{Bd}}{C_{DC}} + 0.25 * (m_B * V_{DC} * \cos(\delta_B) * \frac{m_E * \cos(\delta_E) * x_{dE} + m_B * \cos(\delta_B) * x_{dt}}{2 * CDC * xdE} + m_B * V_{DC} * \sin(\delta_B) * \frac{-m_B * \sin(\delta_E) * x_{qt} + m_E * \sin(\delta_E) * x_{qE}}{2 * C_{DC} * x_{qE}}$$

Appendix B1: Design Parameters of UPFC

x1 = 0.20, delta1 = 0.3588, utd =0.4916, utq =1.3109, itq =0.7022, itd =0.5685, Eq1 =1.4871, EQ = 1.7088, Pe =1.20, Qe = -0.40, ud =0.6320, uq = 1.1972, u = 1.3538, delta = 0.4857, IEd =1.5491, IEq =-1.5960, IBd =-0.4652, IBq = 0.5850, Eq01 =1.7088, Vb0 = 1.3538
Xt = 0.20, Xd1 = 0.310, Xq = 0.70, Xd =1.0300, delta0 =0.4857, Vtd0 = 0.4916, Vtq0 = 1.3109, Vt0 = 1.4000, vEtd = -0.1861, vEtq = -0.0463, vBtd = -0.1342, vBtq = -0.0724, dVdc = -0.1458, a = 0.4590, K1 = 2.6124, K2 = 1.2393, K3 = 0.4146, K4 = 0.8923, K5 = -0.0328, K6 = 0.3672, K7 = 0.1448, K8 = -0.0496, K9 = 0.0208, Kpe = -0.9419, KpdE = 0.1611, Kpb = -0.2411, KpdB = -0.0663, Kpd = -0.1997, Kqd = -0.2155, Kqde = -0.1141, Kqb = -0.0305, KqdB = 0.0071, Kqe =-0.0344, Kvqe = 0.0693, Kvde = 0.1747, Kvb = -0.0333, KvdB = -0.1369, Kvd = -0.0221, Kce = 0.6195, Kcde =0.3086, Kcb = -0.4703, KcdB = 0.0028

A =

0	314.1593	0	0	0
-0.3266	-0.5000	-0.1549	0	0.0250
-0.0970	0	-0.0451	0.1087	0.0234
9.8308	0	-110.1564	-5.0000	6.6305
0.1448	0	-0.0496	0	-0.0208

B =

0	0	0	0	0
0	0.1177	-0.0201	0.0301	0.0083
0	0.0037	0.0124	0.0033	-0.0008
300.0	20.7821	-52.4084	9.9904	41.0621
0	0.6195	0.3086	-0.4703	0.0028

Appendix C: Tana Beles transmission line data

Existing Generator data of Tana Beles

No.	Name	Sn(MVA)	V(kV)	P(MW)	Pmin (MW)	Pmax (MW)	Qmin (MVAR)	Qmin (MVAR)
1	Beles G1	133	15	80	0	115	-130	130
2	Beles G2	133	15	100	0	115	-130	130
3	Beles G3	133	15	90	0	115	-130	130
4	Beles G4	133	15	100	0	115	-130	130

Load buses: $Beles\ 400KV, P_d = 20MW, Q_d = 6.3Mvar$
$Bahirdar\ 230KV, P_d = 65.53MW, Q_d = 30.76Mvar$

Transmission line parameters in pu from Tana Beles 400kV to Bahir Dar

No	From bus	To bus	R(pu)	X(pu)	B(pu)	KA	Km
1	Tana Beles 400	Bahir Dar 400	0.000958	0.012159	0.37713	1341	65

Transformer parameters

Voltage (kV)	**Rating (MVA)**	**R(%)**	**X(%)**	**X/R ratio**
400/230	133	0.176	12.045	68.44
400/15	133	0.215	13.5	62.79

Appendix D: Tana Beles Quarterly hourly station data report

	MW	MVAR	Bus voltage	Generator Voltage	Frequency(Hz)
Max	425.2	-115.8	420	15.07	50.15
Min	167.4	-85.9	409.9	14.92	49.42

Time	BUS END		UNIT-1		UNIT-2		UNIT-3		UNIT-4	
Hours	kV	Hz	MW	MVAR	MW	MVAR	MW	MVAR	MW	MVAR
1:00	420.1	50.11	100.5	-56.6	98.2	-46.8				
2:00	418.8	50.04	106.2	-52.6	105.9	-44				
3:00	419.9	50.08	104.5	-56.4	103.8	-47.5				
4:00	420.9	50.01	106.5	-58.8	105.9	-49.6				
5:00	420.6	49.41	107.1	-58.1	105.6	-49.2				
6:00	420.4	49.97	106.5	-58.1	106	-48.9				
7:00	410.9	50.03	105.1	-34.7	110.3	-24.7	89.5	-20	112.6	-9.7
8:00	410.4	49.82	102.5	-20.8	103.5	-23.5	104.4	-17.4	100.8	-19.2
9:00	408.3	49.37	101.4	-17.2	106.8	-17.8	100.4	-13.2	94.9	-14.2
9:15	409.4	50.07	95.3	-19.8	94.7	-22	96.4	-16	94.1	-17.5
9:30	409.3	50	82.3	-20.5	82.9	-22.7	81.7	-17.1	81.8	-17.8
9:45	409.6	48.8	82	-20.2	83.8	-22.6	83	-16.8	82	-17.8
10:00	409.7	50.0	83	-21.5	83.5	-23.8	83.2	-17.8	81.1	-19
10:15	409.1	50.1	81.8	-22.9	81.2	-24.8	81.2	-18.9	81.1	-19.8
10:30	410.8	50.1	80.1	-23.9	79.3	-26.6	80.2	-20.8	80.9	-21.4
10:45	410.8	50.1	90.9	-23.2	87.8	-25.7	87.3	-19.6	85.1	-20.5
11:00	410.2	49.97	97.3	-21.1	96.7	-23.8	87	-18.3	91	-19.2
11:15	409.8	50.0	94.6	-20.5	99	-23.3	92.7	-16.8	99.6	-16

11:30	408.1	49.9	101.1	-20.3	104.8	-14.8	101.6	-14.8	106.2	-16.8
11:45	410.3	49.86	84.9	-22.6	84.2	-25.1	85.1	-19.5	87.2	-20
12:00	409.7	50.04	96.5	-20.8	98	-22.6	97.4	-16.9	98	-17.7
13:00	410.6	50.10	103.5	-21.5	102.5	-24.1	102.3	-18.1	109	-17.7
14:00	411.6	50.2	105.1	-21.5	104.8	-23	81.7	-20.5	87	-21.4
15:00	409	49.42	102.8	-20.5	100.1	-21.4	103.1	-15.6	102.3	-16.9
16:00	410.7	50.08	97.1	-22.7	95.9	-24.7	95.2	-18.6	99.2	-19.3
17:00	410.2	49.98	98.5	-21.2	95.8	-23.7	97	-17.2	95.9	-18.9

	MW	MVAR	Bus voltage	Generator Voltage	Frequency(Hz)
Max	425.2	-115.8	420	15.07	50.15
Min	167.4	-85.9	409.9	14.92	49.37

Time	BUS END		UNIT-1		UNIT-2		UNIT-3		UNIT-4	
Hours	kV	Hz	MW	MVAR	MW	MVAR	MW	MVAR	MW	MVAR
1:00	417.5	49.45	86.6	-44	80.8	-33.1				
2:00	418	49.85	87	-44.7	85.1	-33.7				
3:00	418.2	50.07	81.4	-45	79.2	-34.3				
4:00	418.8	50.1	82.4	-47.8	80.8	-36.2				
5:00	419.2	50.01	89.4	-47.8	80.6	-37.7				
6:00	418	49.42	98.9	-46.6	81.2	-36.2				
7:00	409.3	50.04	96.5	-21.8	96.2	-10.7	96.1	-27.2	110.9	-23.5
8:00	409.4	49.86	96.5	-21.4	95	-10.8	95.8	-27.2	110.9	-22.7
9:00	409.2	49.71	97	-21.2	97.6	-10.5	95.2	-27.5	111.4	-23.3
9:15	409.2	49.87	97	-21.2	97.6	-10.1	95.2	-27.5	111.4	-22.9
9:30	409.7	49.9	97.9	-23	91.9	-12.6	92.7	-29.4	111.4	-24.8
9:45	409.9	49.92	92.2	-23	93	-12.2	92.8	-28.7	111.1	-24.4
10:00	409.8	49.63	94.4	-22.9	97	-11.3	95.8	-28.1	111.1	-23.9
10:15	409.9	50.01	90.6	-22.7	89.8	-12.3	91.9	-28.5	110.9	-24.1

10:30	409.8	49.91	91.6	-23.5	91.5	-12.3	89.1	-29.3	110.9	-24.7
10:45	410.1	49.45	92.4	-24.1	91.9	-13.1	94.2	-29.8	111.1	-28.5
11:00	410.2	49.83	97.4	-23.9	94	-12.9	96.5	-29.4	95.2	-26.7
11:15	410.2	49.91	97.4	-23.5	96.2	-12.9	96.8	-30	96.1	-26.9
11:30	410.3	49.94	92.4	-24.5	90.9	-14.1	90.7	-30.9	110.9	-26.3
11:45	411.1	50.09	87.2	-26	86.7	-15.6	86.7	-32.2	111.4	-27.2
12:00	410.7	49.71	90.4	-25.4	91.9	-14.8	92.4	-31	110.9	-27
13:00	409.9	49.46	102.5	-23.2	95.7	-12.6	94.6	-29	111.2	-24.9
14:00	410	49.93	89	-24.4	85.5	-13.4	85.7	-29.8	110.8	-24.8
15:00	409.9	49.94	95.3	-22.9	94.4	-14.7	95	-28.1	111.1	-24.2
16:00	409.8	49.96	102.3	-21.5	102.2	-14.4	96.6	-29.5	110.9	-23.9
17:00	410.2	49.92	94.9	-21.8	94.1	-19.9	91.5	-29	110.6	-24.8

Station Data: on date 22/11/2013 E.C

	MW	MVAR	Bus voltage	Generator Voltage	Frequency(Hz)
Max	429.8	-109.6	420.9	15.22	50.20
Min	198.7	-72.7	408.3	14.83	49.77

On date 25/11/2013 E.C

	MW	MVAR	Bus voltage	Generator Voltage	Frequency(Hz)
Max	409.4	-124.6	419.1	15.1	50.13
Min	165.9	-56.2	408.1	14.69	49.78

Appendix E: Interruption data

No.	Unit No.	From		To		Total time HRs	Active power MW	Energy loss MU	Reason
		Date	Time	Date	Time				
1	Unit 1	10/01/2013	15:30:00	10/01/2013	16:06:00	0:36:00	86	51.6	LFO
2	Unit 1	23/01/2013	18:12:00	23/01/2013	18:39:00	0:27:00	98	63.7	LFO
3	Unit 2	17/02/2013	10:39:00	17/02/2013	11:01:00	0:22:00	100	36.67	CB trip

4	Unit 2	25/03/2013	13:47:00	25/03/2013	14:19:00	0:32:00	93	49.6	LFO
5	Unit 1	27/04/2013	17:02:00	27/04/2013	17:22:00	0:20:00	104	34.67	CB open
6	Unit 3	20/05/2013	15:13:00	20/05/2013	15:38:00	0:35:00	92	53.67	LFO
7	Unit 1	02/06/2013	9:37:00	02/06/2013	20:10:00	0:33:00	89	48.95	LFO
8	Unit 2	07/07/2013	14:02:00	07/07/2013	14:34:00	0:32:00	91	48.53	LFO
9	Unit 2	15/08/2013	12:22:00	15/08/2013	12:40:00	0:18:00	106	31.8	N.A
10	Unit 1	27/08/2013	8:19:00	27/08/2013	9:01:00	0:42:00	83	58.1	LFO
11	Unit 3	22/09/2013	15:23:00	22/09/2013	15:50:00	0:27:00	102	45.9	N.A
12	Unit 2	12/10/2013	9:27:00	12/10/2013	9:55:00	0:28:00	99	46.2	N.A
13	Unit 2	02/11/2013	8:32:00	02/11/2013	9:33:00	0:31:00	87	44.95	LFO
14	Unit 1	13/01/2014	17:32:00	13/01/2014	18:10:00	0:38:00	86	54.47	LFO
15	Unit 1	27/01/2014	13:11:00	27/01/2014	13:50:00	0:39:00	93.3	60.65	LFO
16	Unit 1	30/01/2014	7:13:00	30/01/2014	7:48:00	0:35:00	90	52.50	LFO

Appendix F: MATLAB Script code for ALO

Script Code of Antlion optimization algorithm for optimal tuning of controller

```
clear all
clc
SearchAgents_no=40; % Number of search agents
Function_name='LFO'; % Name of the test function
Max_iteration=100; % Maximum number of iterations
% Load details of the selected benchmark function
[lb,ub,dim,fobj]=Get_Functions_details(Function_name);
[Best_score,Best_pos,cg_curve]=ALO(SearchAgents_no,Max_iteration,lb,ub,dim,fobj);
Answer_pos(:,1)=Best_pos;
Answer_cost(:,1)=Best_score;
%% constraint functions
K=Best_pos(1); T1=Best_pos(2); T2=Best_pos(3); T3=Best_pos(4); T4=Best_pos(5);
% A 133MVA, 50Hz Tana Beles HPP has the following system parameters:
f=50; M=8;S=133;H=3.14;Td01=9.2;    %T'd0
Td011=0.1; Tq011=0.1;    % T''d0 and T''q0
xd=1.03;xq=0.7; xd1=0.31; xd11=0.25;  %x''d
xq11=0.25; xL=0.2; D=4;wb=2*pi*f;   % in rad/sec
% Exciter type EXST1 data
KA=60;TA=0.02;
%Transformer Parameter in pu
xT=0.1; xE=0.1; xB=0.1;
%Transmission line data in pu
xtE=1;
% Operating conditions
% Case 1: Nominal loading in pu
%  P0=0.8;  Q0=0.114; Ut=1;  xBV=0.25;
% Case 2: Light loading in pu
%  P0 = 0.2;  Q0 = 0.01;  Ut=0.6; xBV=0.25;
% Case 3: At Heavy loading in pu
P0 = 1.20; Q0 = 0.4; Ut=1.4; xBV=0.25;
% DC link parameter
Vdc=2; Cdc=1;
% controller input
Vdcrf=4;Kdcp = -5; KdcI = 0;Kdp = -5;KdI = -60;Ks=1;Ts=0.05;j=sqrt(-1);
dw=1;wn = sqrt(wb/2*H);s=j*wn;
% UPFC Control input parameters parameter
mB=0.08; %  modulation index of series converter
delta_B=78.21; % phase angle of series converter voltage
delta_E=85.35; % phase angle of shunt converter voltage
mE=0.4;   % modulation index of shunt converter
% Sample times
Ts_PWM = 5e-6; Ts_Control = 50e-6;      % Control systems sample
Ts_Power = Ts_PWM;       % Default value
% Grid parameters
```

```
Fnom = 50;              % Nominal system frequency (Hz)
Vnom_grid = 400e3;      % nominal voltage (L-L rms)
Psc_grid = 15000e6;     % Short-circuit level (VA)
% Shunt Converter parameters
Pnom_dc_3L = 200e6;                 % Nominal DC link Power (VA)
Vnom_dc_3L = Vnom_grid/0.612;
% Nominal DC link voltage (V)
H_3L = 1/Fnom*2;                    % DC link stored energy constant(s) = 2 cycles
Clink_3L = Pnom_dc_3L*H_3L*2 /Vnom_dc_3L^2; % DC link capacitor (F)
Vc_Initial_3L = Vnom_dc_3L/2;           % capacitor initial voltage (V)
% Transformer:
Pnom_3L = Pnom_dc_3L;       % Transformer nominal power (VA)
Vnom_prim_3L = Vnom_grid;   % Nominal primary voltage (V)
m_nom_3L = 0.8;             % Nominal modulation index
Vnom_sec_3L = 0.5*Vnom_dc_3L/sqrt(2)*sqrt(3)*m_nom_3L; % Nominal sec. voltage
(V)
Lact = 0.15*((Vnom_sec_3L/1000)*1e3)^2/(Pnom_3L)/314.159;
% VDC controller
Kp_VDCreg_3L= 3;   Ki_VDCreg_3L= 300;       % Proportional gain and Integral gain
LimitU_VDCreg_3L= 1.5;      % Output (Idref) Upper limit (pu)
LimitL_VDCreg_3L= -1.5;     % Output (Idref) Lower limit (pu)
% Current controller
Kp_Ireg_3L= 0.2/2;          % Proportional gain Kp_VDCreg_3L
Ki_Ireg_3L= 15;             % Integral gain
LimitU_Ireg_3L= 1.5;        % Output (Vdq_conv) Upper limit (pu)
LimitL_Ireg_3L= -1.5;       % Output (Vdq_conv) Lower limit (pu)
%% Mathematical model of SMIB wuth UPFC
P=0.8; Vt=1; Vb=1;
% The reactance equation
xqE=xq+xtE; xdE=xd1+xtE; xBB=xB+xBV; x1d=xE*(1+(xtE+xd1)*(xE+xT)/xE*xT);
x2d=xBB*x1d+xE*xdE; x3d=((xE*xdE/xT)-x1d)/x2d; x4d=(x1d-xE-(xE*xdE)/xT)/x2d;
x1q=xE*(1+(xtE+xq)*(xE+xT)/xE*xT); x2q=xBB*x1q+xE*xqE; xBd=xBB+xdE;
xdt=xd1+xtE+xE; xqt=xq+xtE+xE; xBq=xBB+xqE; r1=0; x1=0.2;
delta1=asin(P0/(sqrt(P0^2+(Q0+Ut^2/xq)^2))); utd=Ut*sin(delta1); utq=sqrt(Ut^2-utd^2);
itq=utd/xq; itd=(P0-utd*utq/xq)/utd;
% Generator output power in terms of q-axis and d-axis components
Eq1=utq+xd1*itd; EQ=Eq1+(xq-xd1)*itd; Pe= utd*itd+utq*itq;
Qe=utd*itq-utq*itd; % dynamic equations relevant to the reactive power deviations
ud=(x1+xq)*itq-r1*itd; uq=EQ-(x1+xq)*itd-r1*itq; u=sqrt(ud^2+uq^2); delta=atan(ud/uq);
%Dynamic d-q based equations of currents relevant to the reference system
IEd=xBB*Eq1/xdE-
mE*sin(delta_E)*Vdc*xBd/2*xdE+xdE*(Vb*cos(delta)+mB*sin(delta_B)*Vdc)/2*xdE;
IEq=mE*cos(delta_E)*Vdc*xBq/2*xqE-
xqE*(Vb*sin(delta)+mB*cos(delta_B)*Vdc/2)/xqE;
IBd=-xdt*(Vb*cos(delta)+mB*sin(delta_B)*Vdc/2)/xdE-
xdE*mE*sin(delta_E)*Vdc/2*xdE+xE*Eq1/xdE;
```

```
IBq=-mE*cos(delta_E)*Vdc*xqE/2*xqE-
xqt*(Vb*sin(delta)+mB*cos(delta_B)*Vdc/2)/xqE;
Eq01=EQ; Vb0=u; Xt=x1; Xd1=xd1; Xq=xq; Xd=xd; delta0=delta; Vtd0=utd; Vtq0=utq;
Vt0=Ut;
% Non-linear dynamic form of UPFC
vEtd =-xE*IEq+Vdc*mE*cos(delta_E)/2; vEtq=xE*IEd+Vdc*mE*sin(delta_E)/2;
vBtd =-xB*IBq+Vdc*mB*cos(delta_B)/2; vBtq=xB*IBd+Vdc*mB*sin(delta_B)/2;
dVdc=3*mE*(cos(delta_E)*IEd+sin(delta_E)*IEq)/4*Cdc+3*mB*(cos(delta_B)*IBd+sin(
delta_B)*IBq)/4*Cdc; % where dVdc is Vdc or dVdc/dt
a=r1^2+(x1+xd1)*(xq+x1);
% linearization constant function of the system coefficients
K1=EQ*u*(r1*sin(delta)+(x1+xd1)*cos(delta))/a+itq*u*((xq-xd1)*(x1+xq)*sin(delta)-
r1*(xq-xd1)*cos(delta))/a;
K2=r1*EQ/a+itq*(1+(x1+xq)*(xq-xd1)/a); K3=(1+(x1+xq)*(xd-xd1)/a)^-1;
K4=u*(xd-xd1)*((x1+xq)*sin(delta)-r1*cos(delta))/a;
K5=utd/Ut*xq*((r1*u*sin(delta)+(x1+xd1)*u*cos(delta))/a)+utq/Ut*xd1*(r1*u*cos(delta)
-(x1+xq)*u*sin(delta))/a; K6=utq*(1-xd1*(x1+xq)/a)/Ut+utd/Ut*xq*r1/a;
K7=3*(x2d*      mE*cos(delta_E)+x4d*mB*cos(delta_B))*Vb*sin(delta)/(4*Cdc*xdE)-
3*(x1q*mE*sin(delta_E)+x2q*mB*sin(delta_B))*Vb*cos(delta)/(4*Cdc*xqE);
K8=3*(mE*cos(delta_E)*x1d+mB*sin(delta_B)*xBd)/(4*Cdc*xdE);
K9=-0.25*Cdc*(mB*sin(delta_B)*(mB*cos(delta_B)*xdt-
mE*cos(delta_E)*xdE)/(2*xdE)-mE*sin(delta_E)*(mE*cos(delta_E)*xBd-
mB*cos(delta_B)*xdt)/(2*xdE)+mB*cos(delta_B)*(mB*sin(delta_B)*xqt-
mE*sin(delta_E)*xqE)/(2*xqE)-mE*cos(delta_E)*(-
mB*sin(delta_B)*xqE+mE*sin(delta_E)*xBq)/(2*xqE));
Kpe=(utd-itq*xd1)*(xBd-xdE)*Vdc*sin(delta_E)/2*xdE+(xq*itd+utq)*(xBq-
xqE)*Vdc*cos(delta_E)/2*xqE;
KpdE=(utd-itq*xd1)*(xBd-xdE)*Vdc*mE*cos(delta_E)/2*xdE+(xq*itd+utq)*(-
xBq+xqE)*Vdc*mE*sin(delta_E)/2*xqE;
Kpb=(utd-itq*xd1)*(xdt-xqE)*Vdc*sin(delta_B)/2*xdE+(xq*itd+utq)*(xqt-
xqE)*Vdc*cos(delta_B)/2*xqE;
KpdB=(utd-itq*xd1)*(xdE+xdt)*Vdc*mB*cos(delta_B)/2*xdE+(xq*itd+utq)*(-
xqt+xqE)*Vdc*mB*sin(delta_B)/2*xqE;
Kpd=(utd-itq*xd1)*((xdt-xdE)*mB*sin(delta_B)/2*xdE+(xBd-
xdE)*mE*sin(delta_E))/2*xdE+(xq*itd+utq)*((xqt-xqE)*mB*cos(delta_B)/2*xqE+(xBq-
xqE)*mE*cos(delta_E)/2*xqE);
Kqd=-(xd1-xd)*(xBd-xdE)*Vdc*sin(delta_E)/2*xqE;
Kqde=-(xd1-xd)*(xBd-xdE)*mE*Vdc*cos(delta_E)/2*xdE;
Kqb=-(xd1-xd)*(xdt-xdE)*Vdc*sin(delta_B)/2*xdE;
KqdB=-(xd1-xd)*(xdE-xdt)*mB*Vdc*cos(delta_B)/2*xdE;
Kqe=-(xd1-xd)*((xBd-xdE)*mE*sin(delta_E)/2*xdE+(xdt-
xdE)*mB*sin(delta_B)/2*xdE);
Kvqe=utd*(xBq-xqE)*Vdc*cos(delta_E)/2*Ut*xqE-utq*(xBd-
xdE)*Vdc*sin(delta_E)/2*Ut*xdE;
Kvde=utd*xq*(xqE-xBq)*mE*Vdc*sin(delta_E)/2*Ut*xqE-utq*xd1*(xBd-
xdE)*mE*Vdc*cos(delta_E)/2*Ut*xqE;
```

```
Kvb=utd*xq*(xqt-xqE)*Vdc*cos(delta_E)/2*Ut*xqE-utq*xd1*(xdt-
xdE)*Vdc*sin(delta_E)/2*Ut*xdE;
KvdB=utd*xq*(xqE-
xqt)*mB*Vdc*sin(delta_E)/2*Ut*xqE+utq*mB*xd1*(xdE+xdt)*Vdc*cos(delta_E)/2*Ut*
xdE;
Kvd=utd*xq*(xBq-xqE)*mE*cos(delta_E)/2*Ut*xqE+(xqt-
xqE)*mB*cos(delta_B)/2*xqE-utq*mE*xd1*(xBd-
xdE)*sin(delta_E)/2*Ut*xdE+mB*(xdt-xqE)*sin(delta_E)/2*xdE;
Kce=0.25*Cdc*Vdc*sin(delta_E)*(mE*cos(delta_E)*xBd-
mB*cos(delta_B)*xdE)/2*xdE+Vdc*cos(delta_E)*(mE*sin(delta_E)*xBq-
mB*sin(delta_B)*xqE)/2*xqE;
Kcde=0.25*mE*(cos(delta_E)*IEq-
sin(delta_E)*IEd)/Cdc+0.25*(mE*Vdc*cos(delta_E)*(mE*cos(delta_E)*xBd-
mB*cos(delta_B)*xdE)/2*Cdc*xdE+mE*Vdc*sin(delta_E)*(mB*sin(delta_B)*xqE+mE*
sin(delta_E)*xBq)/2*Cdc*xqE);
Kcb=0.25*Cdc*Vdc*sin(delta_B)*(-
mE*cos(delta_E)*xdE+mB*cos(delta_B)*xdt)/2*xdE+Vdc*cos(delta_B)*(mB*sin(delta_
E)*xqt-mE*sin(delta_E)*xqE)/2*xqE;
KcdB=0.25*mB*(cos(delta_B)*IBq-
sin(delta_B)*IBd)/Cdc+0.25*(mB*Vdc*cos(delta_B)*(mE*cos(delta_E)*xdE+mB*cos(de
lta_B)*xdt)/2*Cdc*xdE+mB*Vdc*sin(delta_B)*(-
mB*sin(delta_E)*xqt+mE*sin(delta_E)*xqE)/2*Cdc*xqE);
% Constants of state space model of power system
A=[0 wb 0 0 0;-K1/M -D/M -K2/M 0 -Kpd/M; -K4/Td01 0 -K3/Td01 1/Td01 -Kqd/Td01; -
KA*K5/TA 0 -KA*K6/TA -1/TA -KA*Kvd/TA; K7 0 K8 0 -K9];
B=[0 0 0 0 0;0 -Kpe/M -KpdE/M -Kpb/M -KpdB/M;0 -Kqe/Td01 -Kqde/Td01 -Kqb/Td01 -
KqdB/Td01;KA/TA KA*Kvqe/TA -KA*Kvde/TA -KA*Kvb/TA -KA*KvdB/TA;0 Kce
Kcde Kcb KcdB];
delta_E=((Kdp+KdI/s)*dw+(Kdcp+KdcI/s)+(Vdcrf-Vdc))*(Ks/(1+s*Ts));
du=K*(1+s*T1)*(1+s*T3)*dw/((1+s*T2)*(1+s*T4));      % Input to damping controller
%% Results obtained
disp('The best optimal value of the objective function found by ALO : ');
disp('  K          T1          T2          T3          T4');
display([num2str(Best_pos)]);
```